E20-191

ANALYSIS AND MECHANIZATION OF LAUNCH WINDOW AND RENDEZVOUS COMPUTATION PART I. CIRCULAR ORBITS

Research & Analysis Section Tech Memo No. 175

March 1966

By

J. L. Shady

Prepared for:

NATIONAL AERONAUTICS AND SPACE ADMINISTRATION
GEORGE C. MARSHALL SPACE FLIGHT CENTER
AERO-ASTRODYNAMICS LABORATORY

Prepared under Contract NAS8-20082

Reviewed by:

D. L. Cooper
Technical Supervisor

Approved by:

Dr. S. S. Hu
Director
Research & Analysis Section

NORTHROP SPACE LABORATORIES
HUNTSVILLE DEPARTMENT
HUNTSVILLE, ALABAMA

FOREWORD

The enclosed presents the results of work performed by Northrop Space Laboratories, Huntsville Department, while under contract to the Aero-Astrodynamics Laboratory of Marshall Space Flight Center (NAS8-20082). This task was conducted in response to the requirement of Appendix E-1, Schedule Order No. 10. Technical coordination was provided by Mr. Jesco von Puttkamer of the Technical and Scientific Staff (R-AERO-T).

ABSTRACT

This report presents the results of an analytical study to develop the logic for a digital computer subroutine for the automatic computation of launch opportunities, or the sequence of launch times, that will allow execution of various modes of gross circular orbit rendezvous. The equations developed in this study are based on two-body orbital theory.

The Earth has been assumed to have the shape of an oblate spheroid. Oblateness of the Earth has been accounted for by assuming the circular target orbit to be space-fixed and by correcting the rotational rate of the Earth accordingly. Gross rendezvous between the target vehicle and a maneuverable chaser vehicle, assumed to be a standard or uprated Saturn V launched from Cape Kennedy, is in this study accomplished by: 1) direct ascent to rendezvous, or 2) rendezvous via an intermediate circular parking orbit.

When operating, this subroutine will determine the span or sequence of launch times in which a chaser vehicle can be launched to accomplish a pre-selected rendezvous mission. The launch times will be restricted by such mission constraints as:

1) Total propulsive velocity change (ΔV) capability of the chaser vehicle
2) Total allowable chaser flight time
3) Maximum time that can be spent by the chaser vehicle in a parking orbit
4) Range safety restrictions on the chaser vehicle's launch azimuth.

At this point in time, the subroutine is in a state ready for initial programming and checkout.

TABLE OF CONTENTS

NOMENCLATURE

Symbol	Definition	Units
a	Semi-major axis	m
a_2	Semi-major axis of transfer ellipse 2	m
A_Z	Chaser vehicle launch azimuth, measured eastward from the launch site meridian	deg, rad
$(A_Z)_{MAX}$	Maximum allowable launch azimuth	deg, rad
$(A_Z)_{MIN}$	Minimum allowable launch azimuth	deg, rad
D	Chord connecting points A or B and point C of the third-stage-burn-model geometry	m
e	Eccentricity	-
e_2	Eccentricity of transfer ellipse 2	-
E_A	Eccentric anomaly of point A on the variable coast ellipse	rad
E_B	Eccentric anomaly of point B on the variable coast ellipse	rad
E_1	Eccentric anomaly of the point of orbital transfer departure (point a)	rad
E_{2BO}	Eccentric anomaly of the point of chaser second stage burnout on the variable coast ellipse	rad

NOMENCLATURE (Continued)

Symbol	Definition	Units
E_3	Eccentric anomaly of the point of orbital transfer conic intersection with an orbit of radius R_2, (point A)	rad
E_4	Eccentric anomaly of the point of orbital transfer conic intersection with an orbit of radius R_2, (point B)	rad
F	Chaser vehicle third-stage thrust	kg
g_o	Acceleration due to gravity at the Earth's surface, (g_o = 9.8045016 m/sec^2)	-
GMT	Greenwich mean time	sec
GHAΥ	Greenwich hour angle of the vernal equinox, measured westward from the prime meridian	deg
i_T	Target orbit inclination	deg
J	Earth oblateness constant, (J = 1.62345 x 10^{-3})	-
K	Number of completed target revolutions at the launch delay time, relative to the ascending node of the target orbit	-
LHA	Local hour angle, measured westward from the launch site meridian	deg

NOMENCLATURE (Continued)

Symbol	Definition	Units
LHAΥ	Local hour angle of the vernal equinox, measured from the launch site meridian	deg
m_{2BO}	Mass of the chaser vehicle at second-stage burnout	kg
M	Integer number of mean solar days	-
M_a	Mean anomaly of the apogee	rad
M_A	Mean anomaly of point A on the variable coast ellipse	rad
M_B	Mean anomaly of point B on the variable coast ellipse	rad
M_o	Integer number of Earth revolutions	-
M_1	Mean anomaly of the point of orbital transfer departure (point a)	rad
M_{2BO}	Mean anomaly of the point of chaser second-stage burnout on the variable coast ellipse	rad
M_3	Mean anomaly of the point of orbital transfer conic intersection with an orbit of radius R_2, (point A)	rad

NOMENCLATURE (Continued)

Symbol	Definition	Units
M_4	Mean anomaly of the point of orbital transfer conic intersection with an orbit of radius R_2, (point B)	rad
N	Number of target revolutions completed at the launch delay time, relative to the target's position at the reference time	-
N_o	Number of target revolutions per Earth rotation	-
P	Semi-latus rectum	m
P_o	Target orbital period	sec
$(P)_{LP}$	Limiting parabola semi-latus rectum	m
Q	Ratio of the square of the chaser second-stage burnout velocity to the square of the circular orbit velocity at the burnout radius	-
R_1	Parking orbit radius	m
R_2	Target orbit radius	m
R_{2BO}	Chaser second-stage burnout radius	m

NOMENCLATURE (Continued)

Symbols	Definition	Units
R_a	Apogee radius	m
R_{COLN}	Radius to the point the chaser crossed the orbital line of nodes	m
R_e	Earth equatorial radius, ($R_e = 6.378165 \times 10^6$ m)	-
R_p	Perigee radius	m
SHA	Sidereal hour angle	deg
t_{CC}	Flight time from chaser third-stage shutdown to target orbit interception	sec
t'_{CC}	Flight time from chaser third-stage shutdown to target orbit interception, assuming a yaw maneuver is performed	sec
$(t_d)_n$	Launch delay time	sec
$(t_d)_m$	Launch delay time in the true mean solar day	sec
$(t_{EC})_A$	Chaser flight time from second-stage burnout to interception of the variable coast ellipse with a circular orbit of radius R_1 or R_2, (point A)	sec

NOMENCLATURE (Continued)

Symbols	Definition	Units
$(t_{EC})_B$	Chaser flight time from second-stage burnout to interception of the variable coast ellipse with a circular orbit of radius R_1 or R_2, (point B)	sec
$(t_F)_a$	Total chaser ascent flight time	sec
$\left[(t_F)_a\right]_{MAX}$	Maximum allowable chaser ascent flight time	sec
$(t_F)_{E1}$	Chaser flight time along orbital transfer ellipse 1	sec
$(t_F)_{E2}$	Chaser flight time along orbital transfer ellipse 2	sec
$(t_F)_{CC}$	Chaser flight time from second-stage burnout to target orbit interception	sec
$(t_F)_{TC}$	Flight time required for the target to coast from its position at the time of chaser second-stage burnout to the orbital line of nodes, (for a non-coplanar ascent trajectory mode)	sec
$(t_F)_{TC}$	Flight time required for the target to coast from its position at the time of chaser second-stage burnout to the point of gross rendezvous, (for the coplanar ascent trajectory mode)	sec

NOMENCLATURE (Continued)

Symbols	Definition	Units
$(t_F)_{TRANS}$	Chaser orbital transfer time	sec
t_{F_1}	Flight time from perigee to point a on the orbital transfer conic	sec
t_{F_3}	Flight time from perigee to point A on the orbital transfer conic	sec
t_{F_4}	Flight time from perigee to point B on the orbital transfer conic	sec
$t_{FICT\ COAST}$	Coast time spend in the "fictitious" target orbit	sec
$(t_F)_{MISSION}$	Total chaser flight time required to accomplish a given rendezvous mission	sec
$\left[(t_F)_{MISSION}\right]_{MAX}$	Maximum allowable mission flight time	sec
t_{PARK}	Chaser parking orbit time	sec
$(t_{PARK})_{MAX}$	Maximum allowable chaser parking orbit time	sec
t_{12B}	Chaser flight time from lift-off to second-stage burnout	sec

NOMENCLATURE (Continued)

Symbols	Definition	Units
t_{3B}	Chaser third-stage-burn time	sec
$(t)_{\xi}$	Time required for the launch site to rotate through the central angle ξ	sec
$(t)_{\psi_o}$	Time required for the launch site to rotate through the central angle ψ_o	sec
T	Corrected mean solar day	sec
T_o	True mean solar day (T_o = 86,164.099 sec)	-
v_a	Chaser velocity at apogee	m/sec
$(v_a)_1$	Chaser velocity at the apogee of transfer ellipse 1	m/sec
$(v_a)_2$	Chaser velocity at the apogee of transfer ellipse 2	m/sec
$(v_{co})_1$	Circular orbit velocity at radius R_1	m/sec
$(v_{co})_{2BO}$	Circular orbit velocity at the chaser second-stage burnout radius R_{2BO}	m/sec

NOMENCLATURE (Continued)

Symbols	Definition	Units
$(v_{co})_3$	Circular orbit velocity at radius R_2	m/sec
$(v_e)_1$	Chaser velocity at point a on the orbital transfer conic	m/sec
$(v_e)_3$	Chaser velocity at point A on the orbital transfer conic	m/sec
$(v_e)_4$	Chaser velocity at point B on the orbital transfer conic	m/sec
$(v_P)_2$	Chaser velocity at the perigee of transfer ellipse 2	m/sec
$(V)_{COLN}$	Velocity of the chaser at the time it crosses the orbital line of nodes	m/sec
$(V_{EC})_{\substack{A \\ B}}$	Chaser velocity at the point of intersection of the variable coast ellipse with an orbit or radius R_1 or R_2	m/sec
V_{2BO}	Chaser velocity at second-stage burnout	m/sec
X	Whole number	-
Y	Decimal	-

NOMENCLATURE (Continued)

Symbols	Definition	Units
α_o	Position of the target at the reference time, relative to the ascending node	deg, rad
α_{LS}	The central angle, measured in the target orbit plane, from the ascending node to the position of the launch site at the reference time ($i_T > \lambda$)	rad
α_T	Position of the target at the launch delay time, relative to the ascending node	rad
$(\gamma_{EC})_{\substack{A \\ B}}$	Chaser flight path angle at the point of intersection of the variable coast ellipse with a circular orbit of radius R_1 or R_2, measured from the local horizontal	rad
γ_1	Chaser flight path angle at point a on the orbital transfer conic, measured from the local horizontal	rad
γ_{2BO}	Chaser flight path angle at second-stage burnout, measured from the local horizontal	rad
$(\gamma_{2BO})_i$	Chaser flight path angle at second-stage burnout that produces a coast ellipse with an apogee equal to radius R_1 or R_2, measured from the local horizontal	rad
$(\gamma_{2BO})_{MAX}$	Maximum second-stage burnout flight path angle	rad

NOMENCLATURE (Continued)

Symbols	Definition	Units
γ_3	Chaser flight path angle at point A on the orbital transfer conic, measured from the local horizontal	rad
γ_4	Chaser flight path angle at point B on the orbital transfer conic, measured from the local horizontal	rad
Υ	Vernal equinox	-
δ	Plane change angle	rad
δ'	Plane change angle after an impulsive yaw maneuver has been performed	rad
$\Delta\gamma_{2BO}$	Chaser second-stage burnout flight path angle increment	rad
Δn	Orbital transfer conic point of arrival increment	rad
$\Delta\theta_1$	Orbital transfer major axis orientation increment	rad
$\Delta\phi$	Angle of nodal regression per target orbital revolution	rad
Δt	Target orbital period	sec
Δt_d	Launch delay time increment	sec

NOMENCLATURE (Continued)

Symbols	Definition	Units
$(\Delta V)_a$	Total chaser ascent impulsive velocity increment	m/sec
$[\ (\Delta V)_a\ ]_{MAX}$	Maximum allowable chaser ascent impulsive velocity increment	m/sec
$(\Delta V)_{CIR}$	Impulsive velocity increment required to circularize an orbit	m/sec
$(\Delta V)_{MISSION}$	Total chaser impulsive velocity increment required to accomplish a given rendezvous mission	m/sec
$[\ (\Delta V)_{MISSION}\ ]_{MAX}$	Maximum allowable mission impulsive velocity increment	m/sec
$(\Delta V)_{PC}$	Chaser impulsive velocity increment required to perform a plane change maneuver	m/sec
$(\Delta V)_{TRANS}$	Total chaser impulsive velocity increment required to perform an orbital transfer maneuver	m/sec
$(\Delta V)_{YAW}$	Chaser impulsive velocity increment required to perform a yaw maneuver	m/sec
$(\Delta V)_{\gamma EC}$	Chaser impulsive velocity increment required to change the flight path angle to zero at the point of intersection of the variable coast ellipse with an orbit of radius R_1 or R_2	m/sec

NOMENCLATURE (Continued)

Symbols	Definition	Units
$(\Delta V)_{\gamma_{2BO}}$	Chaser impulsive velocity increment required to change the second-stage burnout flight path angle	m/sec
ΔV_1	Chaser impulsive velocity increment number 1	m/sec
ΔV_2	Chaser impulsive velocity increment number 2	m/sec
ΔV_3	Chaser impulsive velocity increment number 3	m/sec
ΔV_4	Chaser impulsive velocity increment number 4	m/sec
η	Angle between point a and point A on the orbital transfer conic	rad
θ_{CC}	Range angle subtended by the chaser while coasting from the point of third-stage shutdown to target orbit or parking orbit interception	rad
θ'_{CC}	Range angle subtended by the chaser while coasting from the point of third-stage shutdown to target orbit interception, assuming a yaw maneuver is performed	rad
θ_{COLN}	Position of the chaser at the end of the required parking time relative to the orbital line of nodes	rad
$(\theta_{EC})^{A}_{B}$	Range angle from the point of chaser second-stage burnout to the point of intersection of the variable coast ellipse (point A or B) with an orbit of radius R_1 or R_2	rad

NOMENCLATURE (Continued)

Symbols	Definition	Units
θ_I	Total chaser intercept range angle	deg, rad
θ_N	Central angle, measured in the target orbit plane, from the launch site meridian, at the launch delay time, to the orbital line of nodes	rad
θ_{NT}	Sum of the central angles θ_N and θ_T	rad
θ_T	Central angle, measured in the target orbit plane, from the launch site meridian at the reference time to the launch site meridian at the launch delay time	rad
θ_{TAN}	Position of the target, relative to the target orbit ascending node, at the time the chaser intercepts an orbit of radius R_1 or R_2	rad
$(\theta_{TAN})_{2BO}$	Position of the target, relative to the target orbit ascending node, at the time of chaser second-stage burnout	rad
θ_{TOLN}	Position of the target, relative to the orbital line of nodes, at the time the chaser intercepts an orbit of radius R_1 or R_2	rad
$(\theta_{TOLN})_{2BO}$	Position of the target, relative to the orbital line of nodes, at the time of chaser second-stage burnout	rad
θ_{TDN}	Position of the target, relative to the descending node, at the time the chaser intercepts the target orbit	rad

NOMENCLATURE (Continued)

Symbols	Definition	Units
θ_1	True anomaly of the point of orbital transfer departure (point a)	rad
θ_{12B}	Range angle from chaser lift-off to second-stage burnout	rad
θ_2	True anomaly of the point of intersection of the "Limiting Parabola" with an orbit of radius R_2	rad
θ_3	True anomaly of the point of orbital transfer conic intersection with an orbit of of radius R_2, (point A)	rad
θ_{3B}	Range angle subtended during chaser third-stage burn	rad
θ_4	True anomaly of the point or orbital transfer conic intersection with an orbit of radius R_2, (point B)	rad
λ	Launch site latitude	deg
λ_o	Launch site longitude	deg
λ_T	Latitude of the target orbit ground track at the launch delay time	rad
μ	Earth gravitational constant, ($\mu = 3.986016 \times 10^4 m^3/sec^2$)	-

NOMENCLATURE (Continued)

Symbols	Definition	Units
ξ	Complementary central angle of ψ_o, measured in the equatorial plane	rad
σ	Central angle, measured in the equatorial plane, between the launch site meridian at the reference time and the target orbit descending node	rad
ϕ_A	True anomaly of point A on the variable coast ellipse	rad
ϕ_B	True anomaly of point B on the variable coast ellipse	rad
ϕ_{TRANS}	Orbital transfer phase angle	rad
ϕ_{TRUE}	True phase angle	rad
$\dot{\phi}$	Catch-up rate of the chaser vehicle	rad/sec
ϕ_{2BO}	True anomaly of the point of chaser second-stage burnout on the variable coast ellipse	rad
	Central angle, measured in the target orbit plane, from the ascending node to the launch site meridian at time $(t_d)_n$	rad

NOMENCLATURE (Concluded)

Symbols	Definition	Units
ψ_o	Central angle, measured in the equatorial plane, between the launch site meridian at the reference time and the launch site meridian at the time of the launch site's second passage through the target orbit plane	rad
ψ_{YAW}	Yaw angle	rad
$(\psi_{YAW})_{MAX}$	Maximum yaw angle	rad
ω_{e_c}	Corrected Earth rotational rate	rad/sec
ω_E	True Earth rotational rate, ($\omega_E = 7.29211513 \times 10^{-5}$ rad/sec)	-
ω_1	Angular velocity of the chaser in a parking orbit	rad/sec
ω_2	Angular velocity of the target	rad/sec
Ω	Angle through which the target coasts during the chaser's orbital transfer maneuver	rad
Ω_{LS}	Angular distance through which the launch site rotates during a launch delay time, measured in the equatorial plane from the launch site meridian at the reference time	rad

LIST OF ILLUSTRATIONS

LIST OF ILLUSTRATIONS (Continued)

LIST OF ILLUSTRATIONS (Continued)

LIST OF ILLUSTRATIONS (Concluded)

SECTION 1

INTRODUCTION

As our national space effort increases, orbital rendezvous will play a more predominant role. Earth-orbital rendezvous will be needed for such missions as:

1. Construction of orbital space stations
2. Supply and maintenance of space stations
3. Assembly of interplanetary space vehicles
4. Rescue operations.

Indications are that many of these and other missions will require not just one but several consecutive launches. Thus, a method for determining the sequence of Earth launch times required to accomplish various rendezvous missions would be a useful tool for mission planning.

This report has been written to present the equations and logic required for the development of a digital computer subroutine for determining the launch opportunities for various types of gross circular orbit rendezvous missions. Because of the Earth's oblateness, true circular orbits are in reality not possible except around the equator. However, the problem of circular orbit rendezvous has been attacked as a stepping stone or building block for the more general problem of elliptical orbit rendezvous.

The problem of gross circular orbit rendezvous can be stated as follows:

A non-maneuverable target vehicle is assumed to be orbiting the Earth in a circular orbit of known orbital inclination and radius. Due to the oblateness of the Earth, the target orbit plane precesses around the Earth's polar axis in a direction opposite to the direction of the target vehicle motion. However, the target orbit plane can be assumed to be fixed in the inertial space if the Earth's rotational rate is corrected accordingly.

Rendezvous between the orbiting target vehicle and an Earth-launched, maneuverable chaser vehicle is said to be accomplished when the two vehicles arrive simultaneously, with the same velocity and flight-path angle, at some point in inertial space. The motion of the target, with respect to a rotating launch site, places strong restrictions on the time during which the chaser vehicle can be launched to achieve rendezvous. Thus emerges the term "launch window". A launch window is a period or span of time in which the target vehicle and the launch site are in favorable positions, allowing the chaser to be launched to accomplish gross rendezvous.

Circular orbit rendezvous can be accomplished by two general methods or modes. These modes are:

1) Direct ascent to rendezvous

2) Rendezvous via an intermediate parking orbit (which is assumed to be circular also).

Direct ascent to gross rendezvous is generally restricted to relatively small launch windows. This is due to the fact that the target and the chaser

must be in approximately the same position at the time of the chaser's injection into the target orbit. Small launch delay times can be compensated for by slight variations in the ascent trajectory itself.

Gross rendezvous accomplished by use of an intermediate parking orbit permits longer launch windows. This is so because large launch delays can be offset by remaining in the parking orbit until the phase angle between the target and the chaser is of the correct magnitude to initiate an orbital transfer maneuver.

Regardless of which rendezvous mode is used, the associated launch times are restricted by the chaser launch vehicle's capabilities and various other mission constraints.

SECTION 2

ASSUMPTIONS AND DEFINITIONS

2.1 Earth Model

The Earth model assumed is a spinning oblate spheroid.

2.1.1 Oblateness Effects

Due to the oblateness of the Earth, the elements of a target vehicle's orbit are perturbed. The major effect of oblateness on an assumed circular target orbit is precession of the orbital plane. This plane, and thus the line of nodes, tends to precess about the Earth's polar axis in a direction opposite the general direction of motion of the orbiting target vehicle. Figure 1 illustrates regression of the line of nodes for an eastwardly travelling target vehicle.

2.1.2 Earth Rotational Rate

Regression of the line of nodes can be best compensated for, in a first approximation, by assuming the target orbit plane to be fixed in inertial space while the Earth rotates inside this orbit at a corrected rotational rate ω_{e_c}. The corrected Earth rotational rate can be defined by the equation

$$\omega_{e_c} = \omega_E \pm \frac{\Delta\phi}{\Delta t} \qquad (2\text{-}1)$$

where

ω_E = True Earth rotational rate ~ rad/sec

$\frac{\Delta\phi}{\Delta t}$ = Regression of the target orbit's line of nodes per orbital period ~ rad/sec.

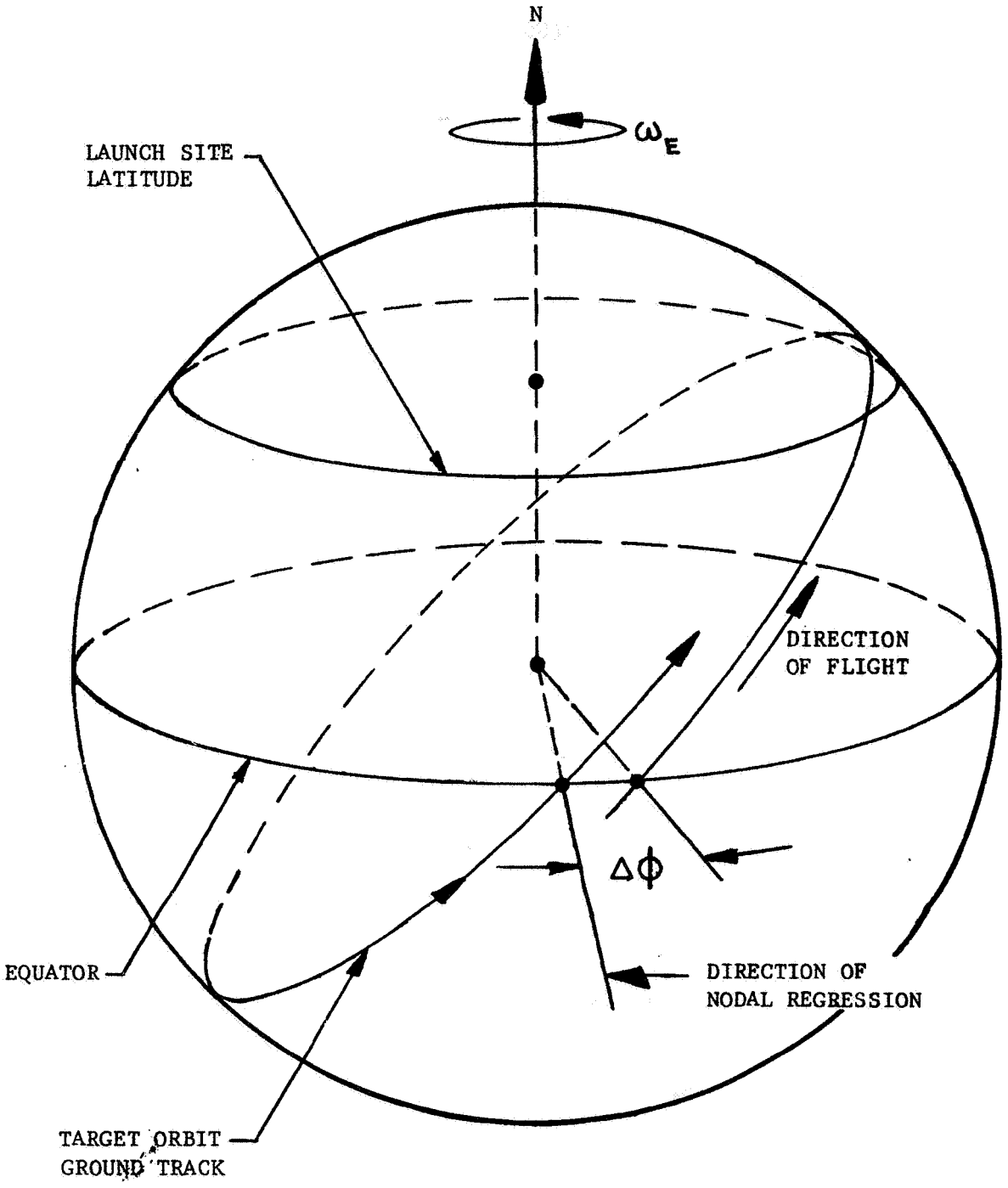

Figure 1. ORBITAL PRECESSION-MOTION OF
A TARGET VEHICLE AROUND AN OBLATE EARTH

The term $\Delta\phi$ has been shown by Blitzer (ref. 3) to be expressed as

$$\Delta\phi = 2\pi J \left(\frac{R_e}{R_2}\right)^2 \cos i_T \qquad (2\text{-}2)$$

The orbital period of the target vehicle is

$$\Delta t = 2\pi \sqrt{\frac{R_2^3}{\mu}} \qquad (2\text{-}3a)$$

The Earth gravitational constant, μ, can also be expressed in terms of Earth constants as

$$\mu = g_o R_e^2 .$$

Thus,

$$\Delta t = 2\pi \left(\frac{R_2}{R_e}\right) \sqrt{\frac{R_2}{g_o}} \qquad (2\text{-}3b)$$

Consequently, the term $\frac{\Delta\phi}{\Delta t}$ can be expressed as

$$\frac{\Delta\phi}{\Delta t} = J \left(\frac{R_e}{R_2}\right)^3 \sqrt{\frac{g_o}{R_2}} \cos i_T \qquad (2\text{-}4)$$

For an eastwardly travelling target vehicle, the corrected Earth rotational rate becomes

$$\omega_{e_c} = \omega_E + J \left(\frac{R_e}{R_2}\right)^3 \sqrt{\frac{g_o}{R_2}} \cos i_T \qquad (2\text{-}5)$$

Hence, it can be seen that for easterly launches

$$\omega_{e_c} > \omega_E .$$

For westwardly travelling target vehicles $\omega_{e_c} < \omega_E$.

2.2 Coordinate System

A geocentric Earth equatorial coordinate system will be used as a reference frame for fixing the target orbit plane in inertial space. This coordinate system has its origin at the center of the Earth. The x-axis lies in the equatorial plane and points toward the vernal equinox or first point of Aries. The z-axis coincides with the Earth's spin axis, while the y-axis completes the right-handed coordinate system. Figure 2 illustrates this coordinate system.

2.3 Reference Time

The subroutine is designed to initiate a sequential launch window computation at some given reference time. Two such reference times will be defined. When the target orbit inclination, i_T, is greater than the launch site latitude, λ, the launch site passes through the target orbit plane twice per day. In this case, the reference time is defined to be the Greenwich mean time, (GMT or ZULU), on a given calendar date, when the target orbit ground-track passes through the launch site with a northerly azimuth. However, when $i_T \leq \lambda$, the reference time is defined as the Greenwich mean time, on a given calendar date, when the launch site is closest to the target orbit plane. This time is referred to as the co-nodal instant because the launch site meridian is midway between the ascending and descending nodes of the target orbit. Figures 3 and 4 illustrate these two reference times.

The reference time is not only the time at which the launch window investigation is initiated, but it also represents the time at which the

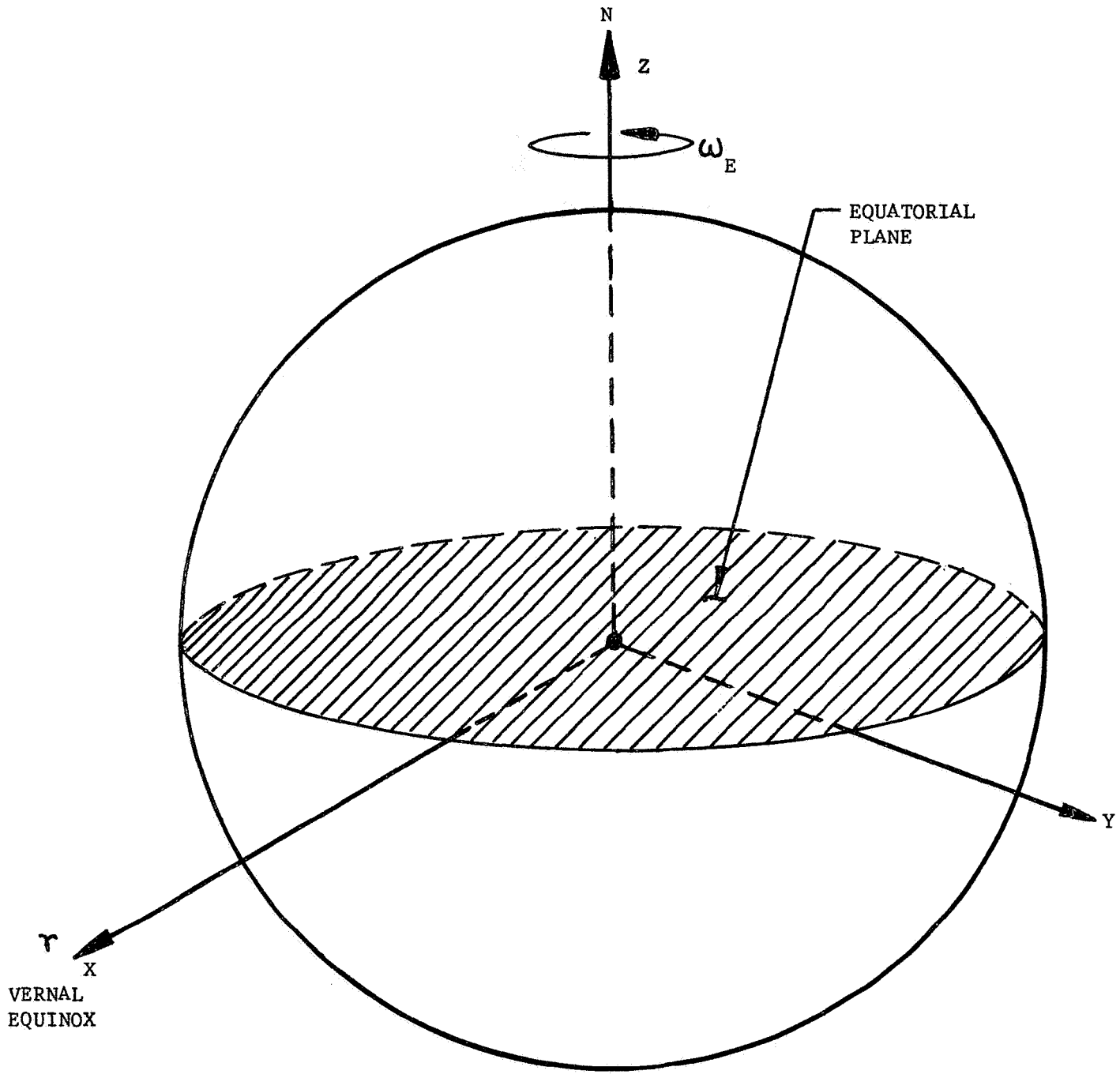

Figure 2. GEOCENTRIC EARTH EQUATORIAL COORDINATE SYSTEM

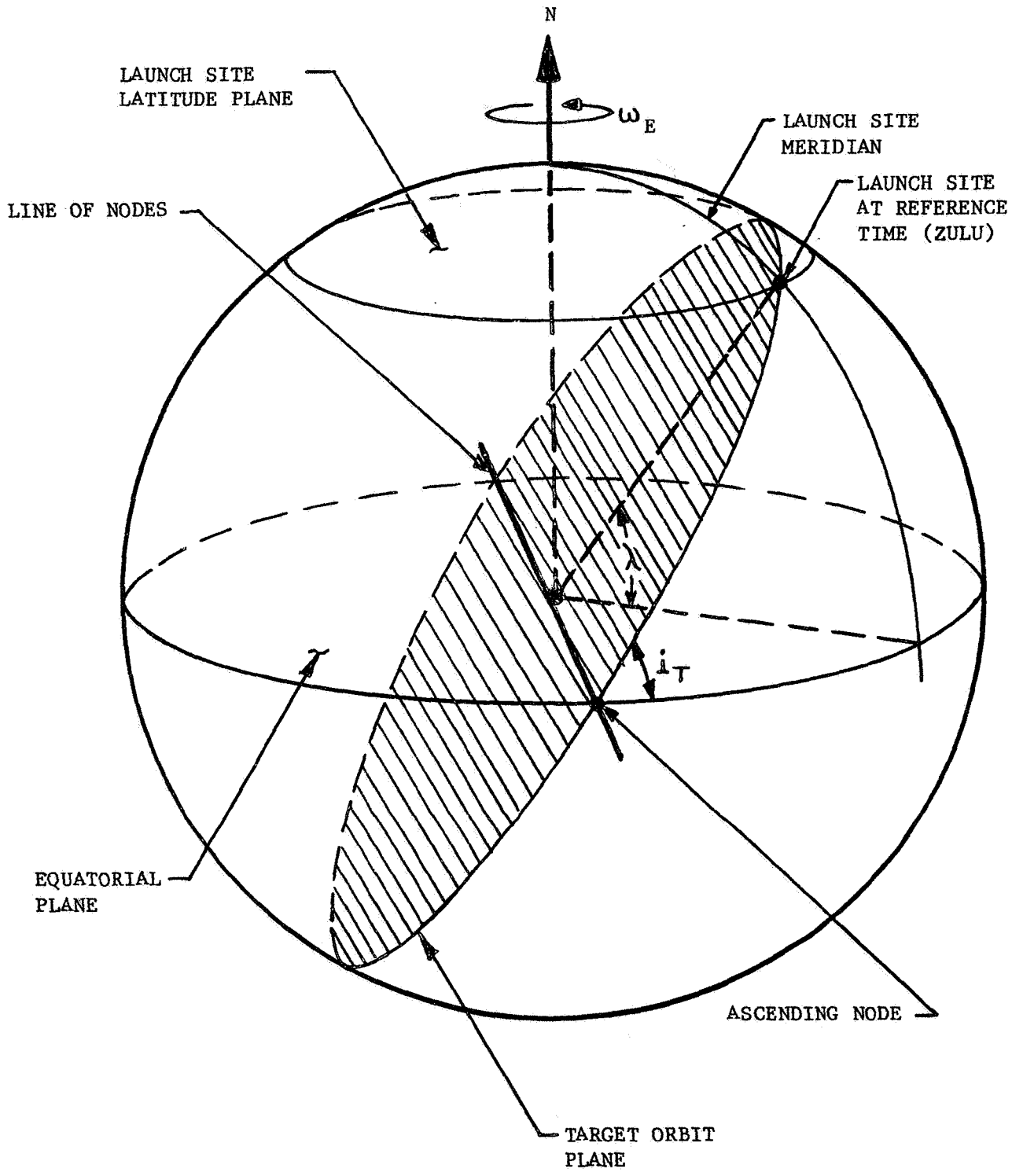

Figure 3. REFERENCE TIME GEOMETRY WHEN $i_T > \lambda$

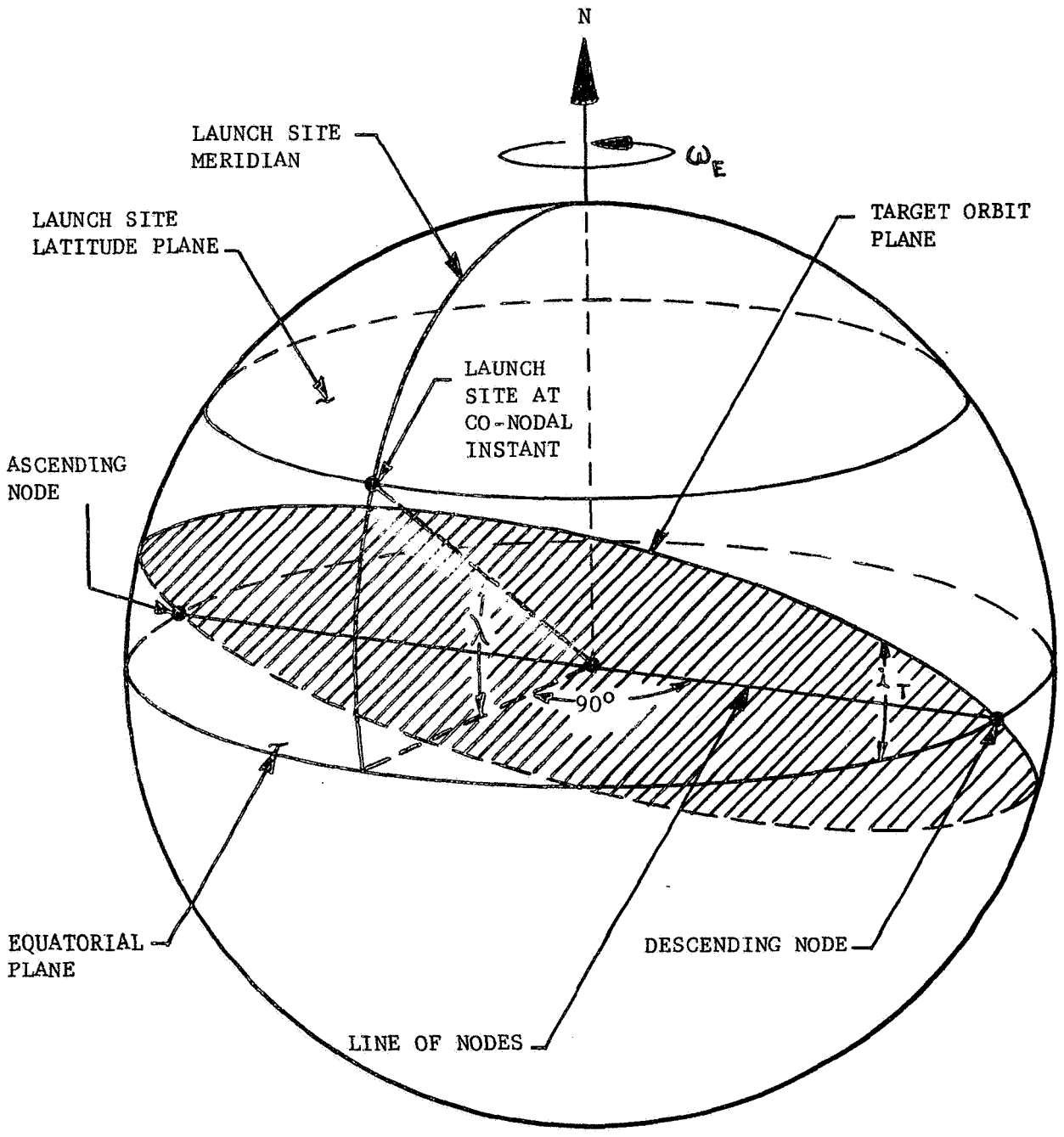

Figure 4. REFERENCE TIME GEOMETRY WHEN $i_T \leq \lambda$ (CO-NODAL INSTANT)

target orbit plane is fixed in inertial space. Thus, there is a need for a method of determining the position of the target orbit plane, relative to the inertial coordinate system, at the reference time.

2.4 Position of the Target Orbit Plane at the Reference Time

With the reference time defined in terms of the Greenwich mean time (GMT or ZULU time), the Greenwich hour angle of the vernal equinox (GHAγ)* can be found by consulting an ephemeris. This angle defines the position of the vernal equinox with reference to the Greenwich hour circle.

The longitude of the launch site, measured westward from the prime meridian, is defined by the symbol λ_o. The local hour angle of the vernal equinox (LHAγ) from the launch site hour circle can be determined by the expressions

$$\begin{aligned} LHA\gamma &= GHA\gamma - \lambda_o \qquad \text{when} \qquad \lambda_o \leq GHA\gamma < 2\pi \\ LHA\gamma &= 2\pi + (GHA\gamma - \lambda_o) \qquad \text{when} \qquad 0 \leq GHA\gamma < \lambda_o \end{aligned} \tag{2-6}$$

Consider Figure 5. This figure illustrates the reference time when $i_T > \lambda$. The local hour angle of the ascending node of the target orbit can be found by the simple trigonometric relation

$$LHA = \sin^{-1}\left[\frac{\tan\lambda}{\tan i_T}\right] \tag{2-7}$$

* Reference is made to Appendix A for the definitions of the terms used in this section.

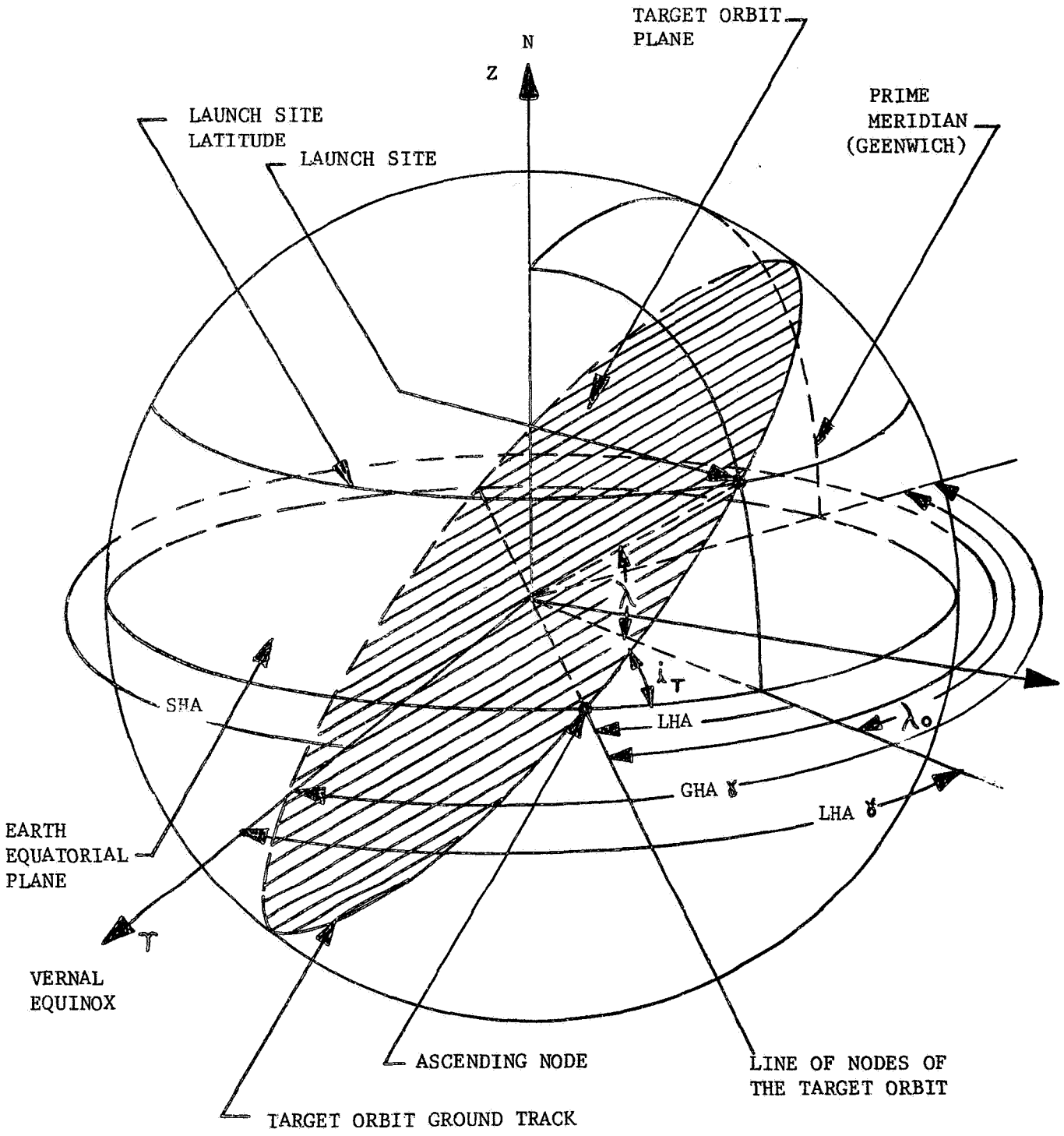

Figure 5. TARGET ORBIT'S POSITION IN THE GEOCENTRIC EQUATORIAL COORDINATE SYSTEM

Hence, the sidereal hour angle (SHA) of the ascending node can be calculated by one of the following expressions:

$$\begin{aligned} &SHA = LHA - LHA^{\gamma} && \text{when } \lambda_o \leq GHA^{\gamma} \leq (\lambda_o + LHA) \\ &SHA = 2\pi + (LHA - LHA^{\gamma}) && \text{when } 0 \leq GHA^{\gamma} < \lambda_o \\ & && (\lambda_o + LHA) < GHA^{\gamma} < 2\pi \end{aligned} \tag{2-8}$$

Thus, the SHA and i_T determine the position of the target orbit plane relative to the vernal equinox at the reference time. Calculation of the SHA, for a target orbit with an inclination less than or equal to the launch site latitude, is similar to the method presented above.

2.5 Launch Delay Time Scale

As the Earth rotates at a corrected rotational rate, the launch site is rotated relative to its position at the reference time. Thus, a time scale is needed to determine the position of the launch site at any given time. This time scale shall be designated as the Launch Delay Time Scale and any given time in this scale will be denoted by the symbol $(t_d)_n$ called launch delay time, where

$$(t_d)_n = (t_d)_{n-1} + \Delta t_d \tag{2-9}$$

$$n = 1,2,3,\ldots$$

Δt_d = launch delay time increment.

The reference time is defined as

$$(t_d)_n = 0.$$

As $(t_d)_n$ is allowed to increase, the position of the launch site, relative to its position at the reference time, can be determined by the expression

$$\Omega_{LS} = (\omega_{e_c})(t_d)_n \tag{2-10}$$

where

Ω_{LS} = central angle through which the launch site rotates in the time $(t_d)_n$.

The true mean solar day is defined to be the time required for the Earth to complete one revolution, or

$$T_o = \frac{2\pi}{\omega_E} \quad (= 23^h\ 56^m\ 4.099^s) \tag{2-11}$$

Because $\omega_{e_c} > \omega_E$, the corrected mean solar day becomes

$$T = \frac{2\pi}{\omega_{e_c}} \tag{2-12}$$

Thus, $T < T_o$.

The launch site completes one revolution around the Earth's polar axis when

$$(t_d)_n = T$$

or

$$\Omega_{LS} = 2\pi.$$

The purpose of the launch delay time scale is to provide a basic reference "clock" in the automatic determination of the launch site's position during the launch window computation. Thus, if it is desired to conduct an investigation

for an integer number of true mean solar days, M, from the reference time, the launch site must be allowed to rotate around the Earth's polar axis for MT seconds or $M(2\pi)$ revolutions.

Launch windows, for various rendezvous modes, are then calculated by determining if rendezvous can be accomplished at various values of $(t_d)_n$, until

$$(t_d)_n = M(T).$$

If gross rendezvous is found to be achievable at any given launch delay time, the value of $(t_d)_n$ must be corrected to its associated time in the true mean solar day. This is accomplished by the following simple expression:

$$(t_d)_n \text{ in the true mean solar day} = (t_d)_n \frac{\omega_{e_c}}{\omega_E}$$

or

$$(t_d)_{n_{TRUE}} = (t_d)_n \frac{\omega_{e_c}}{\omega_E} \qquad (2\text{-}13)$$

All values of the "true launch delay time", that permit gross rendezvous, are then pieced together to give the span of permissible launch times (launch window) in the true mean solar day.

2.6 Target Position at Given Launch Delay Time

The central angle measured, at the reference time, from the ascending node of the target orbit to the position of the target vehicle is defined by the symbol α_o, where $0 \leq \alpha_o \leq 2\pi$. This angle defines the position of the target vehicle in the orbital plane at the reference time $(t_d)_n = 0$. The angle α_o, illustrated in Figure 6, is an input to the subroutine.

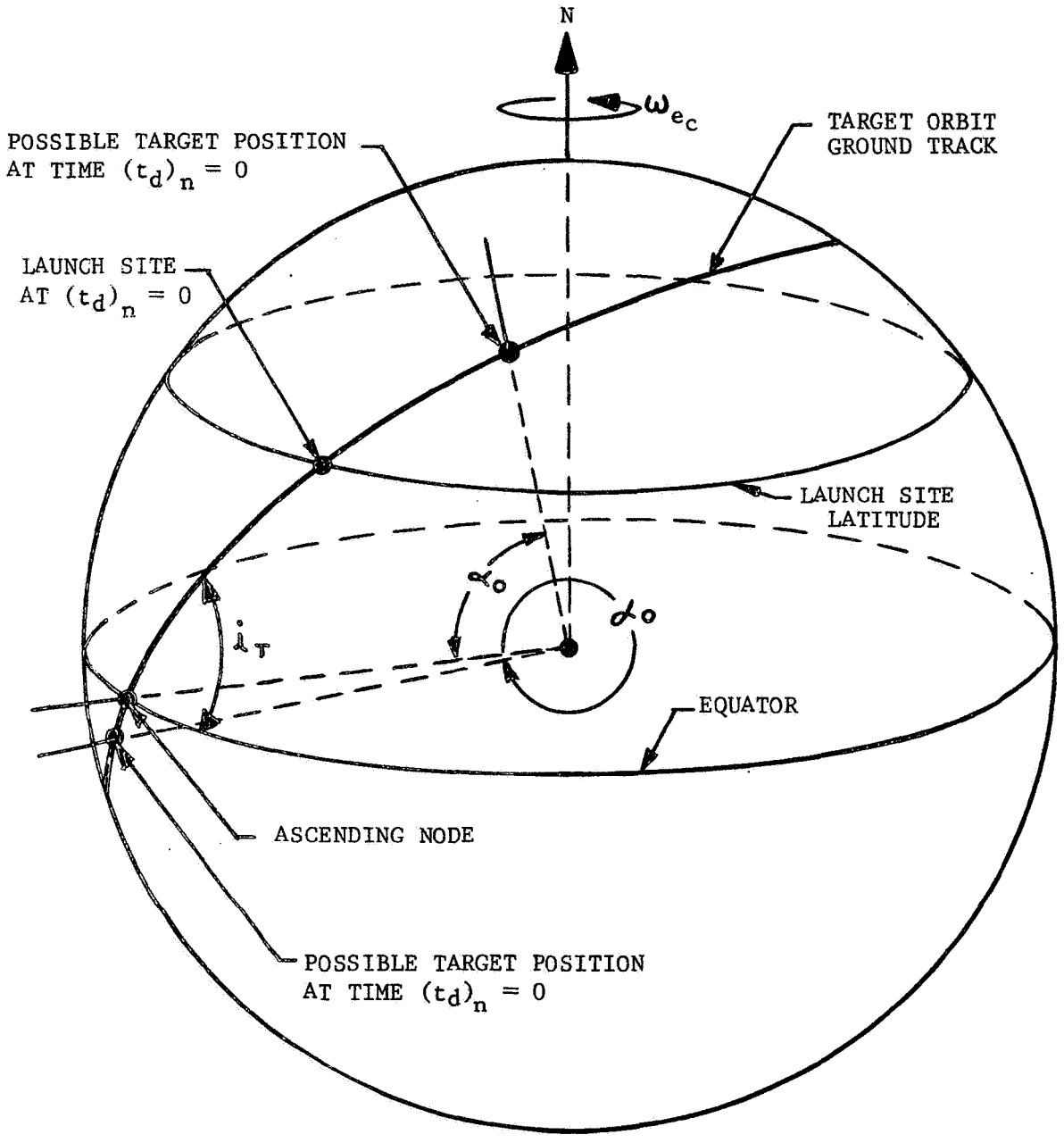

Figure 6. TARGET VEHICLE POSITION AT THE REFERENCE TIME

In order to conduct a launch window investigation, the position of the target relative to the ascending node must be known at any launch delay time, $(t_d)_n$.

The number of orbital revolutions completed by the target vehicle at any launch delay time, $(t_d)_n$, can be given by

$$N = \frac{(t_d)_n}{P_o} \quad * \qquad (2\text{-}14)$$

where

$P_o = 2\pi\sqrt{\frac{R_2^3}{\mu}}$ = target orbital period.

The target's angular distance from the ascending node at any time $(t_d)_n$ can be determined by

$$\alpha_T = \alpha_o + N(2\pi) \qquad (2\text{-}15)$$

A parameter K is introduced which defines the number of completed target revolutions at time $(t_d)_n$, relative to the ascending node, or

$$K = \frac{\alpha_T}{2\pi} \qquad (2\text{-}16)$$

Furthermore, K is a number composed of a whole number and a decimal. Thus,

$$K = X + Y \qquad (2\text{-}17)$$

where

X = whole number

Y = decimal.

---

* The nodal period of the target vehicle is not used in this expression because the target orbit is assumed to be space-fixed. Thus, the nodal period is the orbital period.

The whole number X indicates the number of full revolutions completed by the target at the time $(t_d)_n$. The decimal Y indicates the fractional portion of a revolution completed at time $(t_d)_n$. Thus, the position of the target at any launch delay time, relative to the ascending node, can be written as

$$\alpha_T = Y(2\pi) \tag{2-18}$$

where

$$0 \leq \alpha_T \leq 2\pi.$$

2.7 Rendezvous Compatible Orbits

The term "rendezvous compatibility" applies to target orbits having an orbital inclination, i_T, greater than or equal to the launch site latitude, λ. A rendezvous compatible orbit allows rendezvous to occur nearly directly over the launch site either once or twice per day.

The altitude or radius of an orbiting target vehicle determines its period. Thus, adjustment of altitude is sufficient to permit the target to appear directly above or in the vicinity of the launch site at the same times on successive days. This is known as "once-a-day rendezvous compatibility" and, in principle, is feasible for all inclinations equal to or greater than λ.

However, if (for $i_T > \lambda$) a second rendezvous per day is also desired, the orbital inclination becomes of prime importance. "Twice-a-day rendezvous compatibility" can be achieved only for discrete combinations of altitude and inclination. These combinations of orbital parameters must be such that the

target completes an integral number of revolutions, plus the arc from Points A to B (Figure 7), during the time the launch site rotates from Point A to Point B.

Swanson and Peterson (refs. 16 and 18) have shown that the rendezvous compatibility of a target vehicle, travelling eastward in a circular orbit, can be determined by the expression:

$$\frac{N_o}{M_o} = \frac{T_o}{\frac{2\pi(R_2)^{3/2}}{\sqrt{g_o R_e^2}}\left[1 - \frac{JR_e^2}{R_2^2}(3.0-2.5\sin^2 i_T)\right] + \frac{T_o JR_e^2}{R_2^2}\cos i_T} \qquad (2\text{-}19)$$

If the value of $\frac{N_o}{M_o}$, for a given target orbit, is an integer, the orbit is said to be "twice-a-day rendezvous compatible". That is to say, the target will be located at the same position in its orbit on successive days. Thus, the launch times required to achieve gross rendezvous with the target will be the same on successive days. Consequently, the launch times permitting rendezvous must be determined only for the first day of an M-day investigation. These allowable launch times will then be valid for each successive day of the investigation. If, however, $\frac{N_o}{M_o}$ is not an integer, the launch times allowing rendezvous must be determined for each day of the investigation.

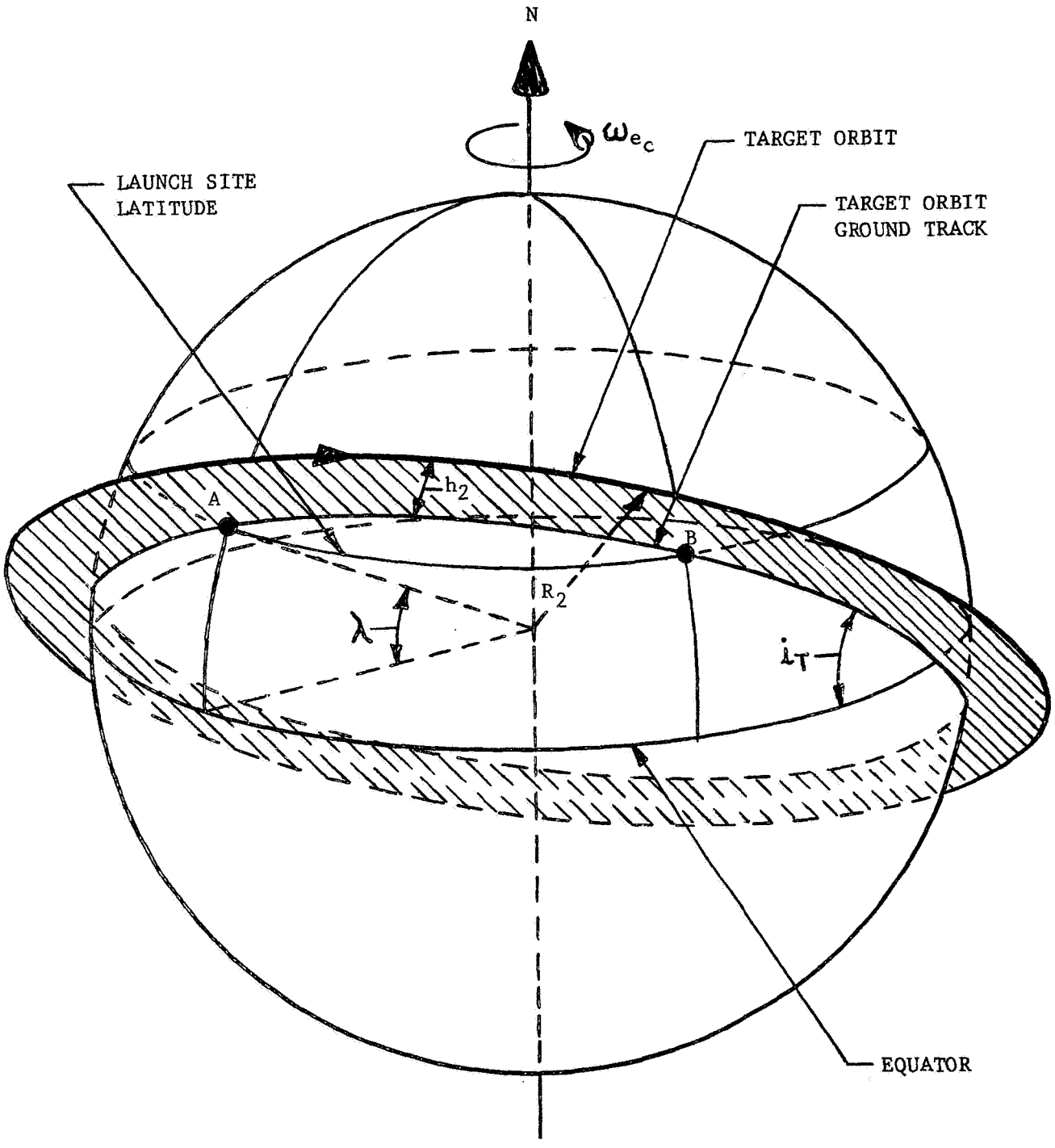

Figure 7. GEOMETRY FOR "TWICE-A-DAY RENDEZVOUS COMPATIBILITY"

SECTION 3

ANALYSIS

3.1 Direct Ascent to Circular Orbit Rendezvous

The general problem of direct ascent to circular orbit rendezvous is illustrated in Figure 8, and can be stated as follows:

A target vehicle is assumed to be revolving around the Earth in a space-fixed, circular orbit while the launch site, on the Earth's surface, rotates beneath the target orbit at a corrected rotational rate. The optimum time to launch a chaser vehicle is the instant the launch site passes through the target orbit plane. This is sometimes called an on-time or coplanar launch.

A coplanar launch is advantageous from the standpoint of fuel consumption because no plane change maneuver is required. Gross rendezvous can be accomplished only if the target is located at a unique point in its orbit at the time of launch of the chaser. However, it is unrealistic to ignore possible launch holds and to assume that the target will always be in the correct position to allow a coplanar direct ascent launch. In case of a delay, the chaser must be launched at some later time (launch delay time) via a non-coplanar ascent trajectory.

If a non-coplanar direct ascent trajectory is used, gross rendezvous cannot be accomplished unless the target's position is within some sector of its orbit. This sector is a function of the target's orbital parameters, the ascent trajectory, the launch azimuth, the plane change angle, and the chaser launch vehicle's maneuver capabilities.

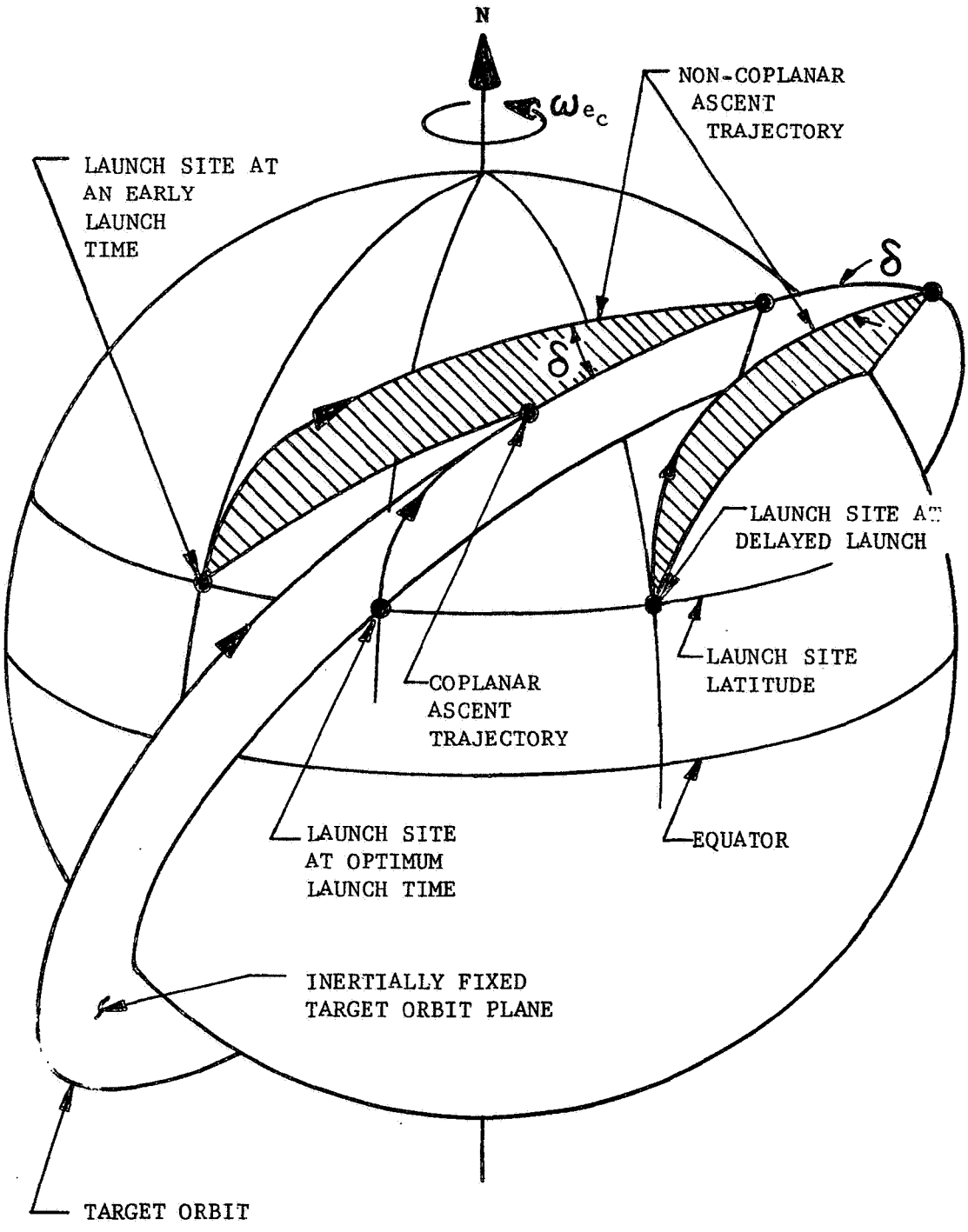

Figure 8. THE DIRECT ASCENT TO RENDEZVOUS PROBLEM

3.1.1 Ascent Trajectory Modes

The reference time has been defined as zero in the Launch Delay Time Scale. At various launch delay times, the launch site is located at different positions relative to the target orbit plane. This fact gives rise to a number of geometrical relationships that occur between the launch site and the target orbit plane. These relationships will be called Ascent Trajectory Modes. They will be categorized according to the position of the launch site at the launch delay time and the target orbit inclination.

3.1.1.1 Coplanar Ascent Trajectory Mode

When the target orbit inclination is greater than the launch site latitude, two optimum coplanar launch opportunities occur daily. One opportunity occurs when the target orbit ground-track passes through the launch site in a northerly direction (reference time), the other when the ground-track passes through the launch site in a southerly direction. The Coplanar Ascent Trajectory Mode refers to the case where the chaser vehicle is launched directly into the target orbit plane during one of the optimum launch opportunities. Figure 9 illustrates both cases of this ascent trajectory mode.

3.1.1.2 Non-Coplanar Ascent Trajectory Modes

The other ascent trajectory modes that apply when the target orbit inclination is greater than the launch site latitude are defined to be non-coplanar. That is to say, the chaser vehicle is launched either before or after the launch site passes through the target orbit plane. As a result,

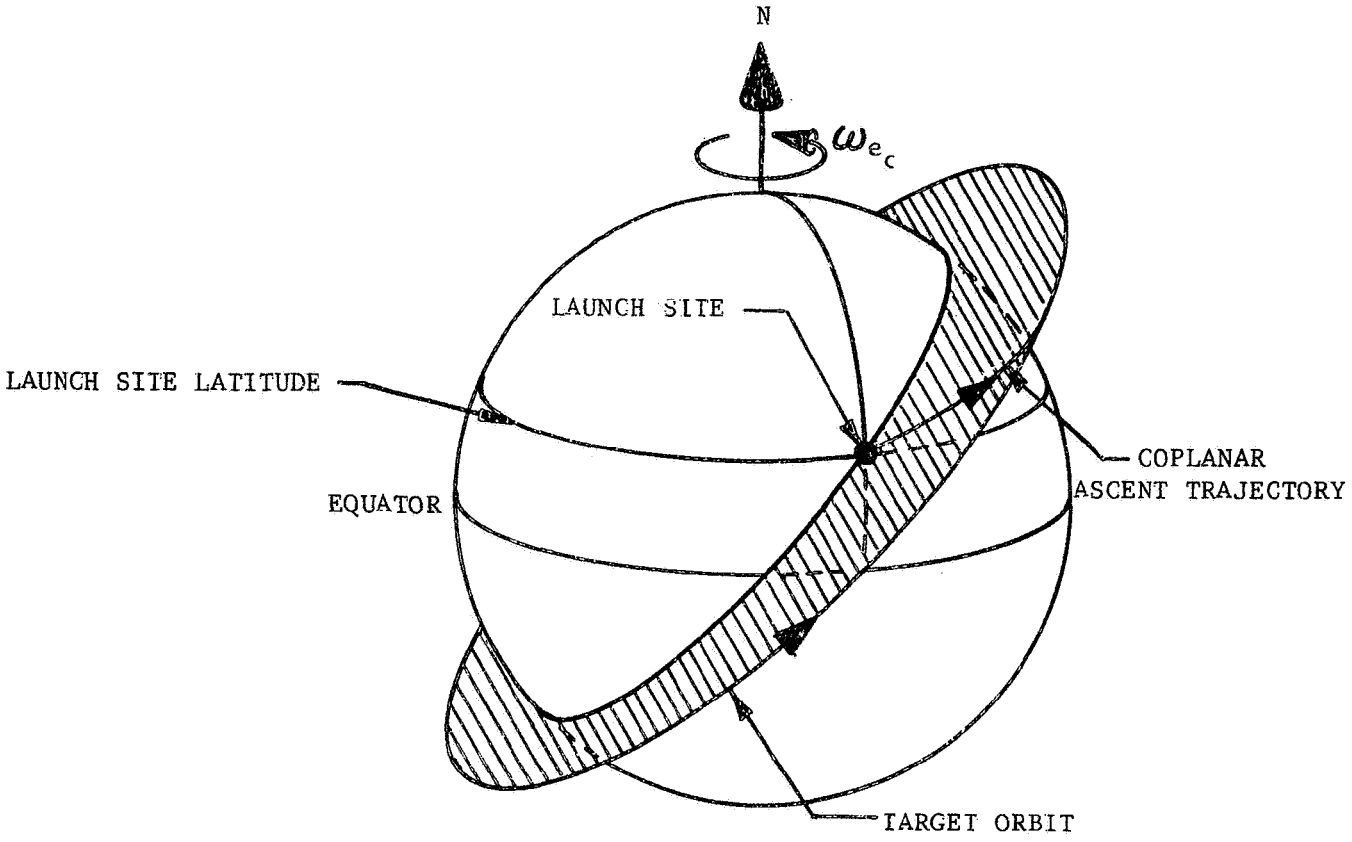

a. NORTHERLY COPLANAR LAUNCH

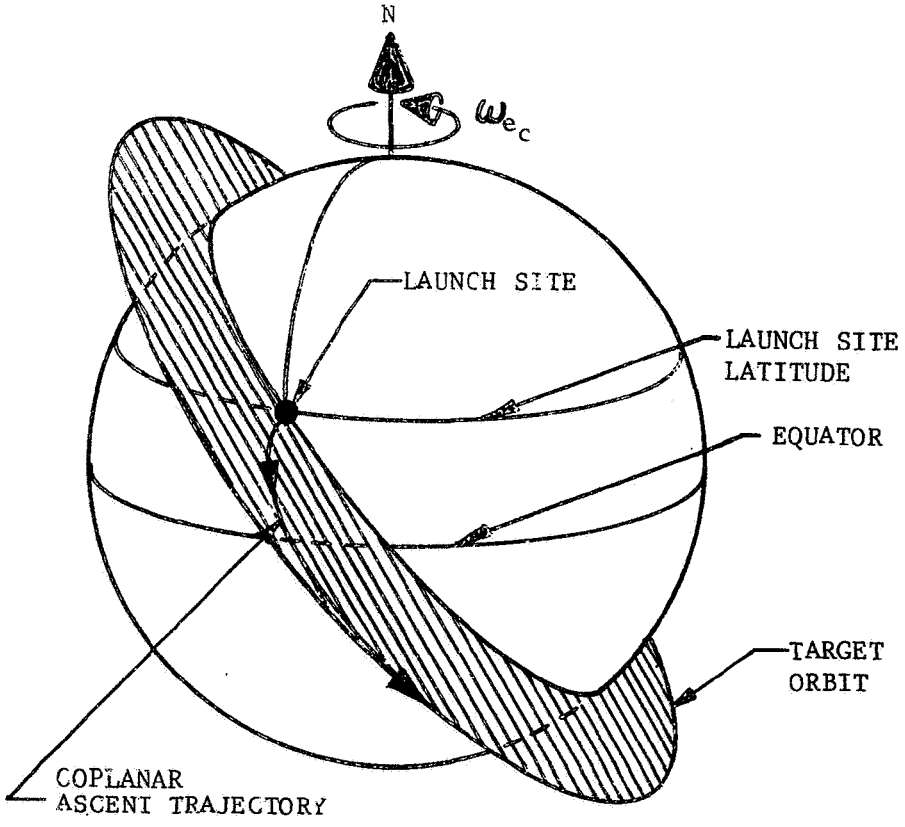

b. SOUTHERLY COPLANAR LAUNCH

Figure 9. THE TWO CASES OF THE COPLANER ASCENT TRAJECTORY MODE ($i_T > \lambda$)

the ascent trajectory lies in an assumed space-fixed plane that intersects the target orbit plane at some angle δ. This angle is known as the plane-change angle because a plane-change maneuver must be performed to inject the chaser into the target orbit. There exists four such non-coplanar ascent trajectory modes. These modes are defined and illustrated in Figures 10 through 13.

Two other ascent trajectory modes apply to target orbits with an inclination less than or equal to the launch site latitude. Since the launch site passes through the target orbit plane only once per day, when $i_T = \lambda$, there exists one optimum launch time that does not require a plane-change maneuver (due east launch). All other launch times require a plane-change maneuver at the chaser's interception of the target orbit. Plane-change maneuvers are also required for all ascent trajectories when $i_T < \lambda$.

The two ascent trajectory modes that occur when $i_T \leq \lambda$ are applicable to either launch before or after the co-nodal instant. These two modes, are defined and illustrated in Figures 14 and 15.

The trigonometric relations pertaining to Ascent Trajectory Modes 1 through 6 are chronologically presented in Appendix B. These equations relate the plane-change angle (δ) and the chaser vehicle's launch azimuth (A_z), for a variable total intercept range angle (θ_I), to any given launch delay time, $(t_d)_n$.

3.1.2 Ascent Trajectory Mode Sequencing

A method will be devised for determining which ascent trajectory mode is applicable for direct ascent to circular orbit rendezvous as a function of the launch delay time. This method will be referred to as Ascent Trajectory Mode Sequencing.

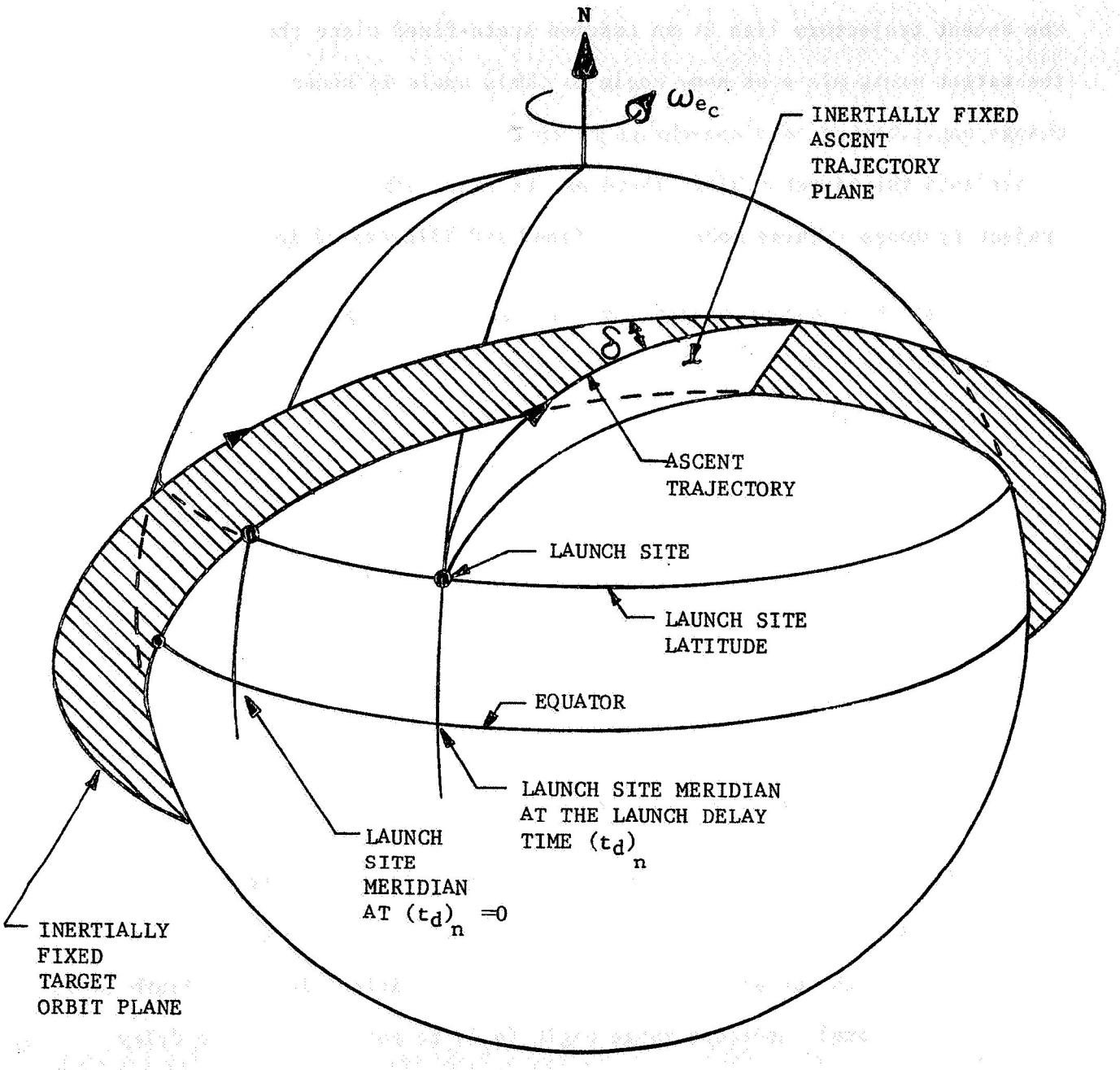

ASCENT TRAJECTORY MODE 1 - THE CHASER VEHICLE IS LAUNCHED WITH A NORTHEASTERLY AZIMUTH, AT SOME LAUNCH DELAY TIME $(t_d)_n$, AFTER THE LAUNCH SITE HAS PASSED THROUGH THE TARGET ORBIT PLANE.

Figure 10. ASCENT TRAJECTORY MODE 1

ASCENT TRAJECTORY MODE 2 - THE CHASER VEHICLE IS LAUNCHED WITH A SOUTHEASTERLY AZIMUTH, AT SOME LAUNCH DELAY TIME $(t_d)_n$, PRIOR TO THE LAUNCH SITE'S SECOND PASSAGE THROUGH THE TARGET ORBIT PLANE.

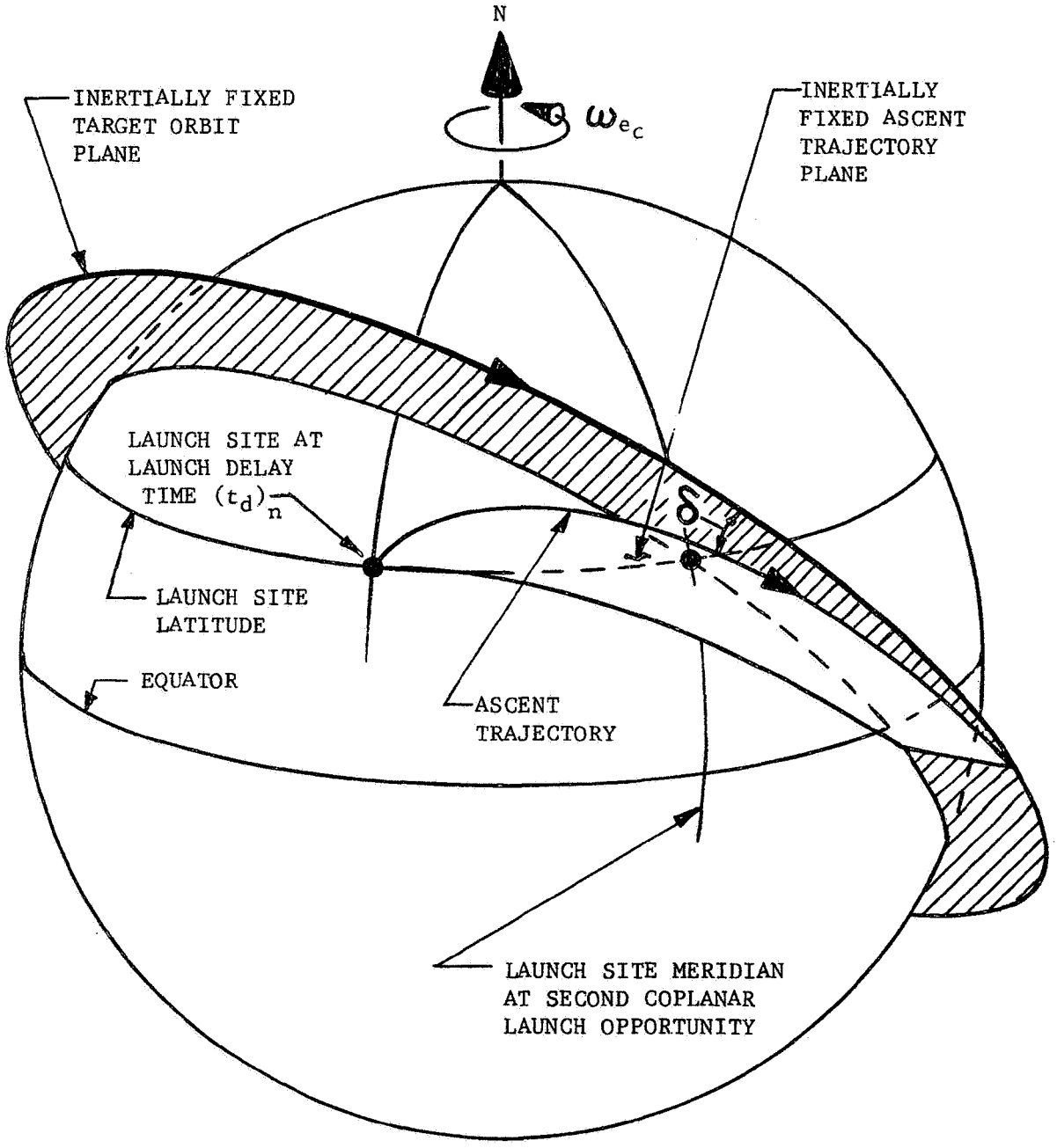

Figure 11. ASCENT TRAJECTORY MODE 2

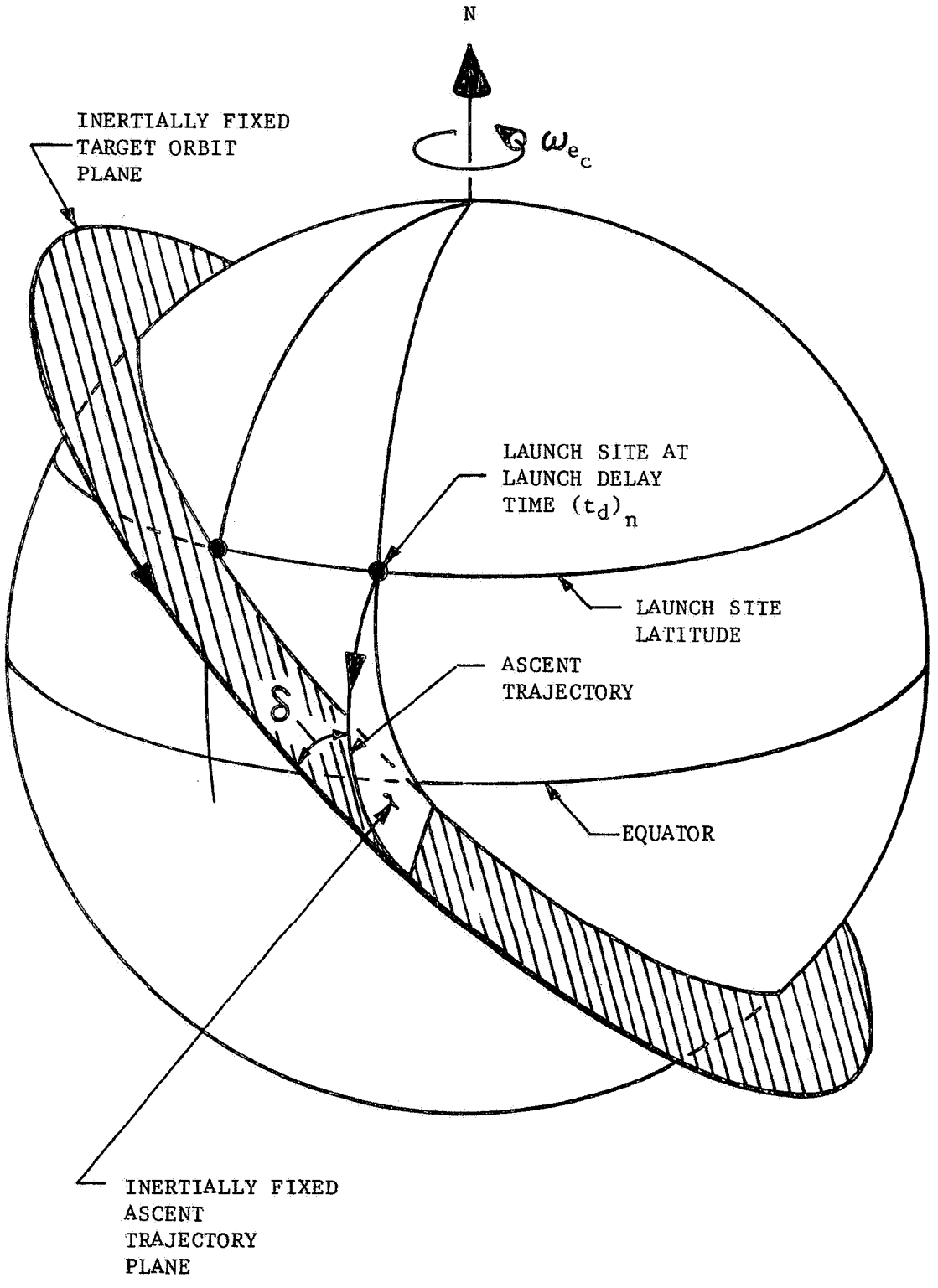

ASCENT TRAJECTORY MODE 3 - THE CHASER VEHICLE IS LAUNCHED WITH A SOUTHEASTERLY AZIMUTH, AT SOME LAUNCH DELAY TIME $(t_d)_n$, AFTER THE LAUNCH SITE'S SECOND PASSAGE THROUGH THE TARGET ORBIT PLANE.

Figure 12. ASCENT TRAJECTORY MODE 3

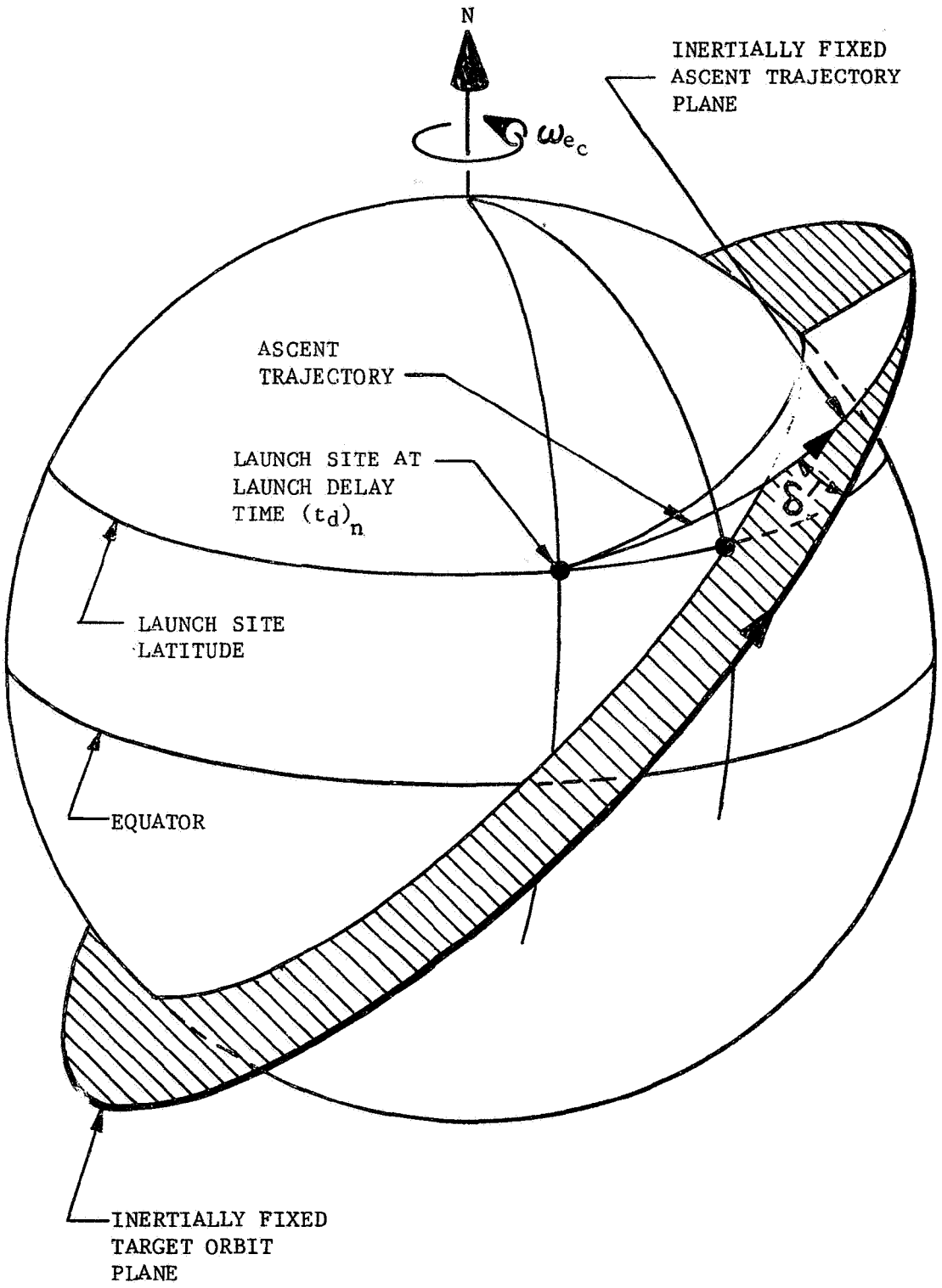

ASCENT TRAJECTORY MODE 4 - THE CHASER VEHICLE IS LAUNCHED WITH A NORTHEASTERLY AZIMUTH, AT SOME LAUNCH DELAY TIME $(t_d)_n$, PRIOR TO THE LAUNCH SITE'S PASSAGE THROUGH THE TARGET ORBIT PLANE NEAR THE END OF A CORRECTED DAY.

Figure 13. ASCENT TRAJECTORY MODE 4

ASCENT TRAJECTORY MODE 5 - THE CHASER VEHICLE IS LAUNCHED WITH A SOUTHEASTERLY AZIMUTH, AT SOME LAUNCH DELAY TIME $(t_d)_n$, AFTER THE CO-NODAL INSTANT.

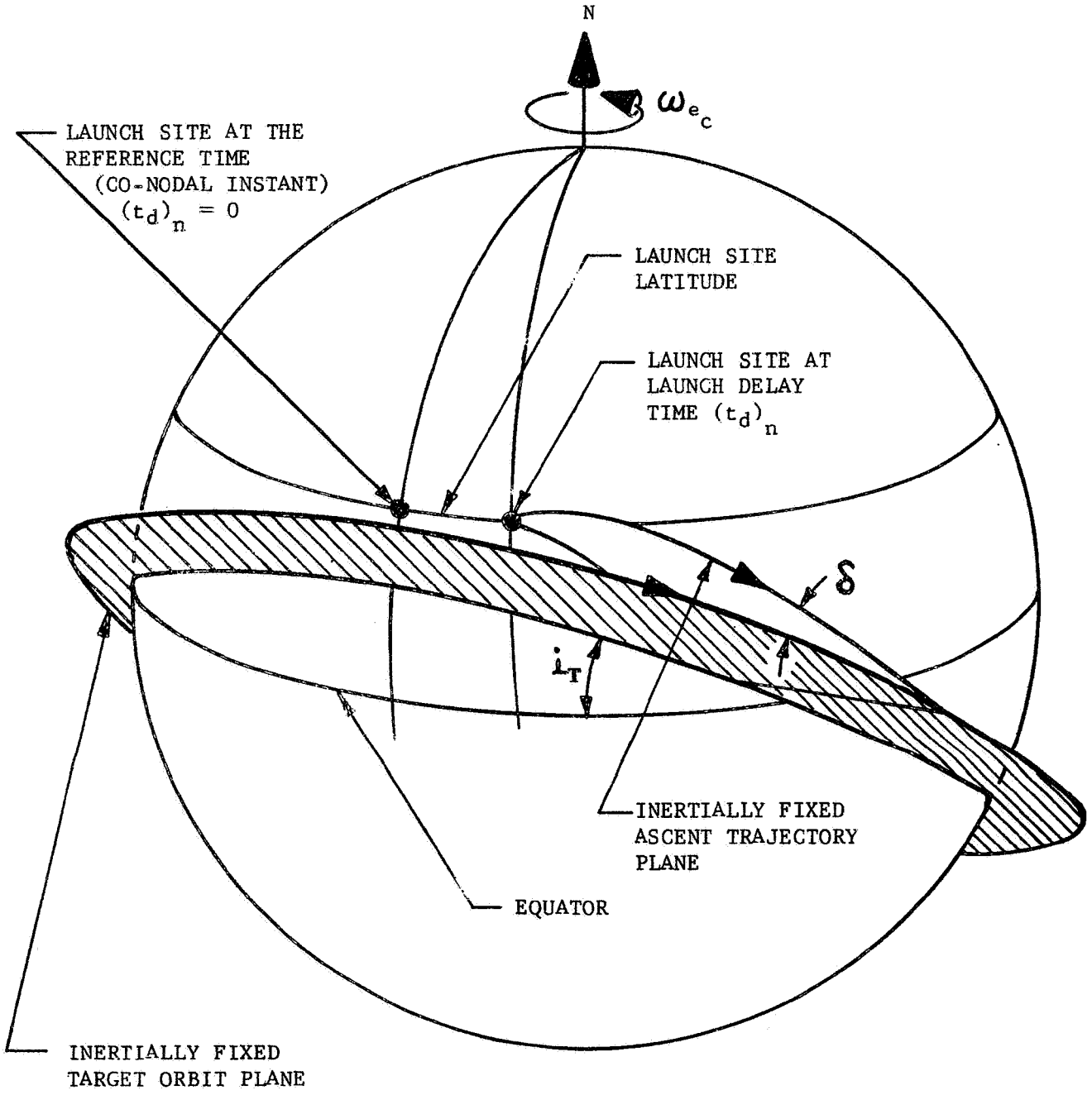

Figure 14. ASCENT TRAJECTORY MODE 5

ASCENT TRAJECTORY MODE 6 - THE CHASER VEHICLE IS LAUNCHED WITH A NORTHEASTERLY AZIMUTH, AT SOME LAUNCH DELAY TIME $(t_d)_n$, BEFORE THE CO-NODAL INSTANT.

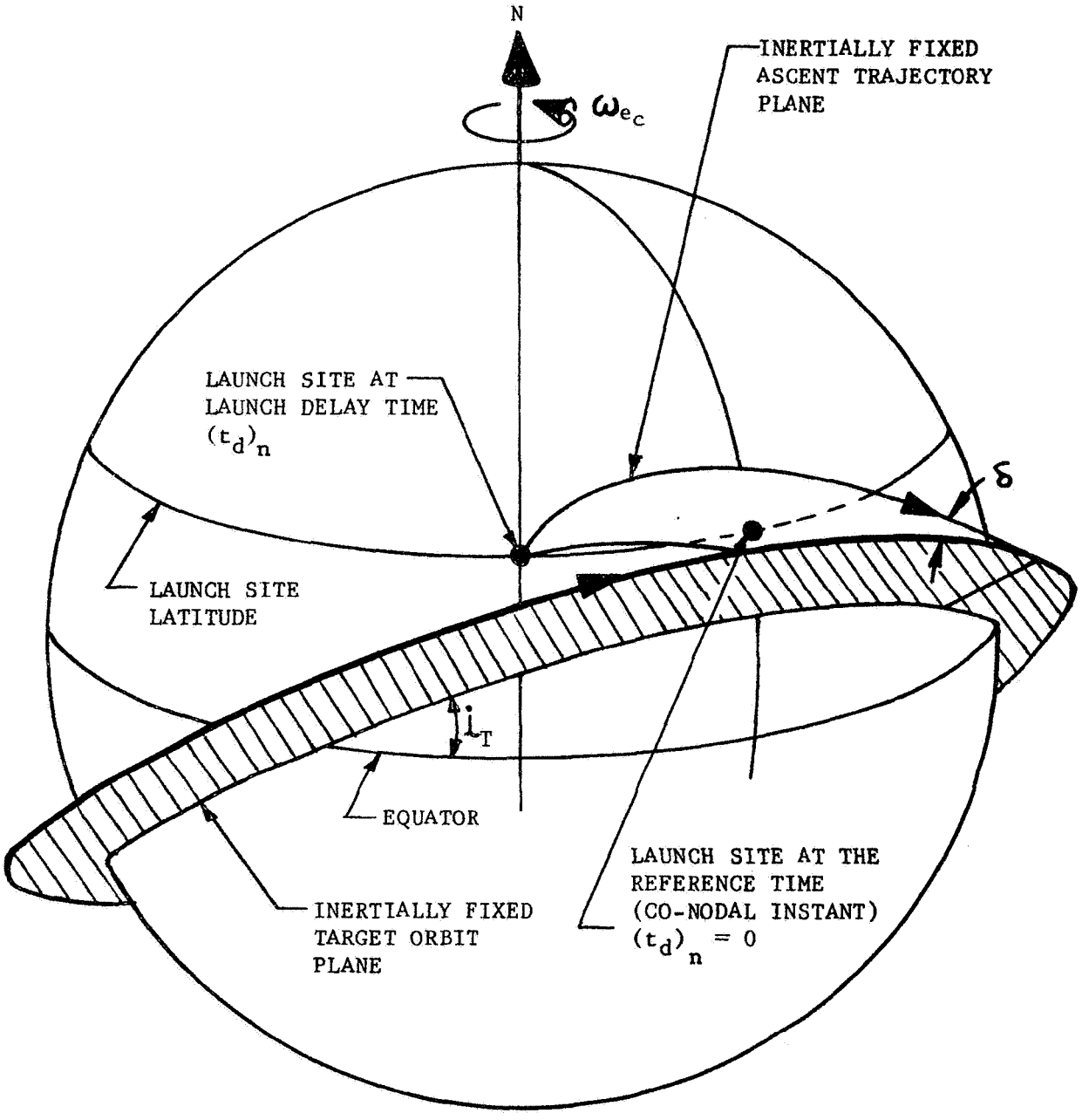

Figure 15. ASCENT TRAJECTORY MODE 6

First, consider the case of a target orbit with an orbital inclination greater than the launch site latitude. Figure 16 represents a sphere of target orbit radius, R_2, as viewed from the North Pole. All points of interest on the Earth's surface have been projected radially outward onto the surface of the sphere. Thus, the Earth's equator appears as the edge of the circle, while the launch site latitude appears as a smaller concentric circle. Furthermore, because the target orbit is inclined to the Earth's equator, the orbit appears as an ellipse.

Point A represents the position of the launch site at the reference time $(t_d)_n = 0$, while Point B represents the position of the launch site when the target orbit plane passes through it in a southerly direction. Points C and D represent the ascending and descending nodes of the target orbit, respectively.

The central angle measured, in the equatorial plane, from the meridian passing through Point A to the meridian passing through Point B is

$$\psi_o = \pi - 2(\text{LHA}) \tag{3-1}$$

and the co-angle ξ is

$$\xi = 2\pi - \psi_o \tag{3-2}$$

Assuming that the target orbit plane is inertially fixed at the reference time $(t_d)_n = 0$, the time required for the launch site to rotate through the central angle, ψ_o, can be written as:

$$(t)_{\psi_o} = \frac{\psi_o}{\omega_{e_c}} \tag{3-3}$$

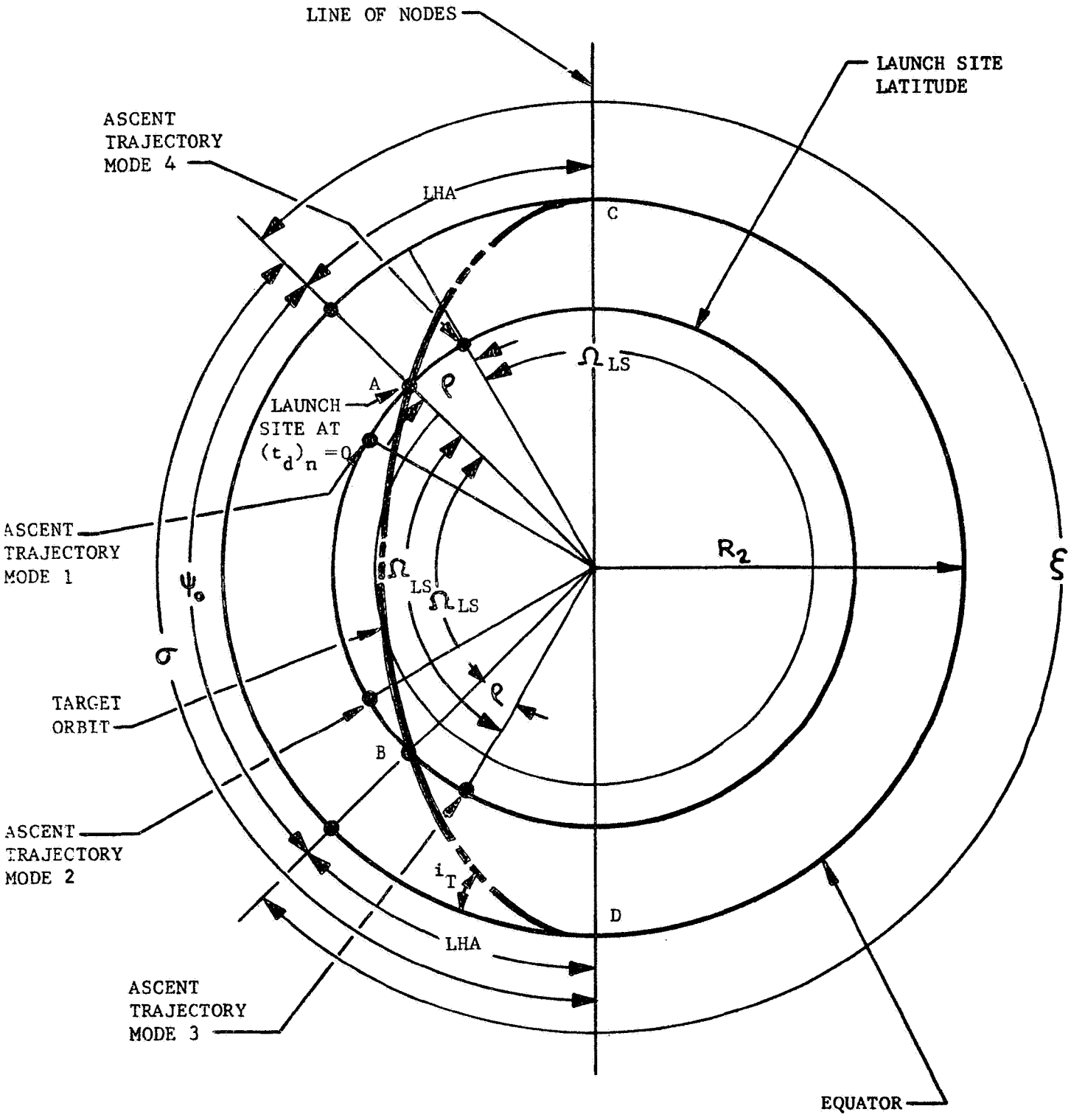

Figure 16. ASCENT TRAJECTORY MODE SEQUENCING WHEN $i_T > \lambda$

Also the time required for the launch site to rotate through the central co-angle, ξ, is

$$(t)_{\xi} = \frac{\xi}{\omega_{e_c}} \tag{3-4}$$

Thus, the time required for the launch site to complete one revolution about the Earth's polar axis (one corrected mean solar day) can be expressed as:

$$\frac{\psi_o}{\omega_{e_c}} + \frac{\xi}{\omega_{e_c}} = \frac{2\pi}{\omega_{e_c}} ,$$

or

$$(t)_{\psi_o} + (t)_{\xi} = T \tag{3-5}$$

If $(t_d)_n = 0$, and likewise $\Omega_{LS} = 0$, the launch site is located at the reference position. In this case, the coplanar ascent trajectory mode must be used in launching the chaser vehicle. However, as $(t_d)_n$ increases, the angle Ω_{LS} increases correspondingly. Consequently, Ascent Trajectory Modes 1 through 4 are applicable under the following conditions:

Ascent Trajectory Mode 1,	when	$0 < \Omega_{LS} \leq \frac{\psi_o}{2}$
Ascent Trajectory Mode 2,	when	$\frac{\psi_o}{2} < \Omega_{LS} < \psi_o$
Coplanar Ascent Trajectory Mode,	when	$\Omega_{LS} = \psi_o$
Ascent Trajectory Mode 3,	when	$\psi_o < \Omega_{LS} \leq (\psi_o + \frac{\xi}{2})$
Ascent Trajectory Mode 4,	when	$(\psi_o + \frac{\xi}{2}) < \Omega_{LS} < 2\pi$
Coplanar Ascent Trajectory Mode,	when	$\Omega_{LS} = 2\pi = 0.$

It should be kept in mind that the above sequence is valid for one corrected revolution of the launch site around the Earth's polar axis, or one corrected mean solar day. If the launch window investigation is to be conducted for several days, the ascent trajectory mode sequence is repeated when the angle Ω_{LS} becomes a multiple of 2π.

In a like manner, an ascent trajectory mode sequence can be defined for a target orbit having an inclination less than or equal to the launch-site latitude. In this case the reference time is, by definition, the time at which the launch-site meridian is midway between the ascending and descending nodes. Consequently, the plane containing the launch site and the Earth's spin axis is perpendicular to the line of nodes at the reference time $(t_d)_n = 0$. Thus, Ascent Trajectory Modes 5 and 6 are applicable under the following conditions:

Ascent Trajectory Mode 5, when $0 < \Omega_{LS} < \pi$

Ascent Trajectory Mode 6, when $\pi < \Omega_{LS} < 2\pi$.

Again, it is pointed out that for launch window computations spanning several days, the sequence must be repeated, for each day, when the angle Ω_{LS} becomes a multiple of 2π.

The above ascent trajectory modes and the mode sequencing procedures will also be used for placing the chaser vehicle in an intermediate circular parking orbit.

3.1.3 Ascent Trajectories

Regardless of whether the chaser vehicle is launched via a coplanar or a non-coplanar ascent trajectory mode, the ascent trajectory itself is assumed to lie in a inertially-fixed plane and to be composed of various stages of flight. These stages, for both the coplanar and non-coplanar trajectories, are listed in Tables 1 and 2, illustrated in Figures 17, 18, and 19, and discussed in subsections 3.1.3.1 through 3.1.3.4.

3.1.3.1 Trajectories from Lift-off to Second-Stage Burnout

The ascent trajectory to a parking orbit or target orbit is assumed to lie in an inertially fixed plane. Thus, it is proposed that, for a given mission (launch vehicle and parking or target orbit), the iterative guidance mode (IGM) be used to generate a table of the following space-fixed parameters, at second-stage burnout, as a function of launch azimuth:

1) Velocity, V_{2BO}

2) Flight path angle, γ_{2BO}

3) Radius, R_{2BO}

4) Range angle, θ_{12B}

5) Flight time, t_{12B}

6) Mass of the chaser vehicle, m_{2BO}.

Table 1. COPLANAR ASCENT TRAJECTORY

1. Continuous powered flight from lift-off to second-stage burnout, assuming a three-stage launch vehicle.

2. Coast along a segment of an ellipse, known as a variable coast ellipse, until the target orbit is achieved.

3. Impulsive velocity increment applied to change the flight path angle, γ_{EC}, to zero.

4. Burning of the third stage to circularize the orbit and effect gross rendezvous.

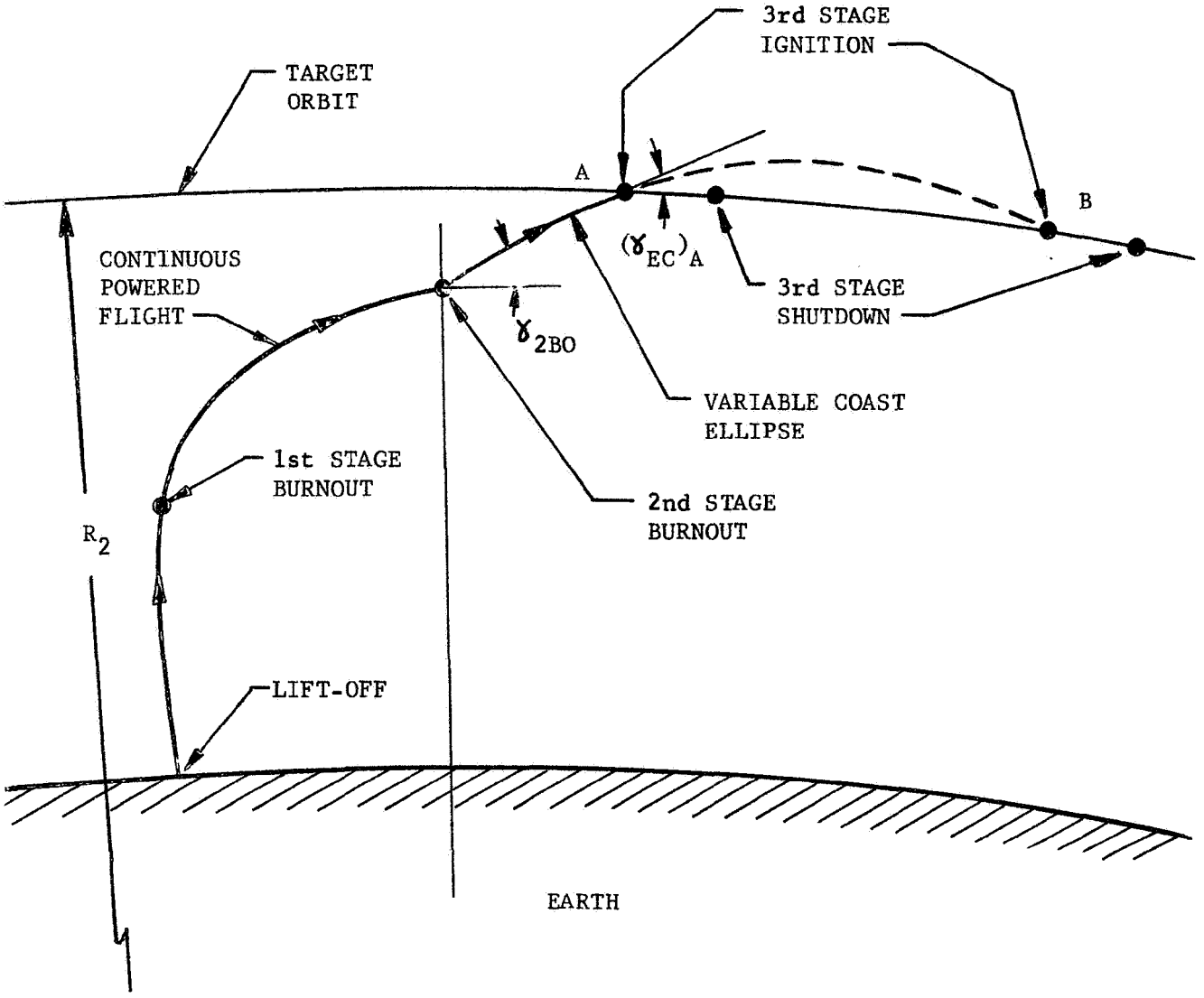

Figure 17. COPLANAR ASCENT TRAJECTORY

Table 2. NON-COPLANAR ASCENT TRAJECTORY

1. Continuous powered flight from lift-off to second-stage burnout, assuming a three-stage launch vehicle.

2. Coast along a segment of an ellipse, known as a variable coast ellipse, until the target orbit radius is achieved.

3. Impulsive velocity increment applied to change the flight path angle, γ_{EC}, to zero.

4. Execution of an impulsive yaw maneuver, if needed, to alleviate lead or lag of the target vehicle.

5. Burning of the third stage to circularize the orbit.

6. Circular coasting from third-stage shutdown to interception of the target orbit.

7. Impulsive velocity increment at interception of the target orbit to perform a plane-change maneuver and effect gross rendezvous.

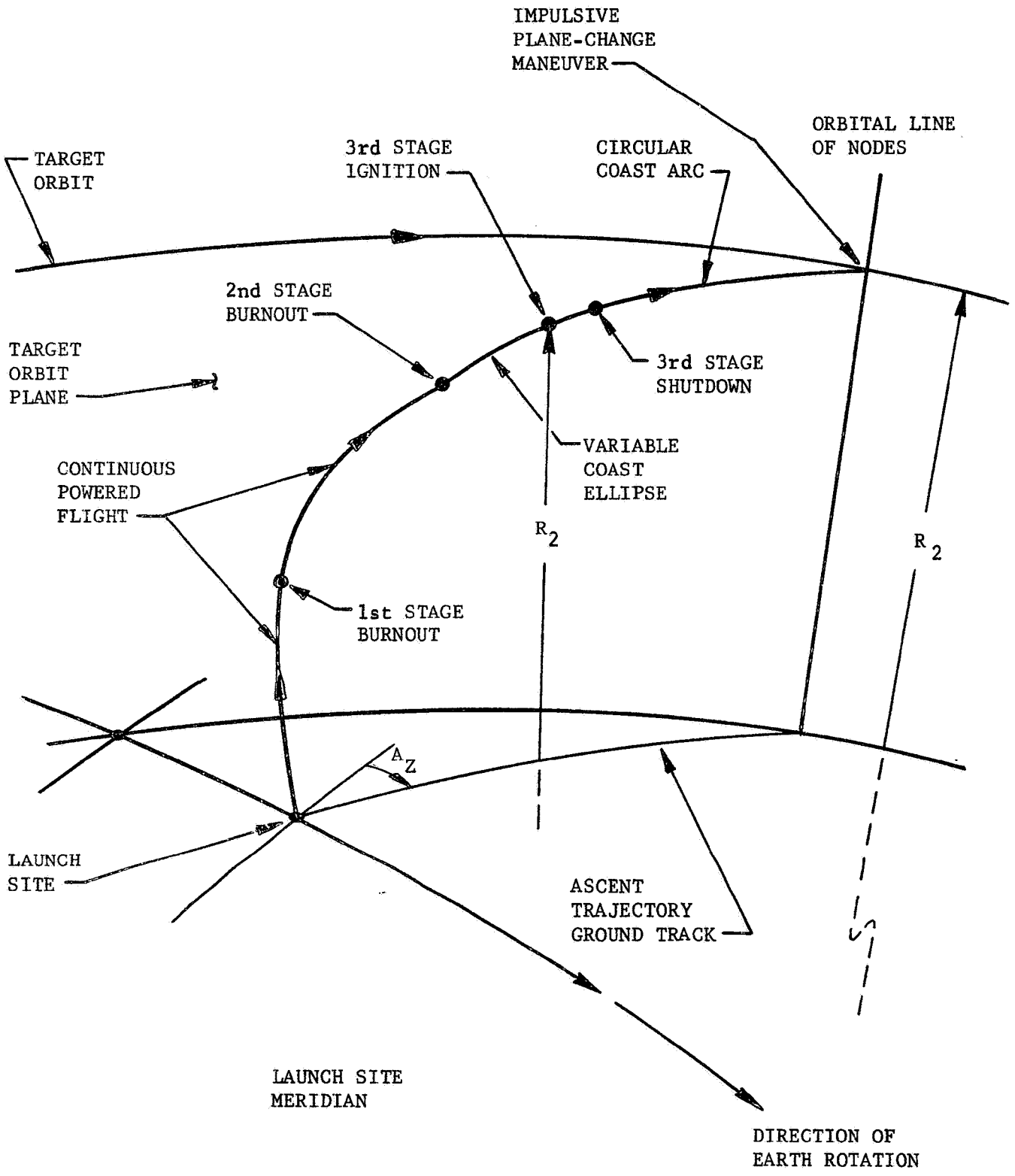

Figure 18. NON-COPLANAR ASCENT TRAJECTORY

This table will be designated the Ascent Trajectory Table and will be generated, for a given launch vehicle and mission, by assuming the chaser follows a fixed tilt program from lift-off to first-stage burnout, and a fixed Chi Table from first-stage burnout to second-stage burnout. First- and second-stage burn times will be fixed. The Ascent Trajectory Table will be placed on tape and used as an input to the subroutine. It is felt that such a table will considerably reduce computer run time.

Development of the Ascent Trajectory Table will be performed under a future extension of the present work assignment.

3.1.3.2 Variable Coast Ellipse

As Tables 1 and 2 indicate, both the coplanar and non-coplanar ascent trajectories make use of a variable coast ellipse from second-stage burnout to third-stage ignition. This coast ellipse is used to increase the total intercept range angle, θ_I, and at the same time achieve the target orbit radius. It is felt that such a variable coast ellipse will lengthen the direct ascent launch windows.

Figures 17, 18, and 19 illustrate typical ascent trajectories for a three-stage chaser launch vehicle. The ascent trajectory is assumed to lie in an inertially fixed plane passing through the center of the Earth, the launch site, and the position of the chaser at second-stage burnout. This trajectory may possess any launch azimuth within range safety constraints.

The second-stage burnout parameters, for a given launch azimuth (V_{2BO}, γ_{2BO}, and R_{2BO}), determine the characteristics of the conic the chaser

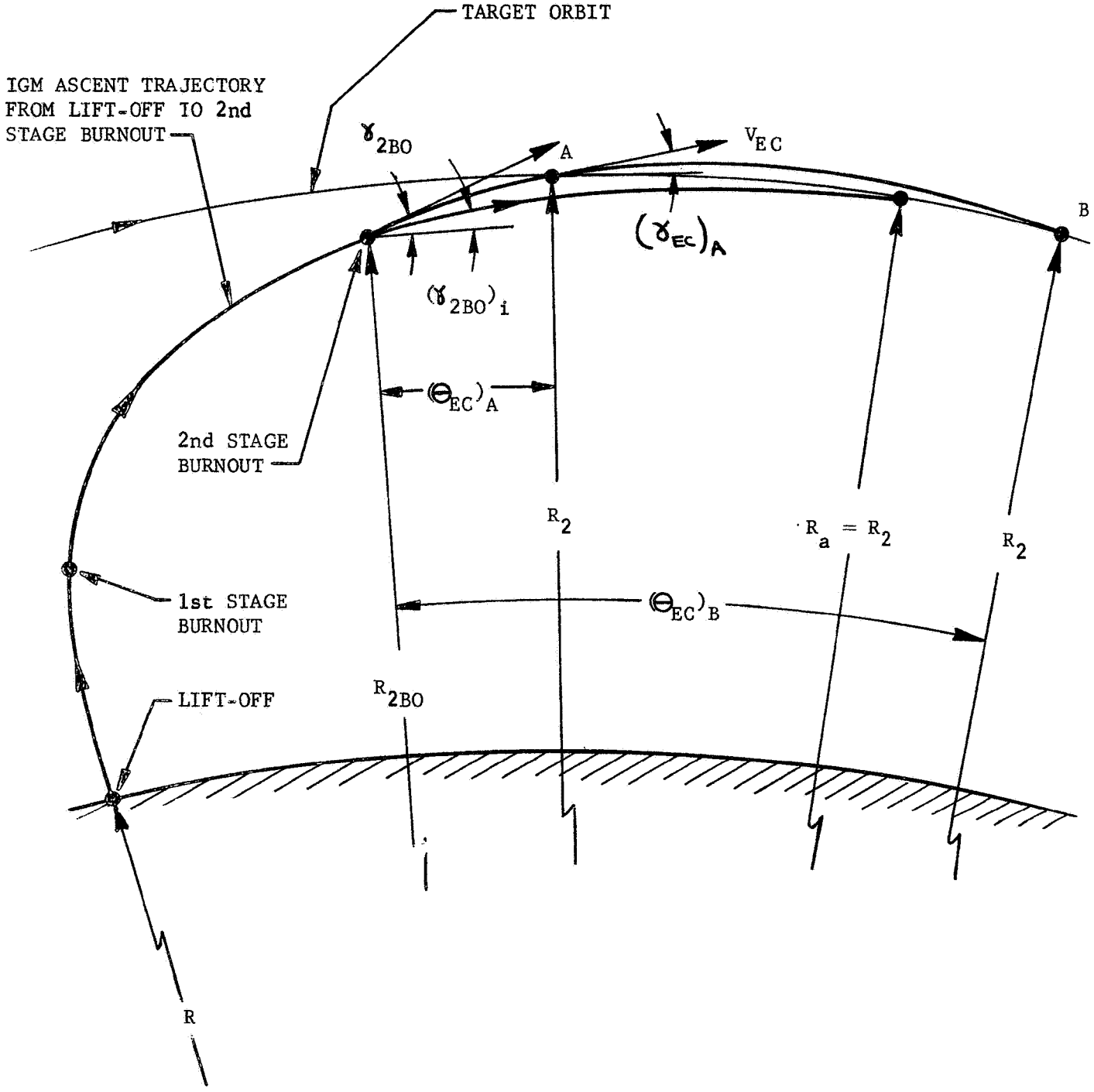

Figure 19. ASCENT TRAJECTORY PROFILE

would follow if it is allowed to coast after second-stage burnout. Because V_{2BO} is sub-circular, the chaser would follow an ellipse producing atmospheric reentry. However, the coast ellipse, following second-stage burnout, can be altered by increasing γ_{2BO} as V_{2BO} is held constant. This has the effect of producing a family of equal energy ellipses such that the apogee increases as γ_{2BO} is increased. Thus, it can be seen that such a coast ellipse would allow the chaser to coast to the desired target orbit radius before the chaser is inserted into circular orbit.

The unaltered burnout parameters must be checked to determine if they produce a coast ellipse with an apogee equal to the target orbit radius. The dimensionless parameter Q is introduced and is defined as

$$Q = \frac{V_{2BO}^2}{(V_{co})^2} = \frac{R_{2BO}(V^2_{2BO})}{\mu} \tag{3-6}$$

The eccentricity of the coast ellipse can be written as

$$e = \sqrt{1 - Q(2-Q)\cos^2 \gamma_{2BO}} \tag{3-7}$$

and the apogee

$$R_a = \frac{R_{2BO}}{(2-Q)}(1+e) \tag{3-8}$$

If $R_a \neq R_2$, the flight path angle, γ_{2BO}, must be changed by an impulsive velocity increment to produce a new equal energy coast ellipse with an apogee equal to R_2. This is illustrated in Figure 19.

Setting R_2 equal to Equation (3-8), the eccentricity of the new ellipse becomes

$$e = (2-Q)\left(\frac{R_2}{R_{2BO}}\right) - 1 \tag{3-9}$$

The flight path angle that produced this ellipse is designated as $(\gamma_{2BO})_i$, where

$$(\gamma_{2BO})_i = \cos^{-1}\left\{\left[\frac{1-e^2}{Q(2-Q)}\right]^{\frac{1}{2}}\right\} \tag{3-10}$$

The impulsive velocity increment required to rotate the velocity vector from γ_{2BO} to $(\gamma_{2BO})_i$ is

$$(\Delta V)_{\gamma 2BO} = 2V_{2BO} \sin \tfrac{1}{2}\left[(\gamma_{2BO})_i - \gamma_{2BO}\right] \tag{3-11}$$

Because R_a does equal R_2, the chaser could be inserted into circular orbit at apogee by burning the third stage. However, such an assumption would be very restrictive because it has the effect of fixing the ascent trajectory. It may also be that the new coast ellipse is not satisfactory to accomplish gross rendezvous. In this case, the ascent trajectory profile can be kept more flexible by holding V_{2BO} constant and increasing $(\gamma_{2BO})_i$ by the impulsive velocity increment

$$(\Delta V)_{\gamma 2BO} = 2B_{2BO} \sin \tfrac{1}{2}\left[(\gamma_{2BO})_i + (\Delta\gamma)_{2BO}\right] \tag{3-12}$$

This would produce an equal energy coast ellipse that would intersect the target orbit in two points (A and B in Figure 19) for a coplanar ascent trajectory. However, in the case of a non-coplanar ascent trajectory, the coast ellipse would intersect a circle of target orbit radius.

The radius of Point A or B is R_2. Thus, the true anomaly of Point A on the coast ellipse can be found by the expression

$$\phi_A = \sin^{-1}\left\{\frac{a(1-e^2)\tan\left[(\gamma_{2B})_i + (\Delta\gamma)_{2BO}\right]}{eR_2}\right\} \tag{3-13}$$

where

$$e = \sqrt{1-Q(2-Q)\cos^2\left[(\gamma_{2BO})_i + \Delta\gamma_{2BO}\right]} \tag{3-14}$$

$$a = \frac{R_{2BO}}{2-Q} \tag{3-15}$$

The true anomaly of the second-stage burnout point is

$$\phi_{2BO} = \sin^{-1}\left\{\frac{a(1-e^2)\tan\left[(\gamma_{2BO})_i + \Delta\gamma_{2BO}\right]}{eR_{2BO}}\right\} \tag{3-16}$$

Hence, the central angle between the burnout point and Point A is

$$(\theta_{EC})_A = \phi_A - \phi_{2BO} \tag{3-17}$$

The flight time required for the chaser to coast along the ellipse from burnout to Point A is determined from the following equations:

$$\sin E_{2BO} = \frac{(1-e^2)^{\frac{1}{2}}\sin\phi_{2BO}}{1+e\cos\phi_{2BO}}$$

$$M_{2BO} = E_{2BO} - e\sin E_{2BO}$$

$$\sin E_A = \frac{(1-e^2)^{\frac{1}{2}}\sin\phi_A}{1+e\cos\phi_A} \tag{3-18}$$

$$M_A = E_A - e\sin E_A$$

$$(t_{EC})_A = (M_A - M_{2BO})\sqrt{\frac{a^3}{\mu}}$$

If the chaser is allowed to coast to Point B, the required equations are:

$$\phi_B = 2\pi - \phi_A \tag{3-19}$$

$$(\theta_{EC})_B = \phi_B - \phi_{2BO} \tag{3-20}$$

$$E_B = \sin^{-1} \frac{(1-e^2)^{\frac{1}{2}} \sin \phi_B}{1+e \cos \phi_B}$$

$$M_B = E_B - e \sin E_B \tag{3-21}$$

$$(t_{EC})_B = (M_B - M_{2BO}) \sqrt{\frac{a^3}{\mu}}$$

3.1.3.3 Third-Stage Burn Model

An analytical approximation will be used to simulate the burning of the third stage of the launch vehicle to inject the chaser into circular orbit. This method is shown in reference 12 to yield highly accurate results for a third-stage burn problem similar to the one presented herein.

With reference to Figure 20, the approximation can be stated as follows:

The chaser vehicle follows an elliptical flight path until it arrives at Point A or B on the coast ellipse. Points A and B have a radius of R_2. The velocity and flight path angle of the chaser at either of these points are:

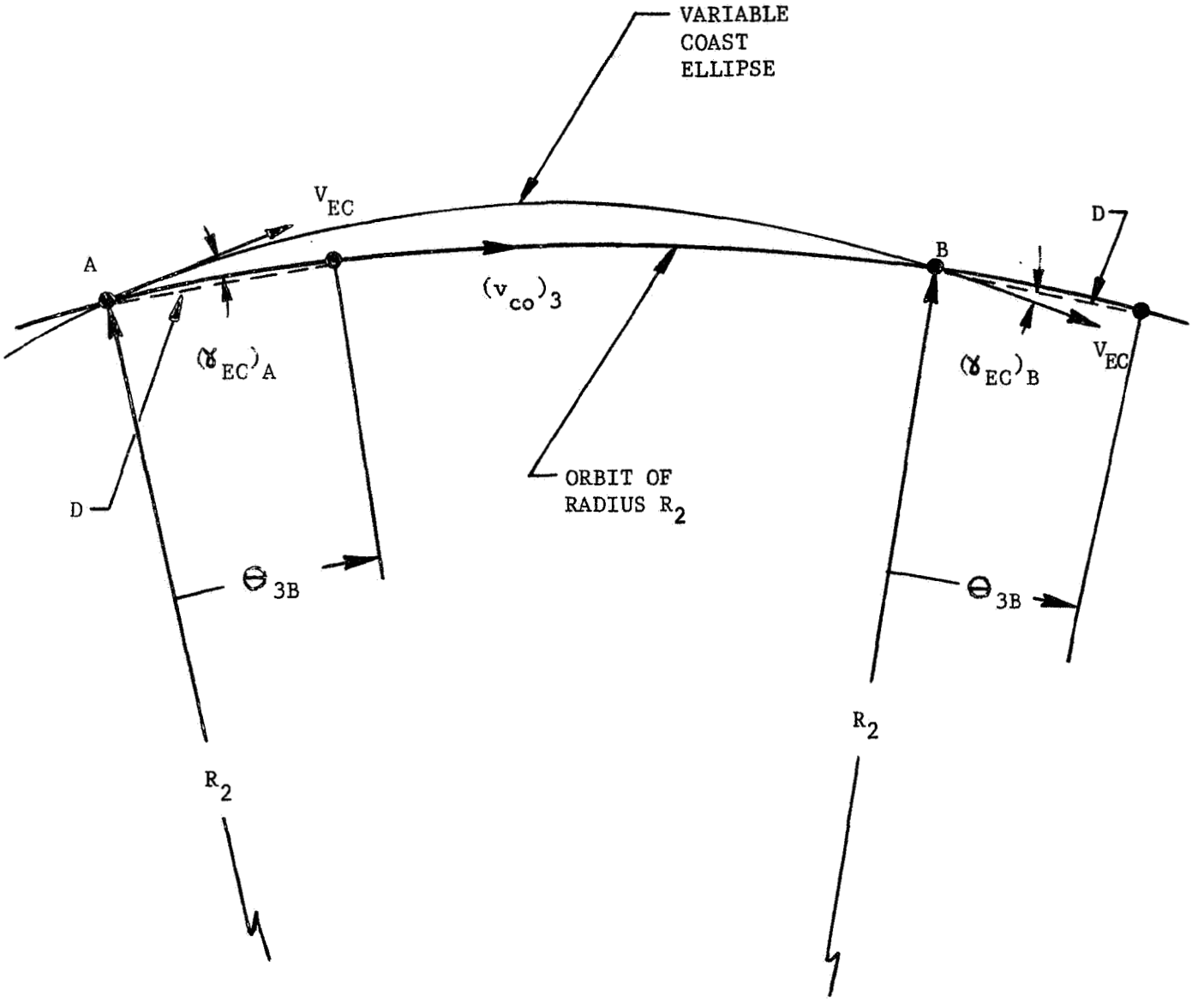

Figure 20. THIRD-STAGE BURN GEOMETRY

$$(V_{EC})_{\substack{A\\B}} = \sqrt{\frac{2\mu}{R_2} - \frac{\mu}{a}} \tag{3-22}$$

and

$$(\gamma_{EC})_A = \tan^{-1}\left[\frac{e \sin \phi_A}{1+e \cos \phi_A}\right]$$

$$\text{or} \quad (\gamma_{EC})_B = \tan^{-1}\left[\frac{e \sin \phi_B}{1+e \cos \phi_B}\right] \tag{3-23}$$

At the instant of arrival of the chaser at Point A or B, the velocity vector is rotated through the angle γ_{EC} by the impulsive velocity increment

$$(\Delta V)_{\gamma_{EC}} = 2(V_{EC})_{\substack{A\\B}} \sin \tfrac{1}{2}(\gamma_{EC})_{\substack{A\\B}} \tag{3-24}$$

This causes the subcircular velocity vector to become oriented normal to the radius vector. At the instant at which the velocity vector becomes perpendicular to the radius vector the third-stage engine is ignited. The engine is allowed to burn for a period of time, t_{3B}, until circular orbit velocity, $(v_{co})_3$, is obtained at Point C.

The circular orbit velocity at the target orbit radius, R_2, is

$$(v_{co})_3 = \sqrt{\frac{\mu}{R_2}} \tag{3-25}$$

Thus, the velocity increment required to inject the chaser into circular orbit can be written as

$$(\Delta V)_{CIR} = (v_{co})_3 - (V_{EC})_{\substack{A\\B}} \tag{3-26}$$

It is assumed that the chaser follows a straight line flight path from Point A or B to Point C, with a constant acceleration, during the burn time, t_{3B}. Thus,

$$(\Delta V)_{CIR} = at_{3B} \tag{3-27}$$

where

$$a = \frac{F}{m_{2BO}}$$

F = thrust of the chaser third stage

m_{2BO} = mass of the chaser third stage at second-stage burnout.

Hence,

$$t_{3B} = \frac{(\Delta V)_{CIR}}{a} = \frac{(\Delta V)_{CIR}}{F/m_{2BO}} \tag{3-28}$$

The chord D connecting Points A and C, or B and C, can be expressed by the expression

$$D = (V_{EC})_{\substack{A \\ B}} t_{3B} + \tfrac{1}{2}\left(\frac{F}{m_{2BO}}\right) t_{3B}^2 \tag{3-29}$$

Consesequently, the central angle θ_{3B} subtended by the chord D can be found by the expression

$$\theta_{3B} = 2 \sin^{-1}\left[\frac{D}{2R_2}\right] \tag{3-30}$$

The angle θ_{3B} is the central range angle obtained during third-stage burn.

3.1.3.4 Non-Coplanar Ascent Trajectory Yaw Maneuver

In all non-coplanar ascent trajectory modes the ascent trajectory plane intersects the target orbit plane at some angle δ, known as the plane-change angle. The intersection of these two planes will be designated as the orbital plane of nodes.

An impulsive yaw maneuver is assumed to be performed by the chaser vehicle at third-stage ignition (Point A in Figures 19 and 20) to delete the target's lead or lag. This endows more flexibility to the non-coplanar ascent trajectory and thus opens up the launch window for a particular ascent mode.

Figures 21 and 22 illustrate a typical non-coplanar ascent trajectory with yaw maneuvers at third-stage ignition.

The total intercept range angle, θ_I, is defined to be a variable. The equations in Appendix A show that as θ_I is changed at various launch delay times, the launch azimuth and plane-change angles vary accordingly. Nevertheless, for a given launch azimuth, A_z, target orbit radius, R_2, and coast ellipse, the angle θ_I is

$$\theta_I = \theta_{12B} + (\theta_{EC})_{\substack{A \\ B}} + \theta_{3B} + \theta_{CC} \tag{3-31}$$

The central angle subtended by the coast arc of the chaser along a circular orbit of radius R_2 from third-stage shutdown to target orbit interception is

$$\theta_{CC} = \theta_I - [\theta_{12B} + (\theta_{EC})_{\substack{A \\ B}} + \theta_{3B}] \tag{3-32}$$

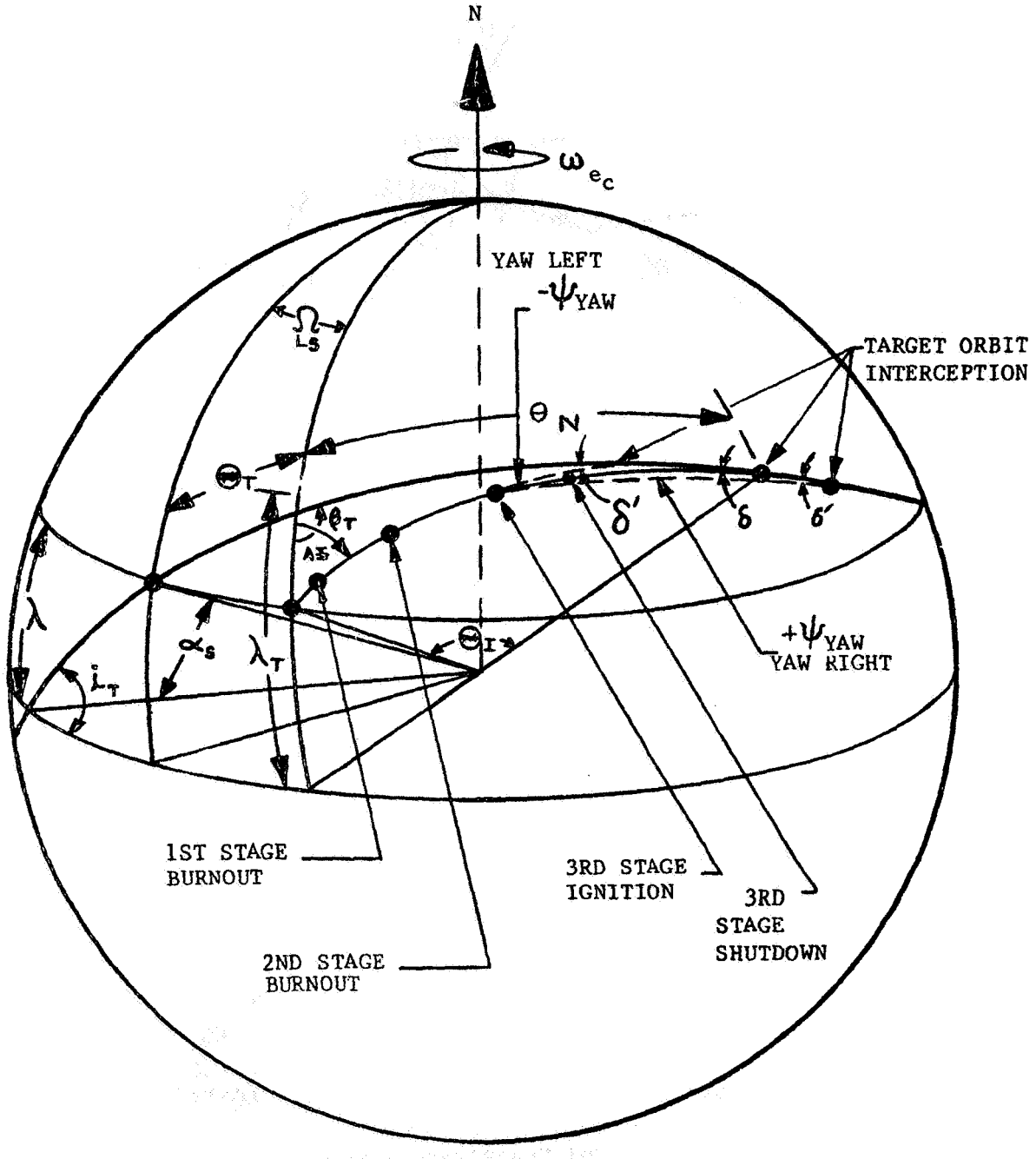

Figure 21a. NON-COPLANAR ASCENT TRAJECTORY WITH YAW MANEUVERS

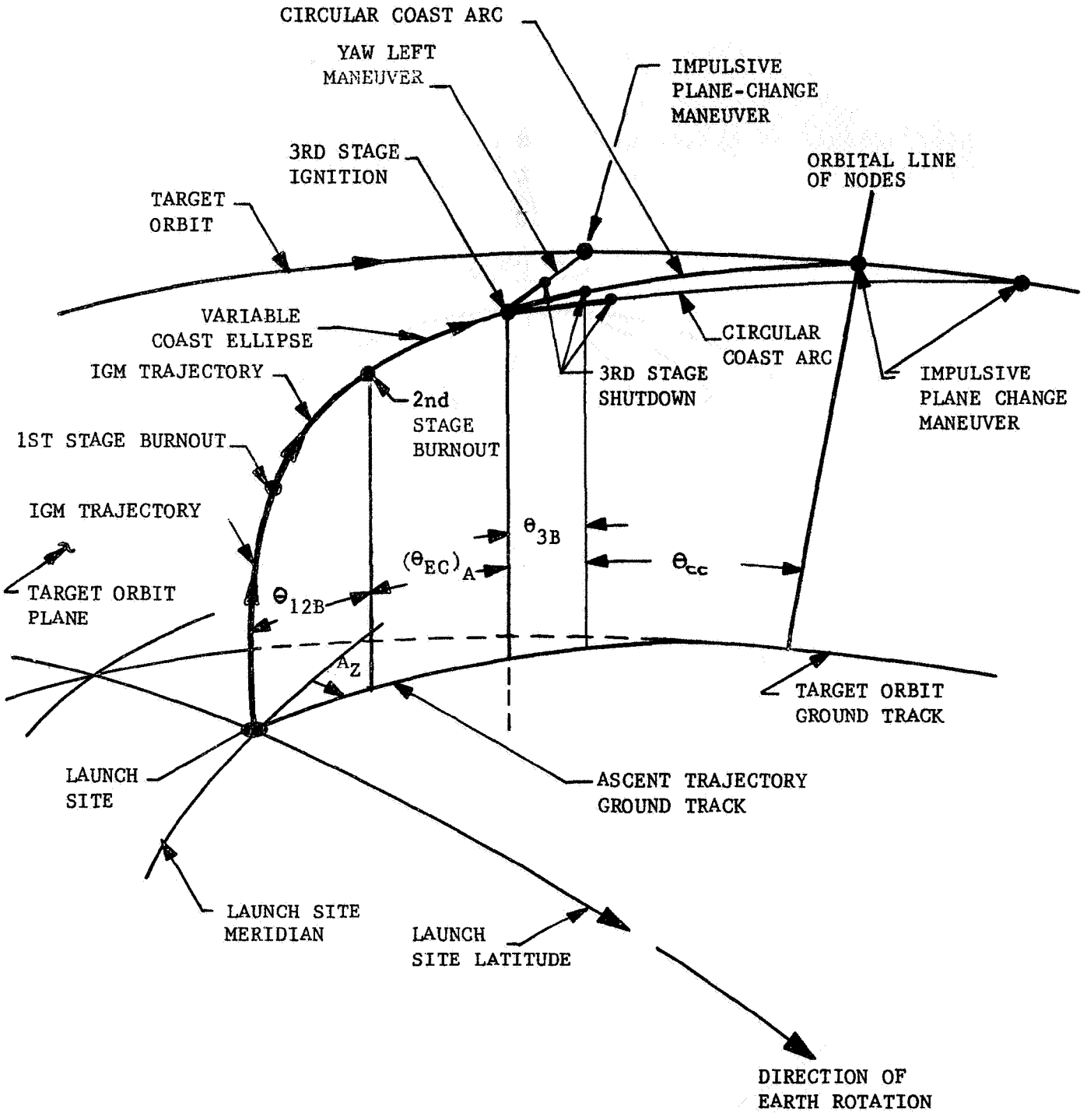

Figure 21b. NON-COPLANAR ASCENT TRAJECTORY WITH YAW MANEUVERS

The flight time corresponding to θ_{CC} can be expressed as

$$t_{CC} = \frac{\theta_{CC}}{\omega_2} \tag{3-33}$$

where

$\omega_2 = \sqrt{\frac{\mu}{R_2^3}}$ = angular velocity of a vehicle in a circular orbit of radius R_2.

Thus, the total chaser flight time from lift-off to target orbit interception is

$$(t_F)_a = t_{12B} + (t_{EC})_{\substack{A \\ B}} + t_{3B} + t_{CC} \tag{3-34}$$

It has been shown that the position of the target at any value of $(t_d)_n$, relative to the ascending node, can be written as

$$\alpha_T = \alpha_o + N(2\pi) \tag{2-15}$$

or

$$\alpha_T = Y(2\pi) \tag{2-18}$$

Thus, the position of the target, from the ascending node of the target orbit, at the time the chaser intercepts the target orbit, is

$$\theta_{TAN} = \alpha_T + (t_F)_a \quad \omega_2 \tag{3-35}$$

The position of the target from the descending node is

$$\theta_{TDN} = \theta_{TAN} - \pi \tag{3-36}$$

The following equations express, for each ascent trajectory mode, the position of the target relative to the orbital line of nodes at the time the chaser intercepts the target orbit:

Ascent Trajectory Mode 1

$$\theta_{TOLN} = \theta_{TAN} - (\theta_{NT} + \alpha_{LS}) \tag{3-37}$$

Ascent Trajectory Mode 2

$$\theta_{TOLN} = \theta_{TDN} - (\theta_{NT} - \chi) \tag{3-38}$$

Ascent Trajectory Mode 3

$$\theta_{TOLN} = \theta_{TDN} - (\theta_{NT} - \alpha_{LS}) \tag{3-39}$$

Ascent Trajectory Mode 4

$$\theta_{TOLN} = \theta_{TAN} - (\theta_{NT} + \chi) \tag{3-40}$$

Ascent Trajectory Mode 5

$$\theta_{TOLN} = \theta_{TDN} - (\theta_{NT} - \pi/2) \tag{3-41}$$

Ascent Trajectory Mode 6

$$\theta_{TOLN} = \theta_{TAN} - (\theta_{NT} + \chi) \tag{3-40}$$

where

$$\alpha_{LS} = \sin^{-1}\left[\frac{\sin\lambda}{\sin i_T}\right] \tag{3-42}$$

$$\chi = \sin^{-1}\left[\frac{\sin \lambda_T}{\sin i_T}\right] \tag{3-43}$$

If θ_{TOLN} is positive, the target is said to lead the chaser when the chaser arrives at the orbital line of nodes. If θ_{TOLN} is negative, the target is said to lag the chaser. However, lead and lag can be compensated for by assuming an impulsive yaw maneuver is performed by the chaser at the point of third-stage ignition.

The spherical triangles representing both right and left yaw maneuvers for Ascent Trajectory Mode 1 are shown in Figure 22. However, the following equations apply to both yaw maneuvers for all ascent trajectory modes:

$$\theta'_{CC} = \cos^{-1}\left[\cos \theta_{TOLN} \cos (\theta_{3B} + \theta_{CC}) + \sin \theta_{TOLN} \sin (\theta_{3B} + \theta_{CC}) \cos \delta\right] - \theta_{3B} \tag{3-44}$$

$$\psi_{YAW} = \sin^{-1}\left[\frac{\sin \theta_{TOLN} \sin \delta}{\sin (\theta_{3B} + \theta'_{CC})}\right] \tag{3-45}$$

$$\delta' = \sin^{-1}\left[\frac{\sin \psi_{YAW} \sin (\theta_{3B} + \theta_{CC})}{\sin \theta_{TOLN}}\right] \tag{3-46}$$

Equation (3-45) has been derived in such a way that ψ_{YAW} is positive for a yaw-right maneuver and negative for a yaw-left maneuver. In either case, the maneuver will be constrained by a subroutine input of $(\psi_{YAW})_{MAX}$. If $|\psi_{YAW}| \leq (\psi_{YAW})_{MAX}$, the yaw maneuver can be effected to achieve gross rendezvous.

The incremental velocity impulse required to accomplish the yaw maneuver can be written as

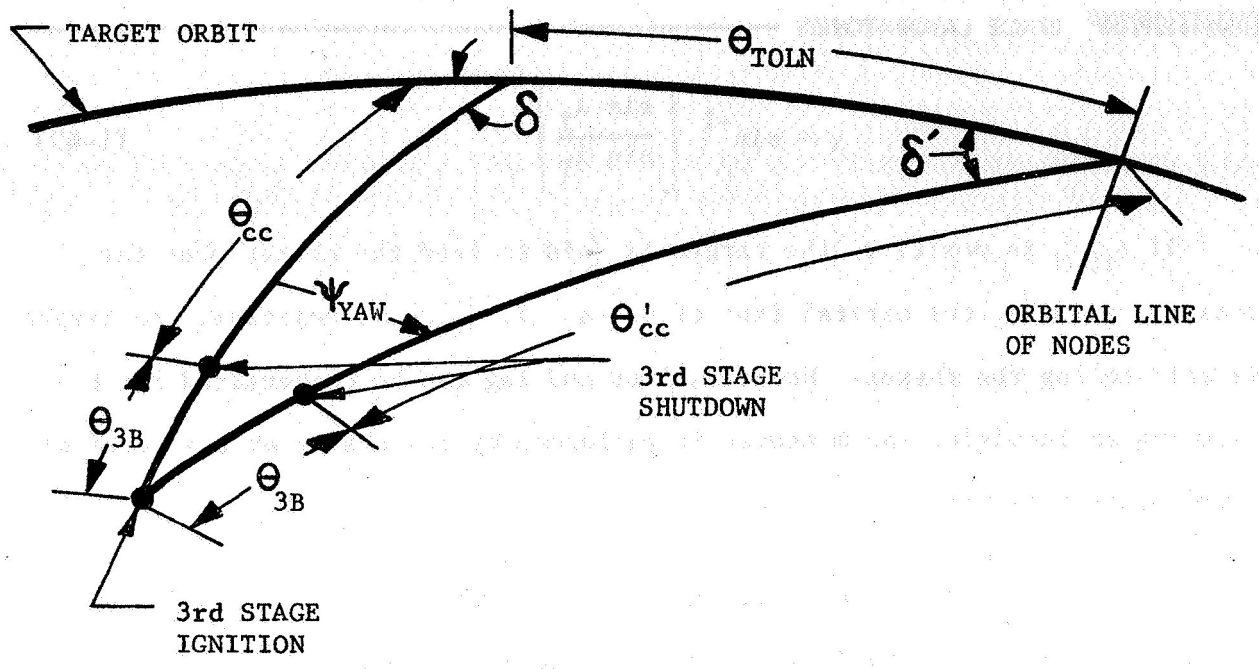

a. RIGHT YAW MANEUVER

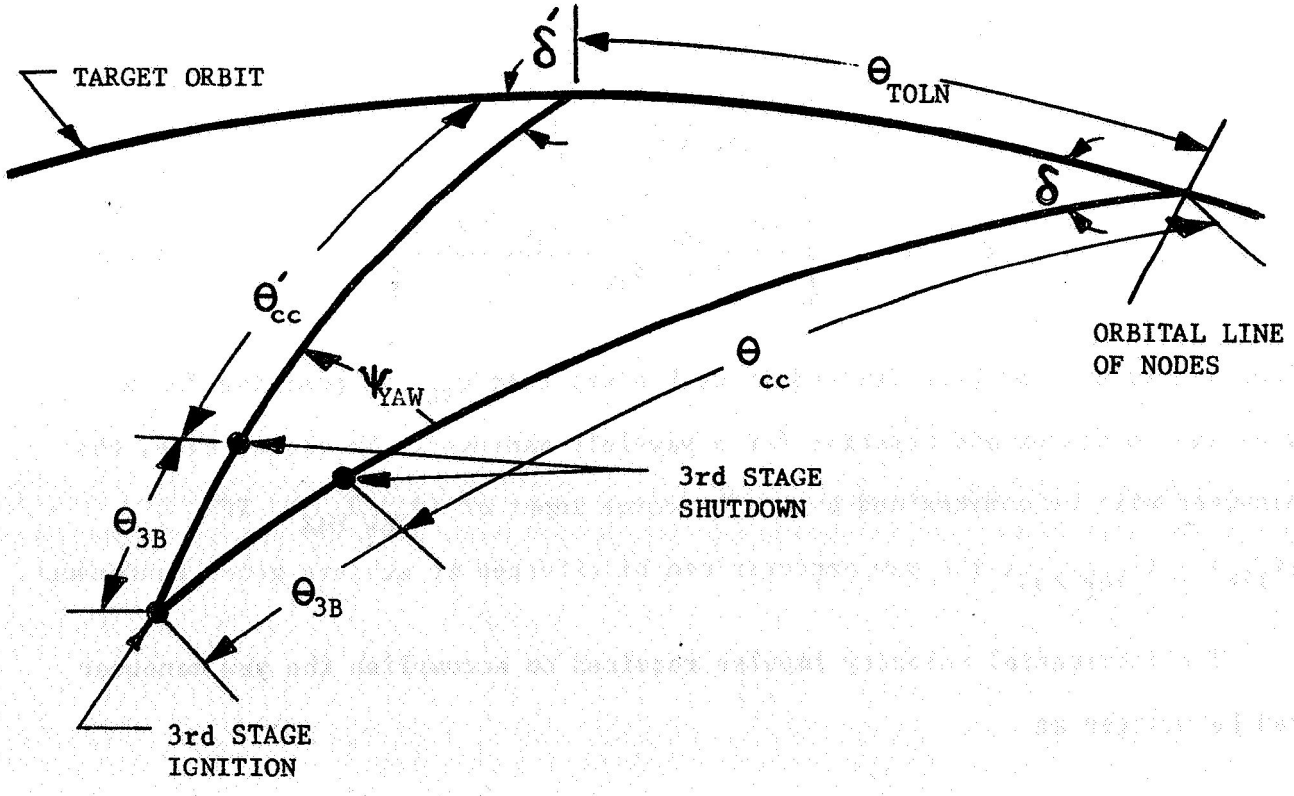

b. LEFT YAW MANEUVER

Figure 22. NON-COPLANAR ASCENT TRAJECTORY YAW MANEUVER GEOMETRIES

$$(\Delta V)_{YAW} = (v_{co})_3 \sin \left| \frac{\psi_{YAW}}{2} \right| \tag{3-47}$$

The velocity increment required to perform the plane-change maneuver is

$$(\Delta V)_{PC} = (v_{co})_3 \sin \left| \frac{\delta'}{2} \right| \tag{3-48}$$

The total chaser flight time from lift-off to gross rendezvous, assuming a yaw maneuver is performed, can be written as

$$(t_F)_a = t_{12B} + (t_{EC}^{A}_{B}) + t_{3B} + t'_{CC} \tag{3-49}$$

where

$$t'_{CC} = \frac{\theta'_{CC}}{\omega_2} \tag{3-50}$$

3.2 Rendezvous via an Intermediate Circular Parking Orbit

The general problem of achieving gross circular orbit rendezvous via an intermediate circular parking orbit can be stated briefly as follows:

A non-maneuverable target vehicle is revolving around the Earth in an inertially fixed circular orbit of known radius R_2 and inclination i_T. The maneuverable chaser vehicle is launched into a circular parking orbit of radius R_1 via the ascent trajectory dictated by the launch delay time, $(t_d)_n$. If the ascent trajectory plane is coplanar with the target orbit plane, the chaser is injected into the parking orbit when the third-stage engine is shutdown. However, if the ascent trajectory mode is non-coplanar, the ascent trajectory and target orbit planes intersect at the orbital line of nodes

and are inclined by the plane-change angle δ. In this case, the chaser is injected into a circular coasting orbit of radius R_1 when third-stage shutdown occurs. The chaser coasts in this coasting orbit until it arrives at the orbital line of nodes.

Upon arrival at the orbital line of nodes, the chaser has two options. These options are:

1) Continue coasting in a parking orbit that lies in the ascent trajectory plane. This parking orbit is non-coplanar with the target orbit since the planes containing these two orbits are inclined by the angle δ.

2) Perform an impulsive plane change maneuver dictated by the magnitude of δ and continue coasting in a parking orbit that is coplanar with the target orbit.

Regardless of the parking orbit used, the chaser is allowed to coast in the parking orbit until the phase angle between the chaser and the target is of the correct magnitude to effect a pre-determined two- or three-impulse transfer maneuver. Gross rendezvous is assumed to be accomplished when the chaser and the target achieve the same position, velocity, and flight-path angle in inertial space.

Figure 23 illustrates coplanar and non-coplanar parking orbits.

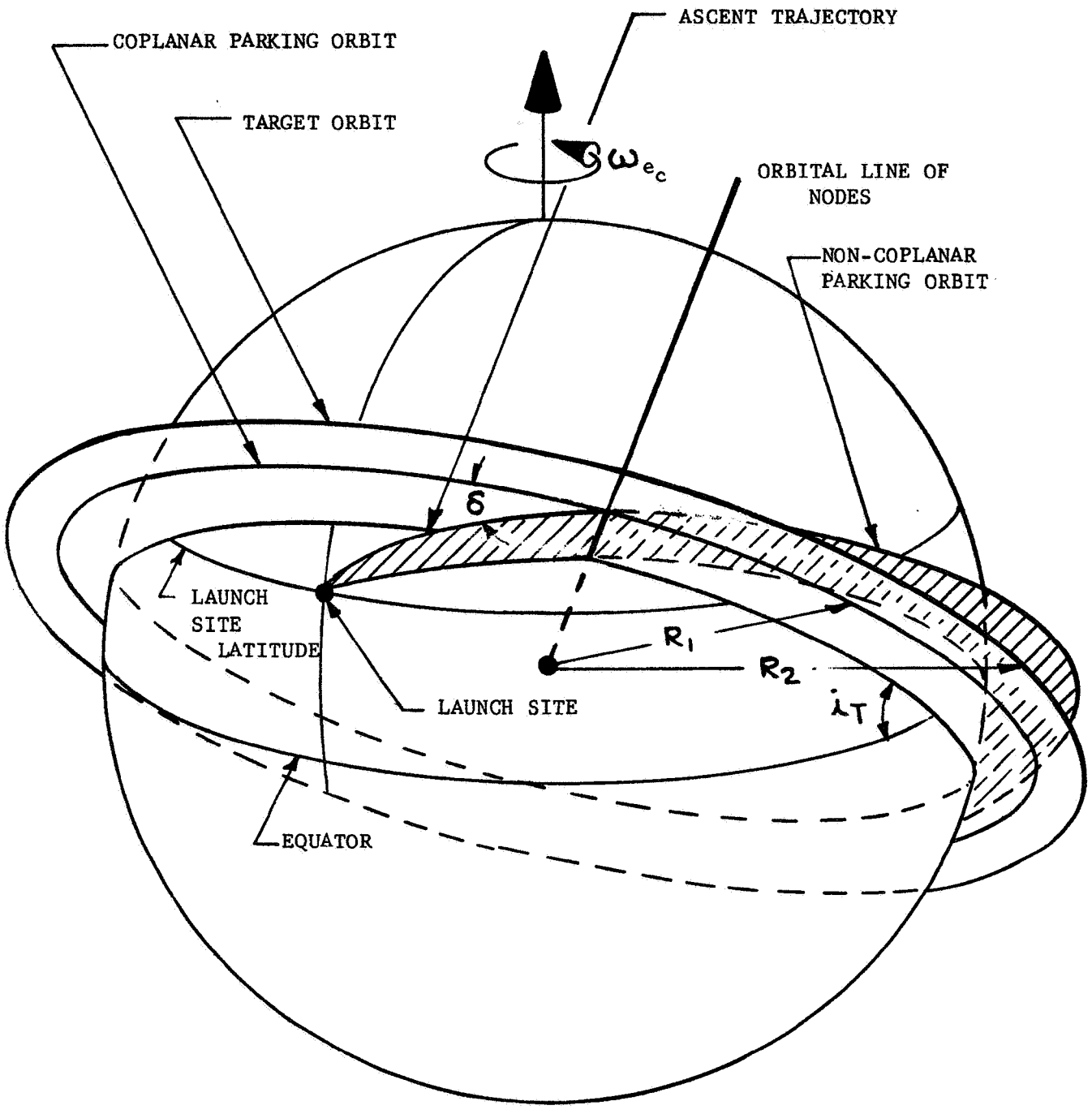

Figure 23. THE PROBLEM OF CIRCULAR ORBIT RENDEZVOUS VIA AN INTERMEDIATE CIRCULAR PARKING ORBIT

3.2.1 Orbital Transfer Maneuvers

Several types of two- and three-impulse maneuvers will be considered for transferring the chaser vehicle from a circular coplanar or non-coplanar parking orbit to a circular target orbit. These maneuvers can be classified as elliptical and parabolic transfer modes. Hyperbolic transfers were not considered due to the extremely high velocity increment required.

3.2.1.1 Transfer from a Coplanar Parking Orbit to the Target Orbit

All orbital transfer modes considered can be initiated at any point in the parking orbit. The transfer conic lies entirely in the plane of the parking orbit. Gross rendezvous is assumed to be accomplished upon completion of the orbital transfer maneuver.

Briefly, the coplanar transfer modes used in this analysis are as follows:

a) Hohmann Transfer Mode - The chaser is given a tangential velocity impulse, ΔV_1, at point a such that the target orbit is intercepted tangentially at point c. A second velocity impulse, ΔV_2, is applied at point c to circularize the chaser's orbit, (Figure 24).

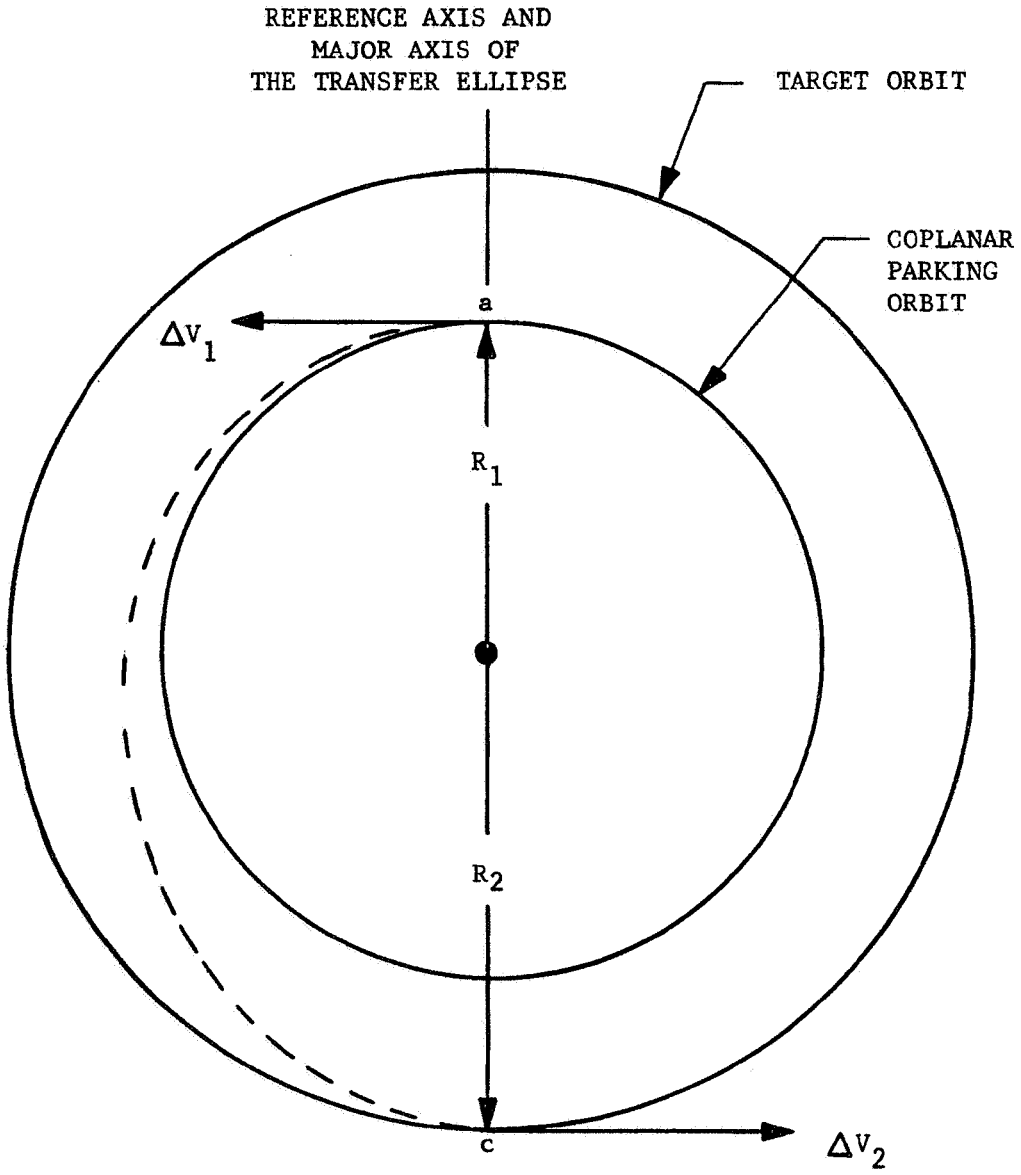

Figure 24. HOHMANN TRANSFER MODE

b) Modified Hohmann Transfer Mode - A tangential velocity impulse is applied to the chaser at point a such that the transfer ellipse intersects the target orbit non-tangentially at points A and B. A second velocity impulse, ΔV_2, is applied at either point A or B to circularize the chaser's orbit (Figure 25).

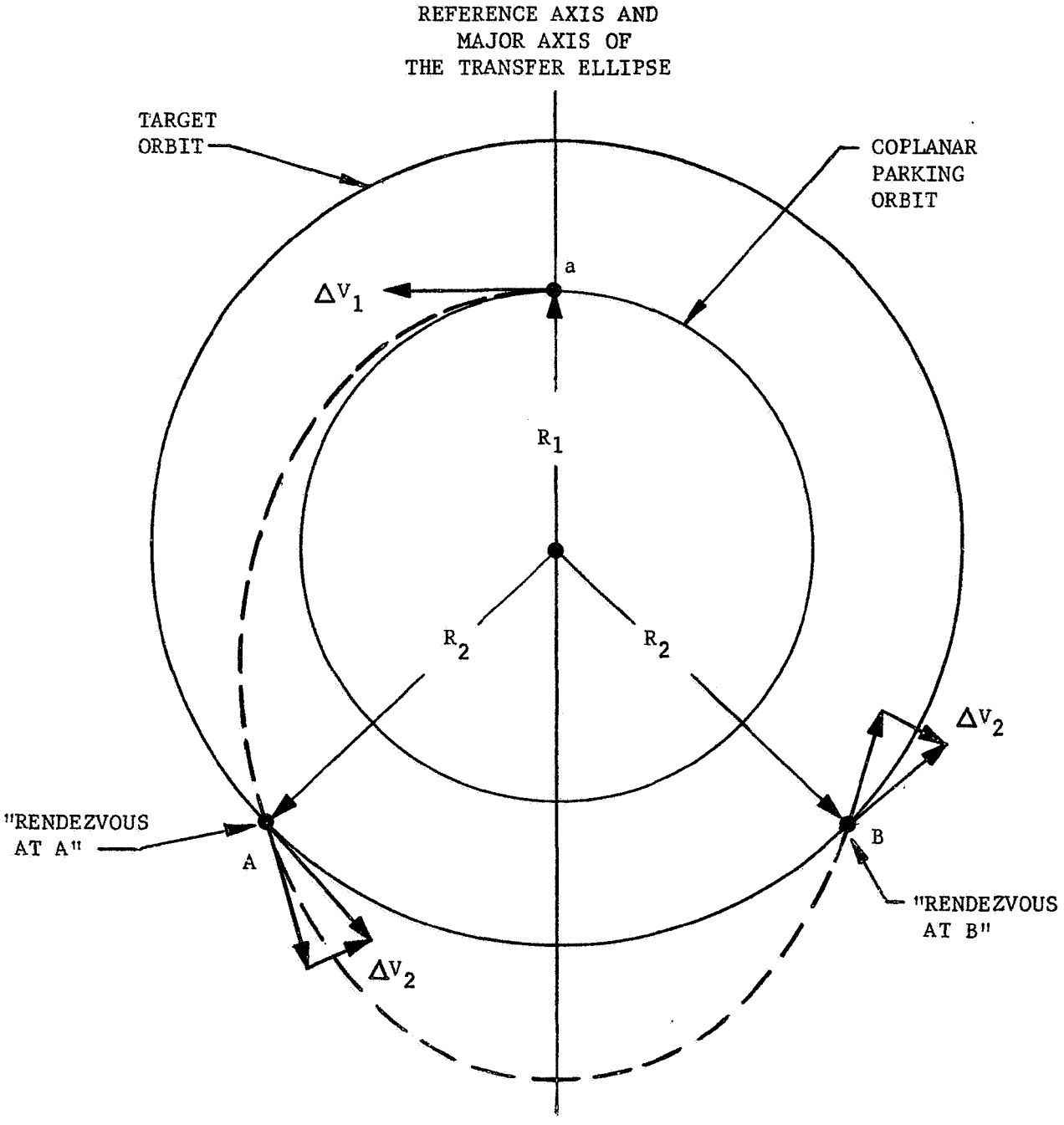

Figure 25. MODIFIED HOHMANN TRANSFER MODE

c) Gamma-Change Transfer Mode - A non-tangential velocity impulse, ΔV_1, is applied to the chaser at point a. The resulting transfer ellipse intersects the target orbit non-tangentially at points A and B. A second velocity impulse, ΔV_2, is applied at either point A or point B to circularize the chaser's orbit (Figure 26).

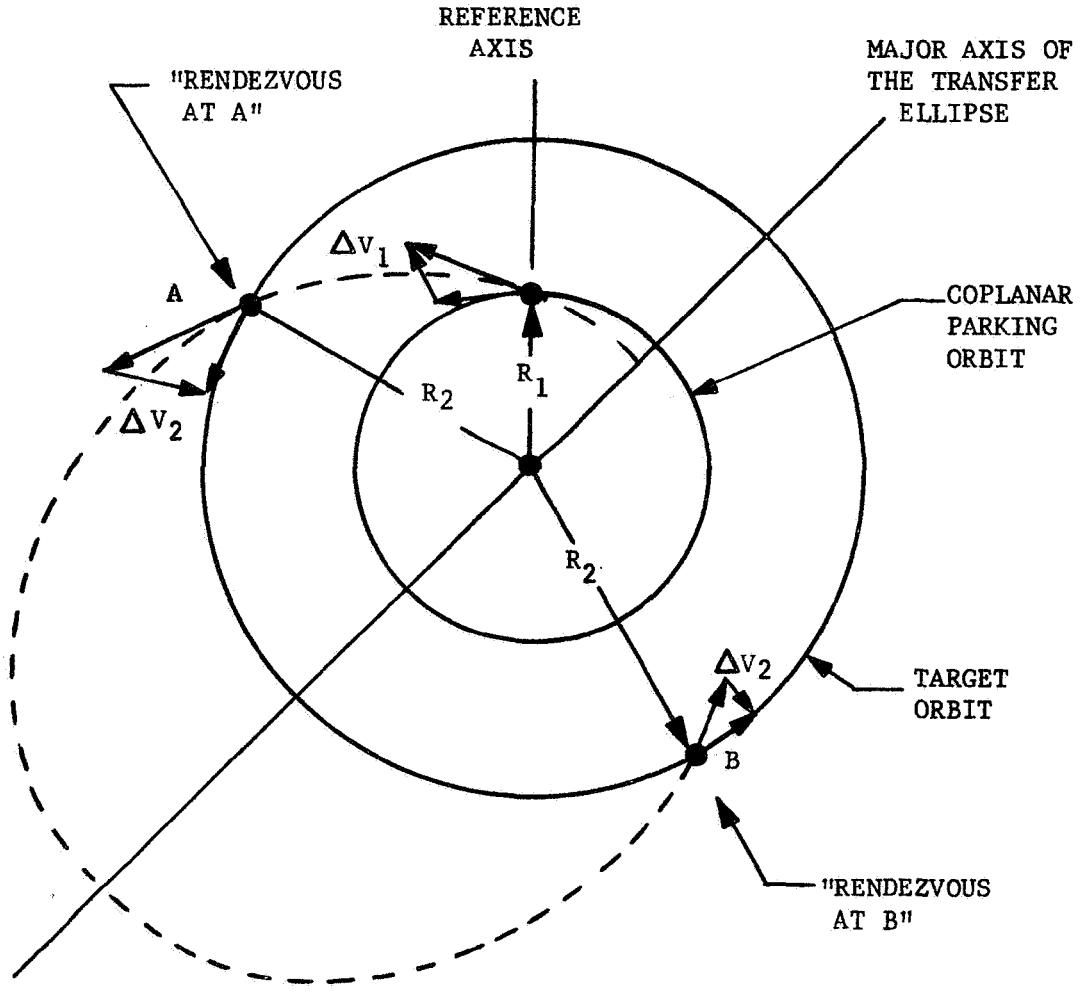

Figure 26. GAMMA-CHANGE TRANSFER MODE

d) Parabolic Transfer Mode - A non-tangential velocity impulse, ΔV_1, is applied to the chaser at point a such that the resulting transfer conic is a parabola. This parabola intersects the target orbit at point A. A second velocity impulse, ΔV_2, is applied at point A to circularize the chaser's orbit (Figure 27).

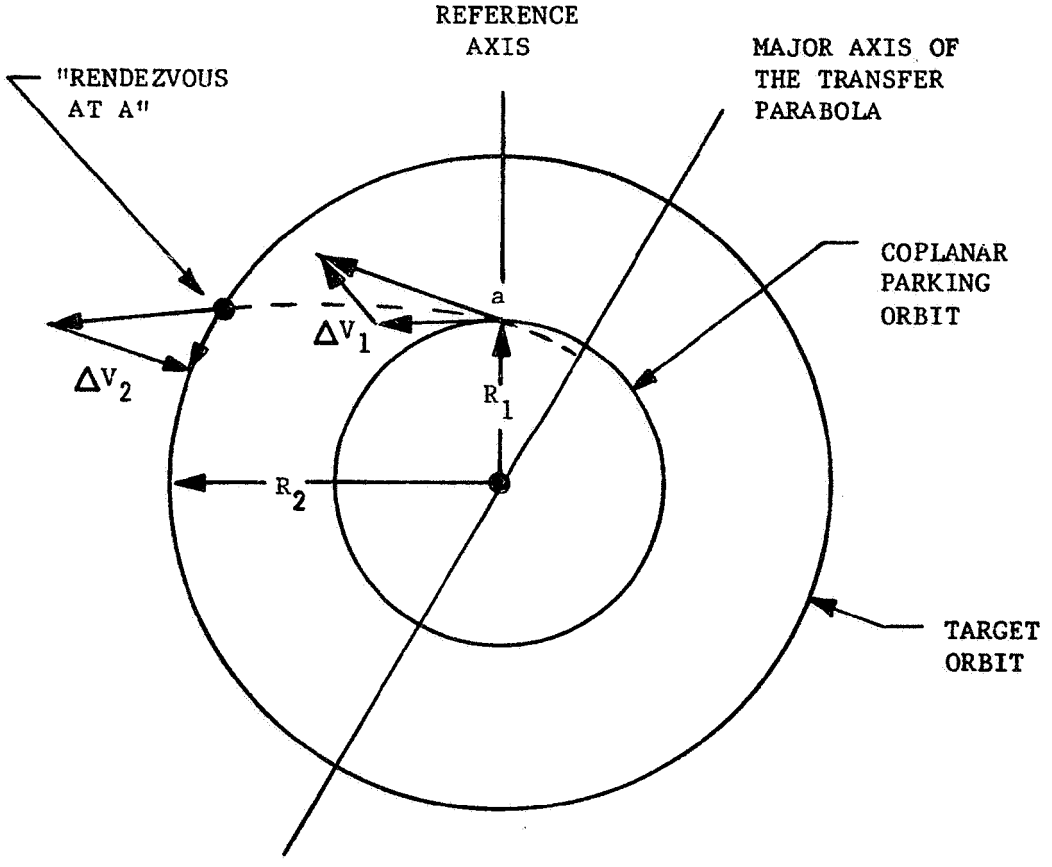

Figure 27. PARABOLIC TRANSFER MODE

e) Concentric Three-Impulse Elliptic Transfer Mode - A tangential velocity impulse, ΔV_1, is applied to the chaser at point a such that the chaser follows a Hohmann ellipse to point c. The second velocity impulse, ΔV_2, is applied tangentially at point c, causing the chaser to follow a second intermediate transfer ellipse and return to point c. The third velocity impulse, ΔV_3, is applied at point c to circularize the chaser's orbit (Figure 28).

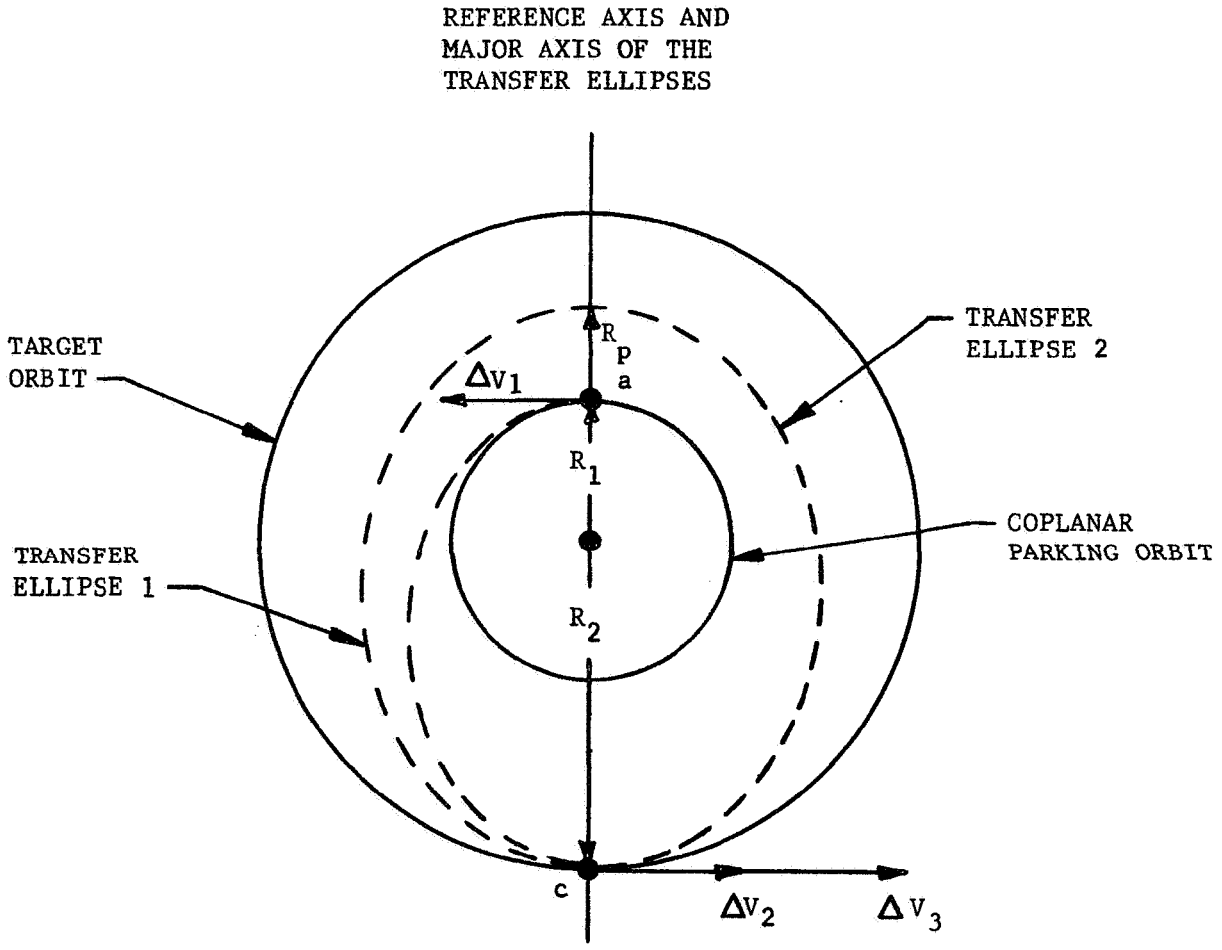

Figure 28. CONCENTRIC THREE-IMPULSE ELLIPTIC TRANSFER MODE

f) Bi-Elliptic Three-Impulse Transfer Mode - This transfer is an application of either the Modified Hohmann of the Gamma - Change Transfer Modes. Either a tangential or non-tangential velocity impulse, ΔV_1, is applied to the chaser at point a. This causes the resulting transfer ellipse to intersect the target orbit at point A. The chaser is allowed to coast on Transfer Ellipse 1 until it arrives at the apogee, point c. A second velocity impulse, ΔV_2, is applied tangentially at point c, causing the chaser to follow Transfer Ellipse 2 to point d. The third velocity impulse, ΔV_3, is applied tangentially at point d to circularize the chaser's orbit (Figure 29).

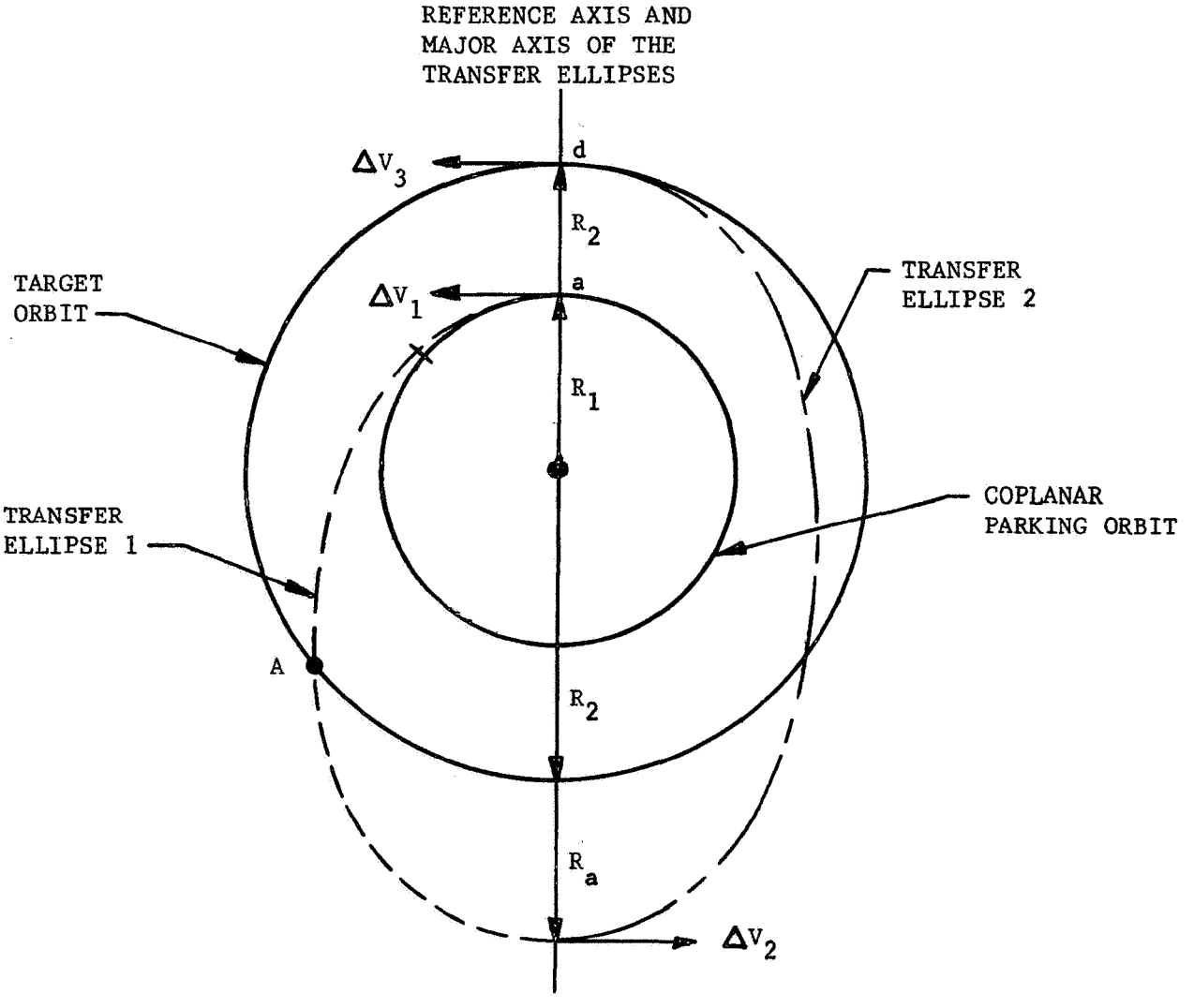

Figure 29. BI-ELLIPTIC THREE-IMPULSE TRANSFER MODE

3.2.1.2 Transfer from a Non-Coplanar Parking Orbit to the Target Orbit

The non-coplanar parking orbit plane intersects the target orbit plane at the so-called orbital line of nodes. These two planes are inclined by the plane-change angle δ .

The previously discussed coplanar orbital transfer modes can be used for non-coplanar transfer it if is assumed that the orbital transfer conic lies in-part in the plane of the parking orbit. Thus, the transfer conic intersects not the target orbit, but an orbit of radius R_2 lying in the parking-orbit plane. This orbit is known as the "fictitious" target orbit, (Figure 30).

It has been stated above that an orbital transfer maneuver can be initiated at any point in the parking orbit. If the points of transfer conic departure and arrival on the "fictitious" target orbit (points a and A, respectively, in Figure 30a) lie on the same side of the orbital line of nodes, the chaser is allowed to follow the transfer conic until it intersects the "fictitious" target orbit. The chaser then undergoes a change in flight-path angle and coasts along the "fictitious" target orbit until it arrives at the nearest node. An instantaneous plane-change maneuver is then performed and gross rendezvous is said to be accomplished. However, if point a and the point of arrival on the "fictitious" target orbit (point B in Figure 30b) lie on opposite sides of the orbital line of nodes, the chaser is allowed to follow the orbital transfer conic until the conic intersects the orbital line of nodes. At this point in time the chaser performs an instantaneous plane-change maneuver enabling the chaser to follow a portion of the transfer conic lying in the target orbit plane. Gross rendezvous is accomplished upon completion of the orbital transfer maneuver at point B' in Figure 30b.

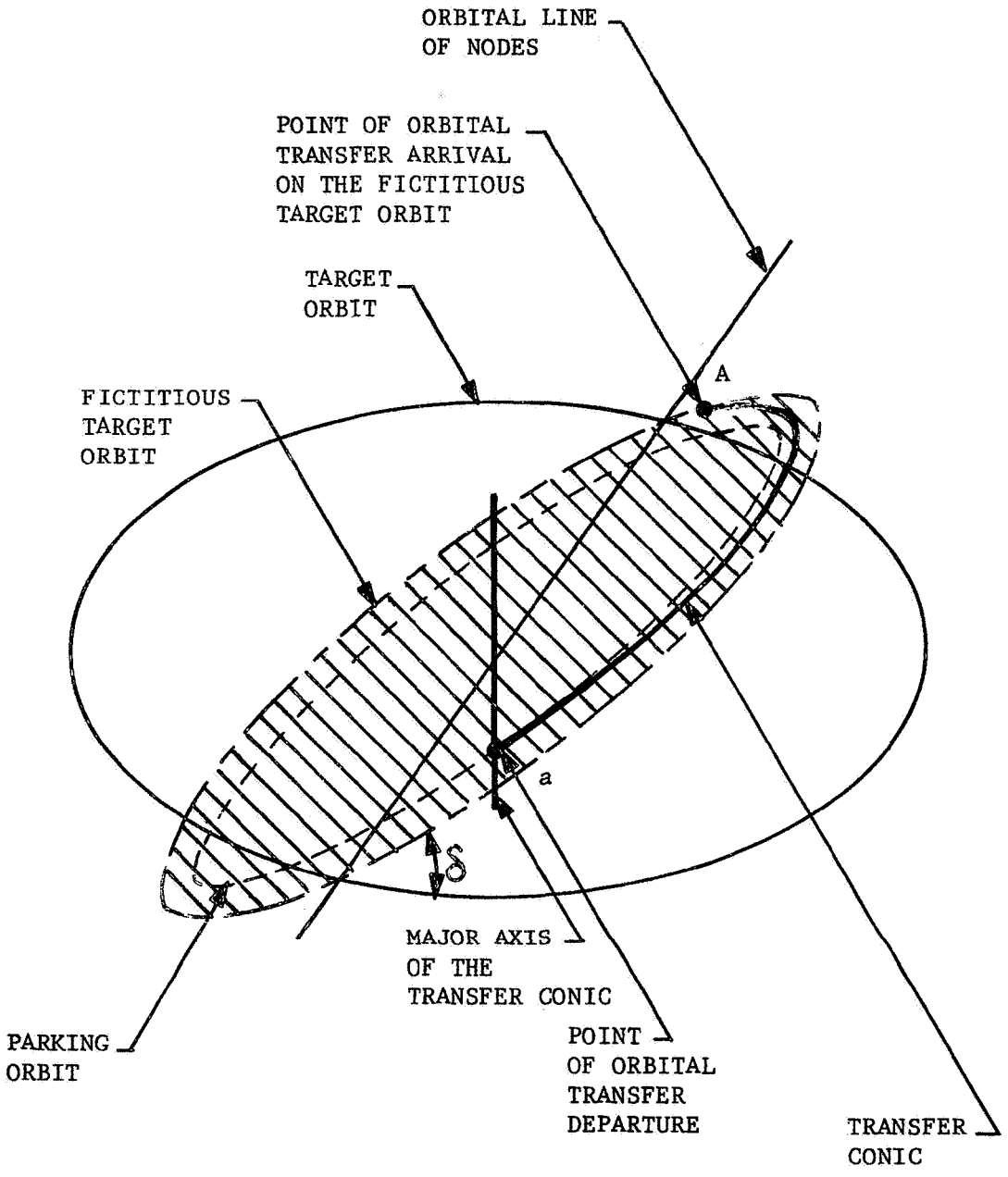

Figure 30a. NON-COPLANAR ORBITAL TRANSFER MANEUVER

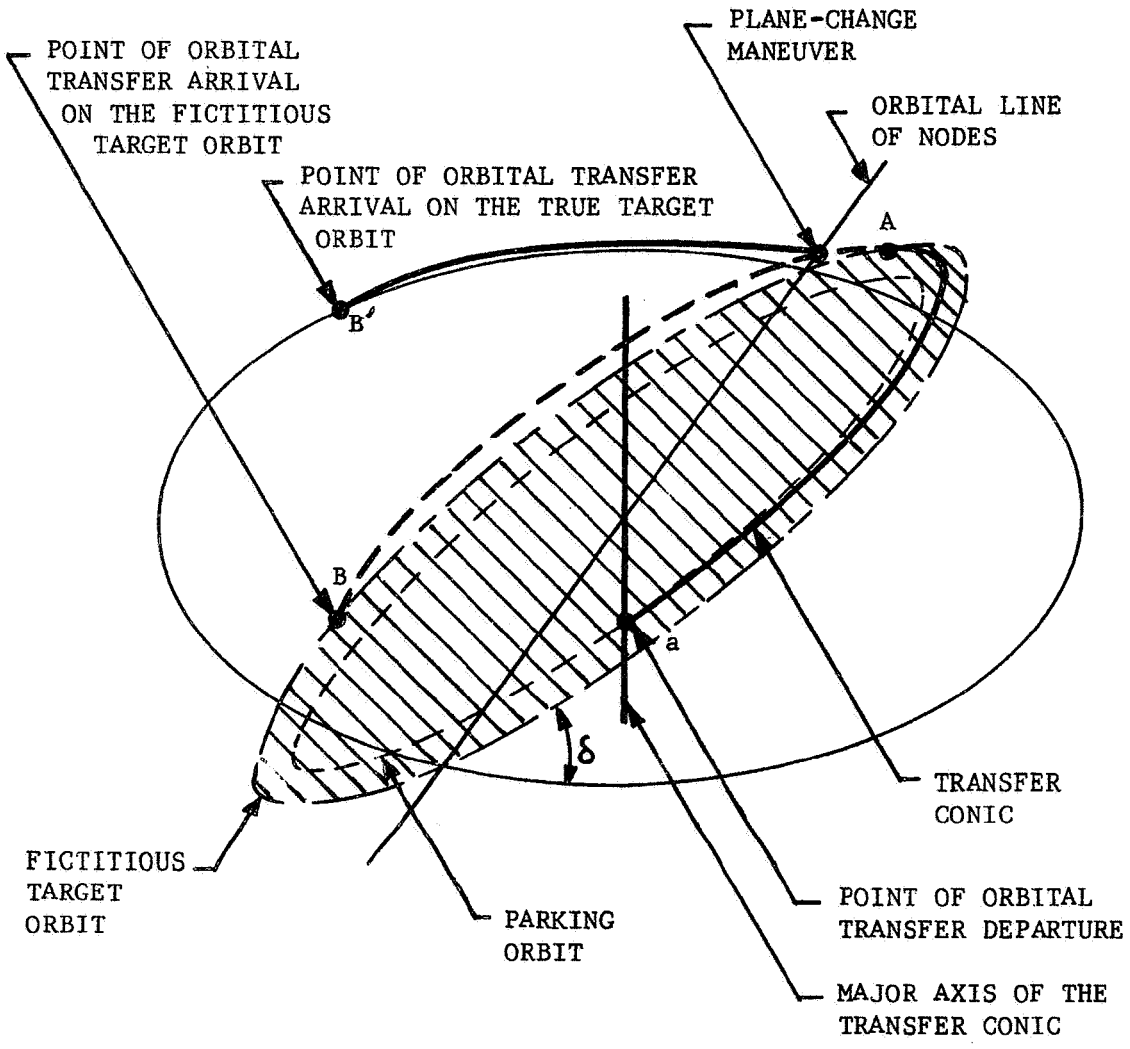

Figure 30b. NON-COPLANAR ORBITAL TRANSFER MANEUVER

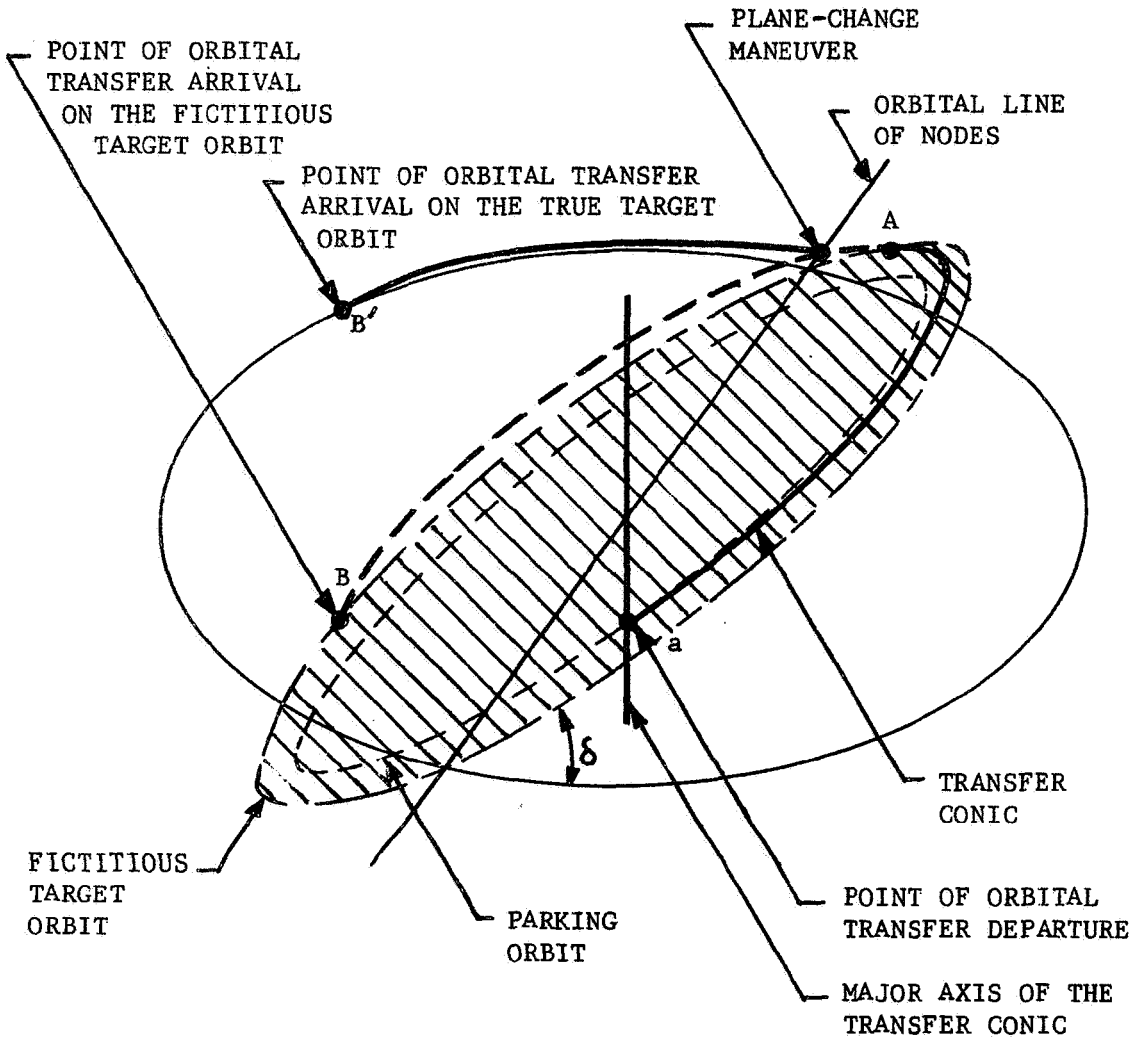

Figure 30b. NON-COPLANAR ORBITAL TRANSFER MANEUVER

3.2.2 Orbital Transfer Mode Matrix

The parameters that are of primary interest for any orbital transfer maneuver are:

$(\Delta V)_{TRANS}$ - Total impulsive velocity increment required to perform the transfer maneuver

$(t_F)_{TRANS}$ - Total flight time required to perform the transfer maneuver

ϕ_{TRANS} - The phase angle or the angle between the chaser and the target at the time of initiation of the transfer maneuver.

These parameters can be generated for a large number of coplanar orbital transfer maneuvers by what will be called the Orbital Transfer Mode Matrix.

It was found during the early development of the equations for the various modes of coplanar and non-coplanar transfer that all two-impulse transfers were a special case of the more general coplanar Gamma-Change Transfer Mode. Both the coplanar and non-coplanar three-impulse transfers were also found to be special applications of the two-impulse modes. All non-coplanar transfer modes differed from the coplanar transfer modes by the added maneuvers outlined in Section 3.2.1.2. Thus, it was found that all of the above mentioned orbital parameters can be generated for a large number of transfer maneuvers by solving the system of equations for the coplanar Gamma-Change Transfer Mode as certain "key" parameters in the geometry of this mode are varied. Additional equations are, however, required for all coplanar three-impulse transfer modes. This method of solution gives rise to the so-called Orbital Transfer Mode Matrix.

The Orbital Transfer Mode Matrix is an orderly array of the transfer parameters generated for any one, any combination, or all of the coplanar transfer modes pre-selected by the user of the subroutine. An example is in order. Assume the user of the subroutine wishes to generate data for the coplanar Gamma-Change Transfer Mode with "rendezvous at A and B". Knowing the parking orbit radius, R_1, and the target orbit radius, R_2, the general set of orbital transfer equations (and the additional equations for "rendezvous at B") are solved as the "key" parameters θ_1 and η (to be discussed later) are varied within certain limits. This produces an array of the orbital transfer parameters for all of the transfer modes so generated. The array or matrix is stored on tape and used as an input to the subroutine.

To set up the equations for the coplanar Gamma-Change Transfer Mode, the geometry related in Figure 31 will be used. Point a is defined as the point of orbital transfer departure. This point lies on the reference axis. The angle θ_1 defines the position of the major axis of the transfer conic relative to the reference axis. The angle η defines the location of the transfer conic's intersection with the target orbit (Point A) relative to the point of transfer departure.

The angle θ_1 will be defined to have any value such that

$$0 \leq \theta_1 < 2\pi.$$

However, for any orientation of the major axis of the transfer conic (θ_1), there is one and only one parabola that has this major axis orientation and passes through point a. This parabola will be designated the "Limiting Parabola".

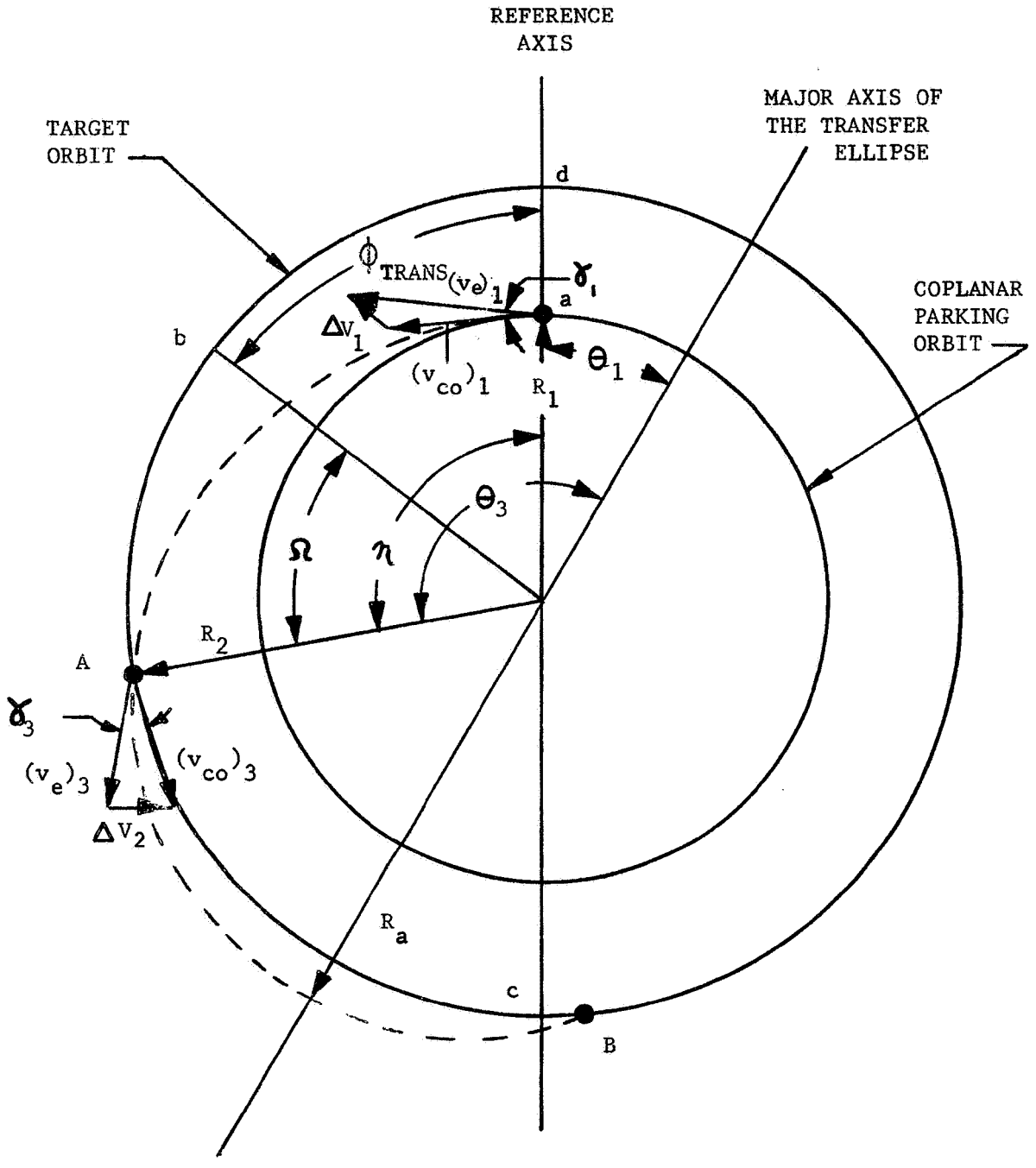

Figure 31. COPLANAR GAMMA-CHANGE TRANSFER MODE GEOMETRY

The "Limiting Parabola" defines a family of concentric transfer ellipses that have the same major axis and pass through point a. Figure 32 illustrates this vital point.

For given values of parking orbit radius, R_1, and target orbit radius, R_2, the "Limiting Parabola" (illustrated in Figure 33) for any value of Θ_1 can be determined as follows:

The angle Θ_1 is the true anomaly of the departure point (a). Because e = 1 for a parabola, the semi-latus rectum of the limiting parabola can be expressed as

$$(P)_{LP} = R_1 \ (1 + \cos \theta_1) \tag{3-51}$$

or

$$(P)_{LP} = R_2 \ (1 + \cos \theta_2) \tag{3-52}$$

where

θ_2 = true anomaly of the point of intersection of the "Limiting Parabola" with an orbit of radius R_2.

Equating expressions (3-51) and (3-52) the angle Θ_2 is

$$\theta_2 = \cos^{-1}\left[\frac{R_1}{R_2} \ (1 + \cos \theta_1) - 1\right] \tag{3-53}$$

The family of the transfer conics, defined by the limiting parabola, intersects an orbit of radius R_2 in an infinite number of points. The range of intersections is

$$\theta_2 \leq \theta < (2\pi - \theta_2),$$

where

θ = true anomaly of the point of intersection of the transfer conic with the target orbit.

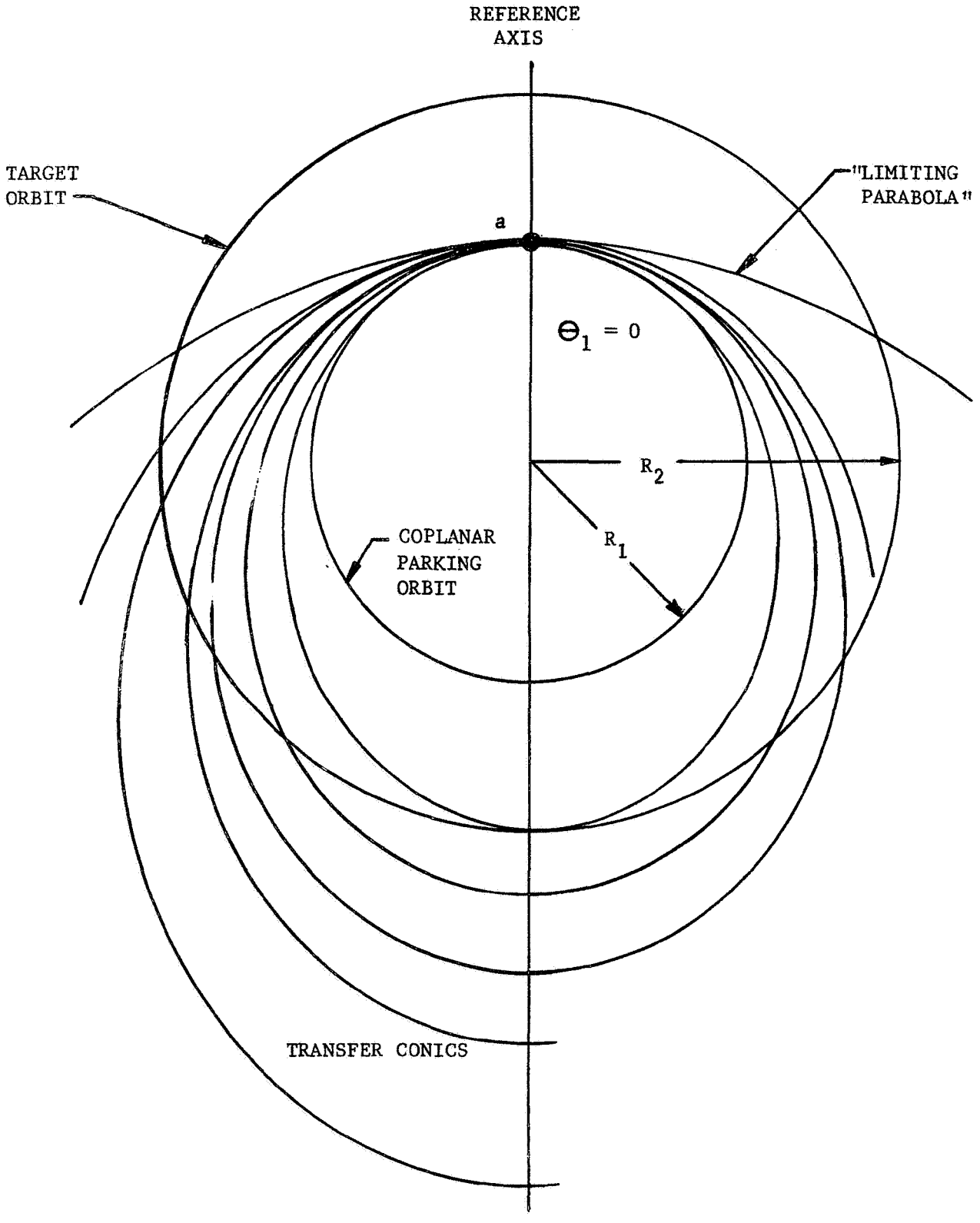

Figure 32 "LIMITING PARABOLA" AND ASSOCIATED FAMILY OF TRANSFER CONICS

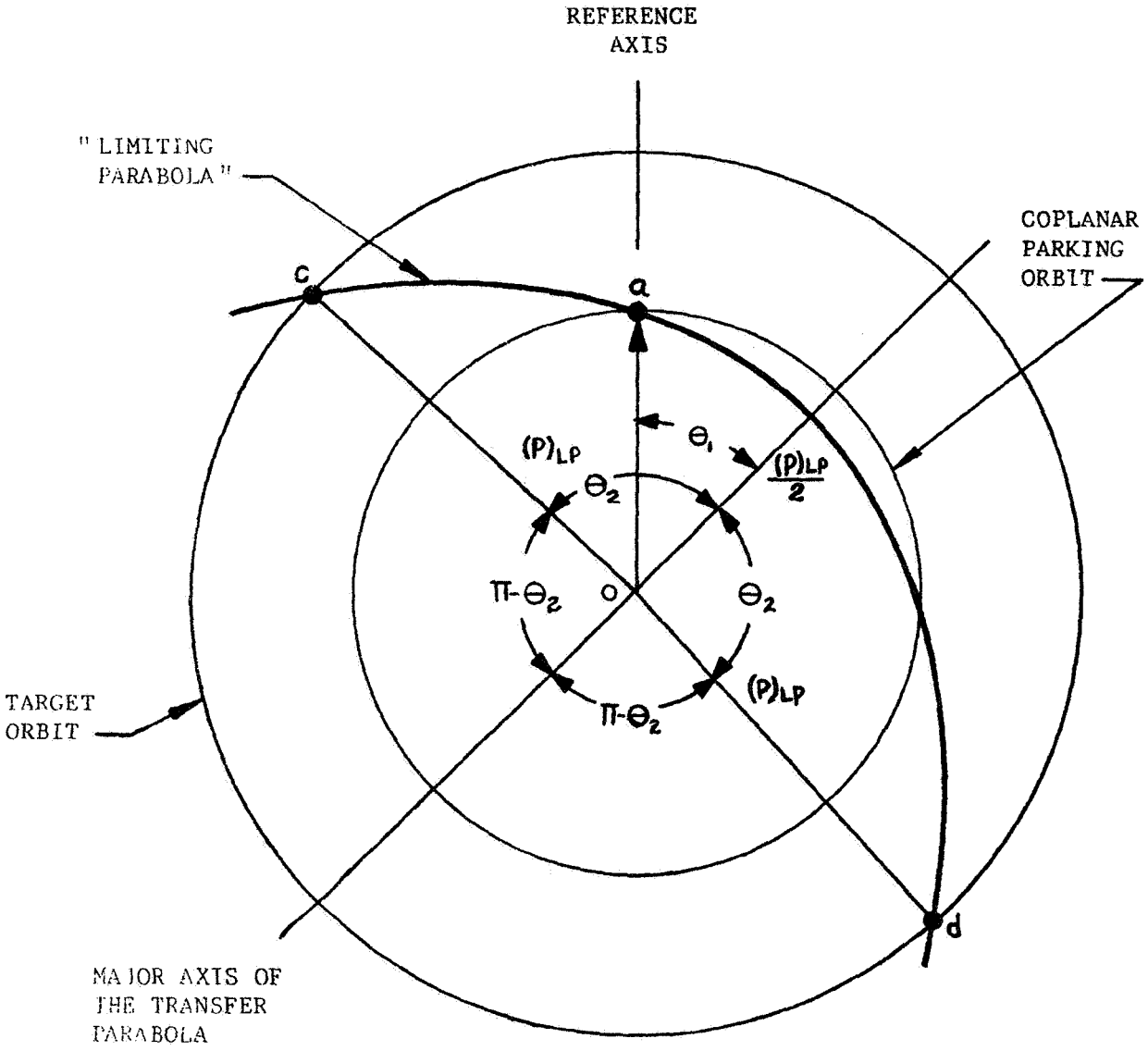

Figure 33. "LIMITING PARABOLA" GEOMETRY

Consider Figure 34, which illustrates the "Limiting Parabola" superimposed upon the Gamma-Change Transfer Mode geometry. In most cases the transfer conic intersects the target orbit in two points, A and B. When $\theta = \theta_3$, the intersection is point A and when $\theta = \theta_4$, the intersection is point B. This is known as "rendezvous at A" and "rendezvous at B", respectively. Parabolic transfer modes are applicable when $\theta = \theta_2$.

However, for every transfer intersection at point A, when

$$(\theta_2 - \theta_1) \leq \eta < (\pi - \theta_1),$$

there is an associated point of intersection B. Thus, to reduce computation time, the general equations for the coplanar Gamma-Change Transfer Mode are set up in terms of the point of intersection A, or "rendezvous at A". An additional set of equations is provided for "rendezvous at B".

The general set of equations for the coplanar Gamma-Change Transfer Mode for "rendezvous at A", with reference to Figure 31, are as follows:

The point at which the "Limiting Parabola" intersects the target orbit, of radius R_2, is determined by equation (3-53).

From this equation the range of acceptable values of θ_3 is found to be

$$\theta_2 \leq \theta_3 \leq (\pi - \theta_2) \tag{3-54}$$

where

$$\theta_3 = \theta_1 + \eta \tag{3-55}$$

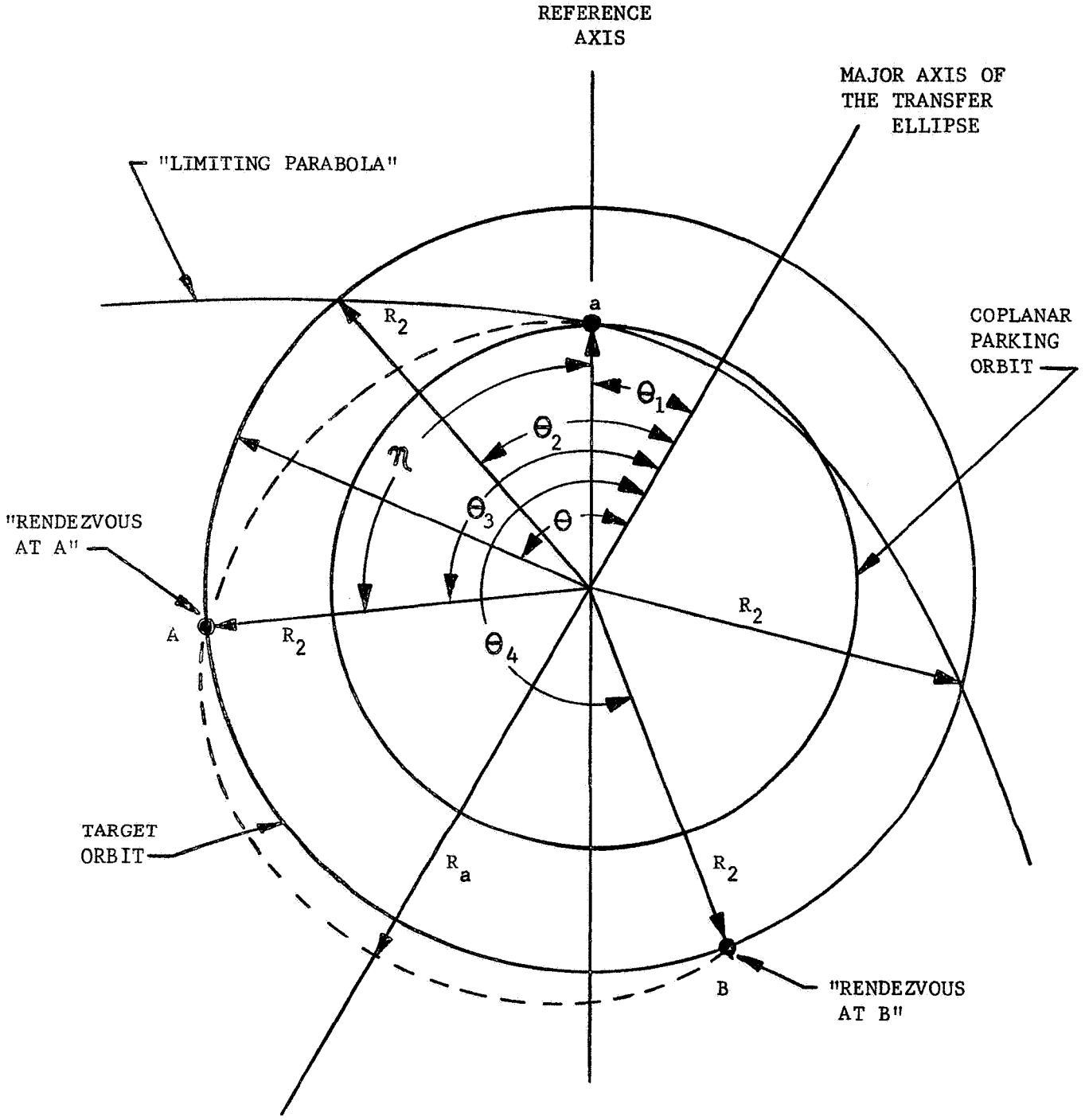

Figure 34. "LIMITING PARABOLA" AND THE GAMMA-CHANGE TRANSFER MODE GEOMETRY

Since the angle η has been defined as a "key" parameter, it is advantageous to express the range of acceptable η's as

$$(\theta_2 - \theta_1) \leq \eta \leq (\pi - \theta_1) \tag{3-56}$$

The eccentricity, e, of the orbital transfer conic can be written in terms of θ_1 and θ_3 as

$$P = R_1 (1 + e \cos \theta_1)$$

$$P = R_2 (1 + e \cos \theta_3)$$

$$R_1 (1 + e \cos \theta_1) = R_2 (1 + e \cos \theta_3)$$

$$e(R_1 \cos \theta_1 - R_2 \cos \theta_3) = R_2 - R_1.$$

Thus,

$$e = \frac{R_2 - R_1}{R_1 \cos \theta_1 - R_2 \cos \theta_3} \tag{3-57}$$

Knowing e, the semi-latus rectum can be determined

$$P = R_1 (1 + e \cos \theta_1) \tag{3-58}$$

As well as the semi-major axis

$$a = \frac{P}{1 - e^2} \tag{3-59}$$

The above equations determine the geometric parameters of the transfer conic. However, the following equations are the expressions required for "rendezvous at A":

The eccentric anomaly of the point of transfer departure (point a), measured from the major axis of the transfer conic, is:

$$\sin E_1 = \frac{(1 - e^2)^{\frac{1}{2}} \sin \theta_1}{1 + e \cos \theta_1} \tag{3-60a}$$

or

$$E_1 = \sin^{-1} \left[\frac{(1 - e^2)^{\frac{1}{2}} \sin \theta_1}{1 + e \cos \theta_1} \right] \tag{3-60b}$$

The eccentric anomaly of point "A" is

$$\sin E_3 = \frac{(1 - e^2)^{\frac{1}{2}} \sin \theta_3}{1 + e \cos \theta_3} \tag{3-61a}$$

or

$$E_3 = \sin^{-1} \left[\frac{(1-e^2)^{\frac{1}{2}} \sin \theta_3}{1 + e \cos \theta_3} \right] \tag{3-61b}$$

The mean anomalies of points a and A are

$$M_1 = E_1 - e \sin E_1 \tag{3-62}$$

and

$$M_3 = E_3 - e \sin E_3 \tag{3-63}$$

The flight time of a vehicle traveling from the perigee of the transfer conic to point a is

$$t_{F_1} = M_1 \sqrt{\frac{a^3}{\mu}} .$$

The flight time of a vehicle travelling from the perigee of the transfer conic to point A is

$$t_{F_3} = M_e \sqrt{\frac{a^3}{\mu}} .$$

Thus, the total transfer flight from point a to point A is

$$(t_F)_{TRANS} = (M_3 - M_1) \sqrt{\frac{a^3}{\mu}} \tag{3-64}$$

Now a relationship is needed to express the phase angle, ϕ_{TRANS}, required to accomplish gross rendezvous.

During the time, $(t_F)_{TRANS}$, the chaser vehicle travels from point a to point A along the transfer conic; through a central angle of η. Also during this time the target vehicle travels from point b to point A along the target orbit, of radius R_2; an angle of Ω.

Thus,

$$\eta = \Omega + \phi_{TRANS} \tag{3-65}$$

but

$$\Omega = \omega_2 \, (t_F)_{TRANS} \tag{3-66}$$

where

ω_2 = angular velocity of the target

$$\omega_2 = \sqrt{\frac{\mu}{R_2^3}} \tag{3-67}$$

Hence,

$$\eta = \phi_{TRANS} + \omega_2 \, (t_F)_{TRANS} .$$

Solving for the phase angle ϕ_{TRANS}

$$\phi_{TRANS} = \eta - \omega_2 \, (t_F)_{TRANS} \tag{3-68}$$

It is now of importance to examine the total velocity increment required, $(\Delta V)_{IRANS}$, to accomplish gross rendezvous.

The flight path angle at point a, (γ_1), measured from the local horizontal and expressed in terms of the true anomaly of point a, is:

$$\tan\gamma_1 = \frac{e \sin\theta_1}{1 + e \cos\theta_1} \tag{3-69a}$$

or

$$\gamma_1 = \left| \tan^{-1} \left[\frac{e \sin \theta_1}{1 + e \cos \theta_1} \right] \right| \tag{3-69b}$$

The circular orbit velocity of the chaser vehicle in the parking orbit is

$$(v_{co})_1 = \sqrt{\frac{\mu}{R_1}} \tag{3-70}$$

The velocity of the chaser at point a on the transfer conic can be expressed as

$$(v_e)_1 = \sqrt{\frac{2\mu}{R_1} - \frac{\mu}{a}} \tag{3-71}$$

Thus, the impulsive velocity increment required for the chaser vehicle to leave the parking orbit at point a and travel along the transfer conic is

$$\Delta V_1 = \left| \left[(v_e)_1^2 + (v_{co})_1^2 - 2(v_e)_1 \, (v_{co})_1 \cos \gamma_1 \right]^{\frac{1}{2}} \right| \tag{3-72}$$

The flight path angle at point A, (γ_3), measured from the local horizontal, is

$$\tan \gamma_3 = \frac{e \sin \theta_3}{1 + e \cos \theta_3} \tag{3-73a}$$

or

$$\gamma_3 = \left| \tan^{-1} \left[\frac{e \sin \theta_3}{1 + e \cos \theta_3} \right] \right| \tag{3-73b}$$

The circular orbit velocity of a vehicle in an orbit of radius R_2 is

$$(v_{co})_3 = \sqrt{\frac{\mu}{R_2}} \tag{3-74}$$

and the velocity of the chaser vehicle at point A on the transfer ellipse is

$$(v_e)_3 = \sqrt{\frac{2\mu}{R_2} - \frac{\mu}{a}} \tag{3-75}$$

Hence, the impulsive velocity increment required for the chaser vehicle to leave the transfer conic at point A and travel along the target orbit can be written as

$$\Delta V_2 = \left| \left[(v_e)_3^2 + (v_{co})_3^2 - 2(v_e)_3 (v_{co})_3 \cos \gamma_3 \right]^{\frac{1}{2}} \right| \tag{3-76}$$

Therefore, the total impulsive velocity increment required to accomplish the orbital transfer maneuver is

$$(\Delta V)_{TRANS} = \Delta V_1 + \Delta V_2 \tag{3-77}$$

Reference is made to Appendix C for the values of θ_1 and η that dictate which coplanar orbital transfer mode is applicable as the range of η's is examined. The appendix also presents the additional equations required for

1) Coplanar "rendezvous at B"

2) Coplanar Concentric Three-Impulse Elliptic Transfer Mode

3) Coplanar Bi-Elliptic Three-Impulse Transfer Mode.

Figure 35 presents a semi-detailed logic flow chart for the Orbital Transfer Mode Matrix. The matrix is generated for any one, any combination, or all of the coplanar orbital transfer modes by inputting R_1 and R_2 and the following control parameters:

A = 1 Coplanar "rendezvous at A" and/or "rendezvous at B"

A = 2 Coplanar "rendezvous at A" and/or "rendezvous at B" and Coplanar Concentric and/or Bi-Elliptic Three-Impulse Transfer Mode(s)

A = 3 Coplanar Concentric and/or Bi-Elliptic Three-Impulse Transfer Mode(s)

B = 1 Coplanar "rendezvous at A"

B = 2 Coplanar "rendezvous at A" and/or "rendezvous at B"

B = 3 Coplanar "rendezvous at B"

C = 1 Coplanar "rendezvous at A"

C = 3 Coplanar "rendezvous at A and B"

D = 1 Yes - - - Coplanar Three-Impulse Transfer Modes

D = 2 No - - - Coplanar Three-Impulse Transfer Modes

E = 1 Yes - - - Coplanar Concentric Three-Impulse Elliptic Transfer Mode

E = 2 No - - - Coplanar Concentric Three-Impulse Elliptic Transfer Mode

F = 1 Yes - - - Coplanar Bi-Elliptic Three-Impulse Transfer Mode

F = 2 No - - - Coplanar Bi-Elliptic Three-Impulse Transfer Mode.

Figure 35 indicates that the orbital transfer parameters for all generated coplanar transfer modes are arranged by decreasing order of the transfer phase angle, ϕ_{TRANS}. This matrix or array of transfer parameters is stored and used as an input to the subroutine.

3.2.3 Orbital Transfer Maneuvers and Phasing Relationships

A parking orbit, whether it is coplanar or non-coplanar with the target orbit, is utilized by the chaser for waiting until the phasing relationship between the chaser and the target is correct to initiate an orbital transfer maneuver.

If the launch delay time, $(t_d)_n$, is such that the Coplanar Ascent Trajectory Mode is applicable, the chaser is injected into a coplanar parking orbit. This is illustrated in Figure 36. The true phase angle between the chaser and the target at the time of chaser orbital injection is determined as follows:

$$\alpha_{LS} = \sin^{-1}\left[\frac{\sin\lambda}{\sin i_T}\right] \tag{3-42}$$

$$\theta_{TAN} = \alpha_T + (t_F)_a \quad \omega_2 \tag{3-35}$$

If $$[\alpha_{LS} + \theta_{12B} + (\theta_{EC})_A + \theta_{3B}] < \theta_{TAN}$$

$$\phi_{TRUE} = \theta_{TAN} - [\alpha_{LS} + \theta_{12B} + (\theta_{EC})_A + \theta_{3B}] \tag{3-78}$$

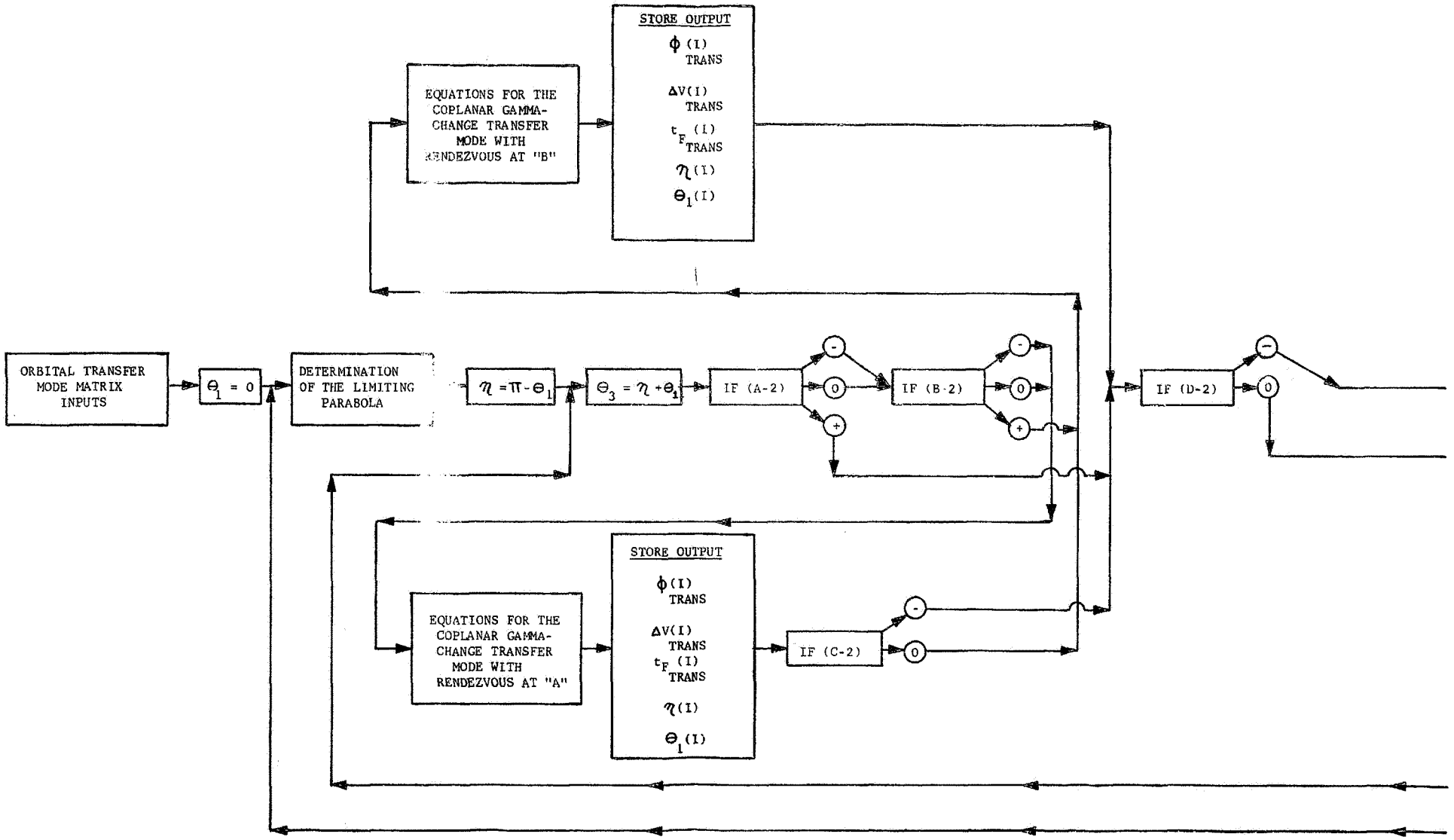

Figure 35. LOGIC FLOW CHART FOR THE ORBITAL TRANSFER MODE MATRIX

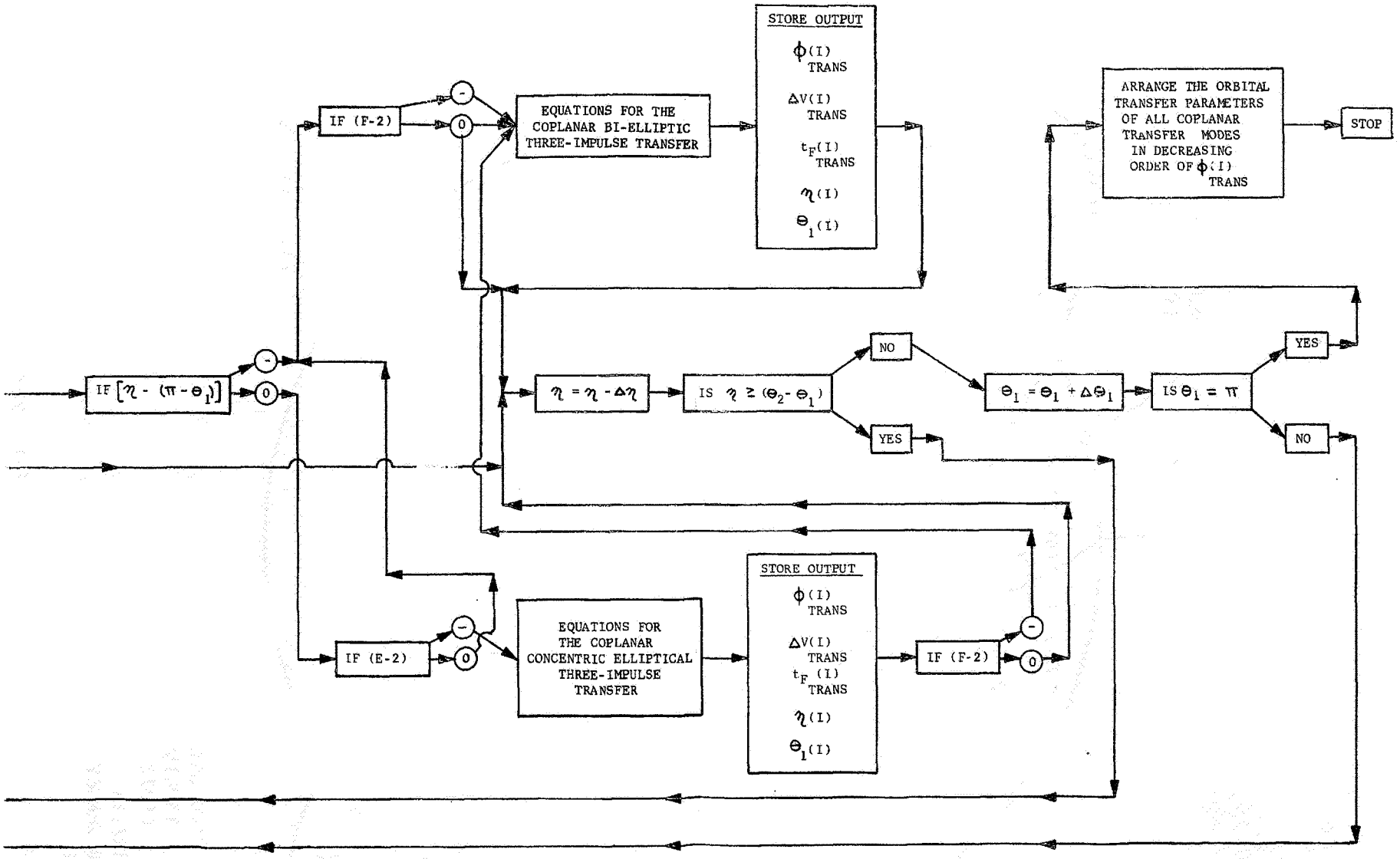

Figure 35. LOGIC FLOW CHART FOR THE ORBITAL TRANSFER MODE MATRIX (concluded)

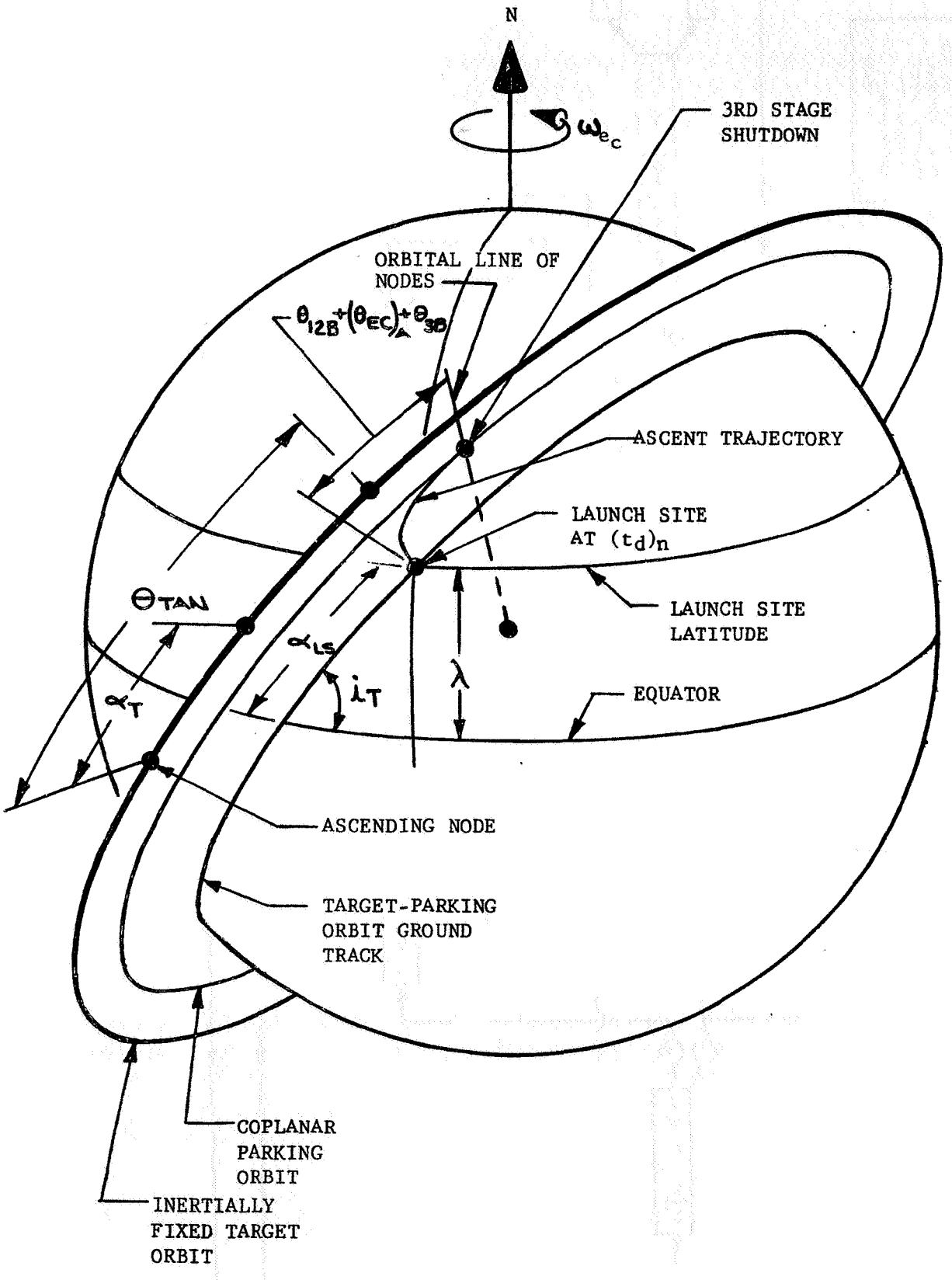

Figure 36. TYPICAL COPLANAR ASCENT TO PARKING ORBIT

If $$[\alpha_{LS} + \theta_{12B} + (\theta_{EC})_A + \theta_{3B}] > \theta_{TAN}$$

$$\phi_{TRUE} = 2\pi - \{\theta_{TAN} - [\alpha_{LS} + \theta_{12B} + (\theta_{EC})_A + \theta_{3B}]\} \tag{3-79}$$

Once the true phase angle is known, the Orbital Transfer Mode Matrix is searched for a ϕ_{TRANS} that is equal to ϕ_{TRUE}. If a suitable transfer phase angle is found, the orbital transfer mode associated with ϕ_{TRANS} can be initiated. However, if a transfer phase angle cannot be found such that

$$\phi_{TRANS} = \phi_{TRUE},$$

the chaser must remain in the parking orbit until the phasing relationship is suitable for initiation of a transfer maneuver. The next transfer phase angle in the descending sequence of phase angles is then examined to determine the required parking time. This parking time is determined by

$$t_{PARK} = \frac{\phi_{TRUE} - \phi_{TRANS}}{\dot{\phi}} \qquad \text{for } 0 \leq \phi_{TRUE} \geq \phi_{TRANS}$$

or (3-80)

$$t_{PARK} = \frac{(2\pi - \phi_{TRANS}) - \phi_{TRUE}}{\dot{\phi}} \qquad \text{for } 0 \leq \phi_{TRUE} < \phi_{TRANS}$$

where

$\dot{\phi}$ = chaser catch-up rate

$$\dot{\phi} = \omega_1 - \omega_2 \tag{3-81}$$

$$\omega_1 = \sqrt{\frac{\mu}{R_1^3}} \tag{3-82}$$

Thus, the Orbital Transfer Mode Matrix is searched for an orbital transfer mode that can be accomplished within certain parking time restrictions. An acceptable transfer maneuver is, however, restricted by the allowable total mission velocity increment and total mission flight time. The semi-detailed subroutine logic flow chart in Section 4 illustrates this approach.

If the launch delay time, $(t_d)_n$, is such that a Non-Coplanar Ascent Trajectory Mode is applicable, the chaser coasts from third-stage shutdown to the orbital line of nodes. When the chaser arrives at the orbital line of nodes, the chaser can perform either of the two options outlined in Section 3.2. If a plane change is performed and a coplanar parking orbit utilized, the procedure for finding an acceptable transfer mode is the same as above. However, the use of a non-coplanar parking orbit requires a somewhat different approach.

Ascent into a non-coplanar parking orbit is accomplished by a non-coplanar ascent trajectory similar to the one used for direct ascent to rendezvous. Figure 37 illustrates this point. The true phase angle existing when the chaser arrives at the orbital line of nodes, for any ascent trajectory mode, is found by

$$\phi_{TRUE} = \theta_{TOLN} \tag{3-83}$$

or

$$\phi_{TRUE} = 2\pi - \theta_{TOLN} \tag{3-84}$$

where

θ_{TOLN} is determined by equations (3-37) through (3-40).

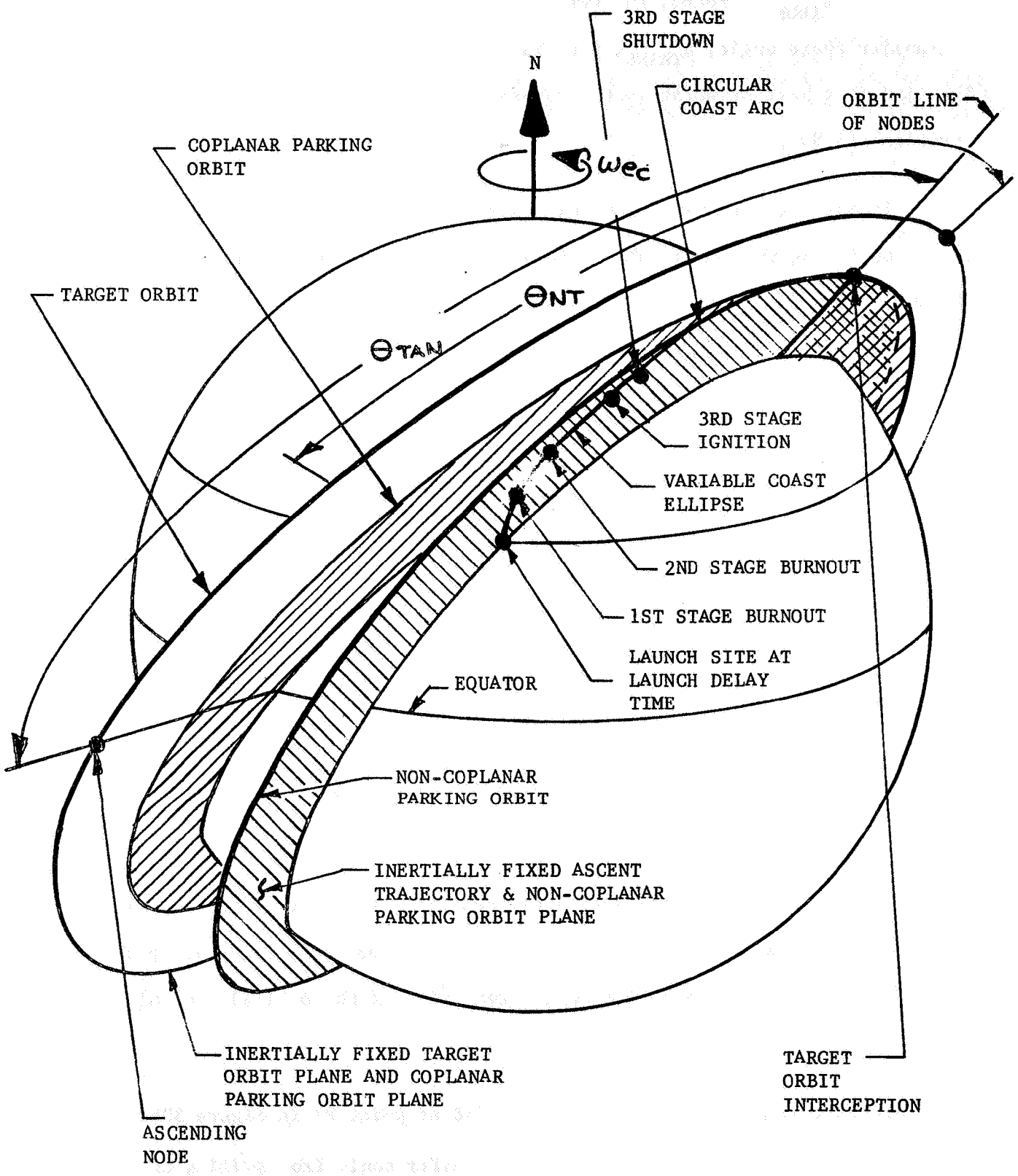

Figure 37. TYPICAL NON-COPLANAR ASCENT AND NON-COPLANAR PARKING ORBIT

When ϕ_{TRUE} is found, the Orbital Transfer Mode Matrix is searched for a transfer phase angle, ϕ_{TRANS}, that is equal to or slightly less than ϕ_{TRUE}. The time that must be spent in the non-coplanar parking orbit is found by equation (3-80).

It must be remembered that the parking orbit is non-coplanar with the target orbit and that these planes intersect at the orbital line of nodes (Figure 30b). Thus, the position of the chaser at the end of required parking time, relative to the orbital line of nodes, must be determined.

Figure 38 illustrates the Non-Coplanar Gamma-Change Transfer Mode geometry as viewed from vertically above the parking orbit plane. The position of the chaser from the orbital line of nodes for any parking time is

$$\theta_{COLN} = \omega_1 \ (t_{PARK}) \qquad (3\text{-}85)$$

If gross rendezvous is desired at point e in Figure 38, the chaser would follow the transfer conic from point a to point A on the "fictitious" target orbit. The chaser would then coast in the "fictitious" target orbit until it arrives at the nearest orbital node. At the node, the chaser would perform a plane-change maneuver and effect rendezvous.

Appendix D contains the additional equations required for non-coplanar orbital transfers if the point of departure and the point of arrival, on the "fictitious" target orbit, both lie on the same side of the orbital line of nodes.

However, if gross rendezvous is desired at point B' in Figure 30b, the chaser would be allowed to follow the transfer conic from point a to

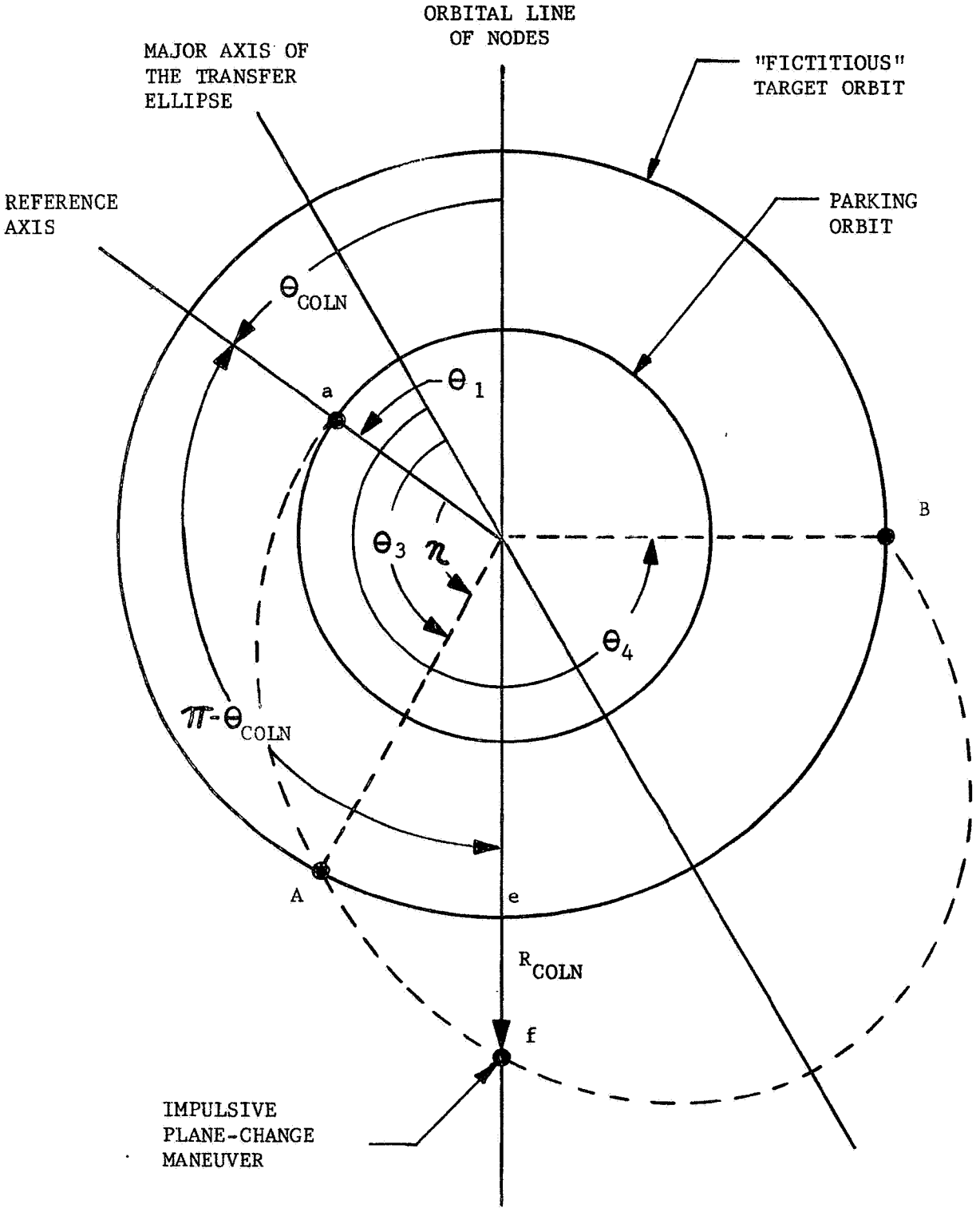

Figure 38. NON-COPLANAR GAMMA-CHANGE TRANSFER MODE

the orbital line of nodes (point f in Figure 38). The radius at point f on the orbital transfer conic is

$$R_{COLN} = \frac{P}{1 + e \cos (\pi - \theta_{COLN} + \theta_1)} \tag{3-86}$$

The chaser's velocity is

$$(V)_{COLN} = \sqrt{\frac{2\mu}{R_{COLN}} - \frac{\mu}{a}} \tag{3-87}$$

Thus, the impulsive velocity increment required to perform the plane-change maneuver is

$$(\Delta V)_{PC} = 2(V)_{COLN} \sin \tfrac{1}{2} \delta \tag{3-88}$$

After performing the plane change, the chaser continues coasting along the transfer conic, lying in the target orbit plane, until it arrives at Point B'. Gross rendezvous is effected at this point.

SECTION 4

RESULTS AND CONCLUSIONS

4.1 Subroutine Logic Flow Chart

Figure 39 presents a semi-detailed logic flow chart for the entire subroutine. It is suggested that the Ascent Trajectory Table and the Orbital Transfer Mode Matrix be input tapes. The subroutine has the following inputs:

a) Target orbit radius, R_2

b) Target orbit inclination, i_T

c) Position of the target from the ascending node at the reference time, α_0

d) Launch site latitude, λ

e) Launch site longitude, λ_0

f) Local hour angle of the vernal equinox, measured from the launch site hour circle at the reference time, LHAY

g) Total ΔV capability of the chaser launch vehicle, $[(\Delta V)_{MISSION}]_{MAX}$

h) Total allowable chaser flight time, $[(t_F)_{MISSION}]_{MAX}$

i) Total allowable parking orbit time, $(t_{PARK})_{MAX}$

j) Chaser launch azimuth range safety constraints, $(A_Z)_{MAX}$ and $(A_Z)_{MIN}$

k) Desired parking orbit radius, R_1

l) Maximum allowable yaw angle, $(\psi_{YAW})_{MAX}$

m) Maximum allowable chaser 2nd-stage burnout flight path angle, $(\gamma_{2BO})_{MAX}$

n) Earth oblateness constant, $J = 1.62345 \times 10^{-3}$

o) Earth equatorial radius, $R_e = 6.378156 \times 10^6$ m

p) Earth gravitational constant, $\mu = 3.986016 \times 10^{14}$ m^3/sec^2

q) Acceleration due to gravity at the Earth's surface, $g_o = 9.8045016$ m/sec^2

r) Length of the true mean solar day, $T_o = 86{,}164.099$ sec

s) True Earth rotational rate, $\omega_E = 7.29211513 \times 10^{-5}$ rad/sec

t) Reference time in terms of GMT or ZULU time

u) Number of days of required launch window investigation, M

v) Chaser vehicle third-stage thrust, F

w) Maximum allowable chaser ascent impulsive velocity increment, $[(\Delta V)_a]_{MAX}$

x) Launch delay time increment, Δt_d

y) Chaser 2nd-stage burnout flight path angle increment, $\Delta\gamma_{2BO}$

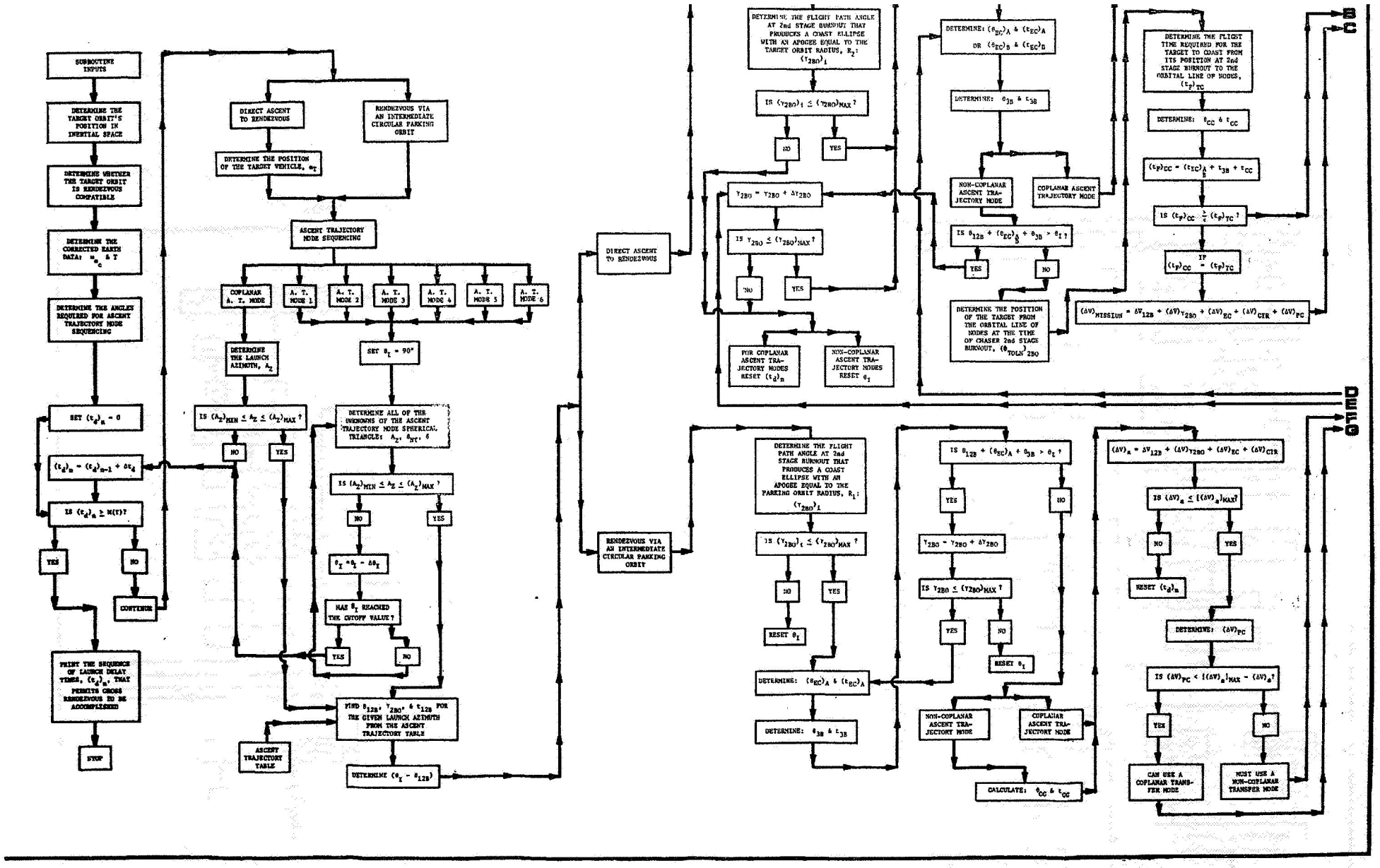

Figure 39. LOGIC FLOW CHART FOR THE SUBROUTINE (Sheet 1 of 2)

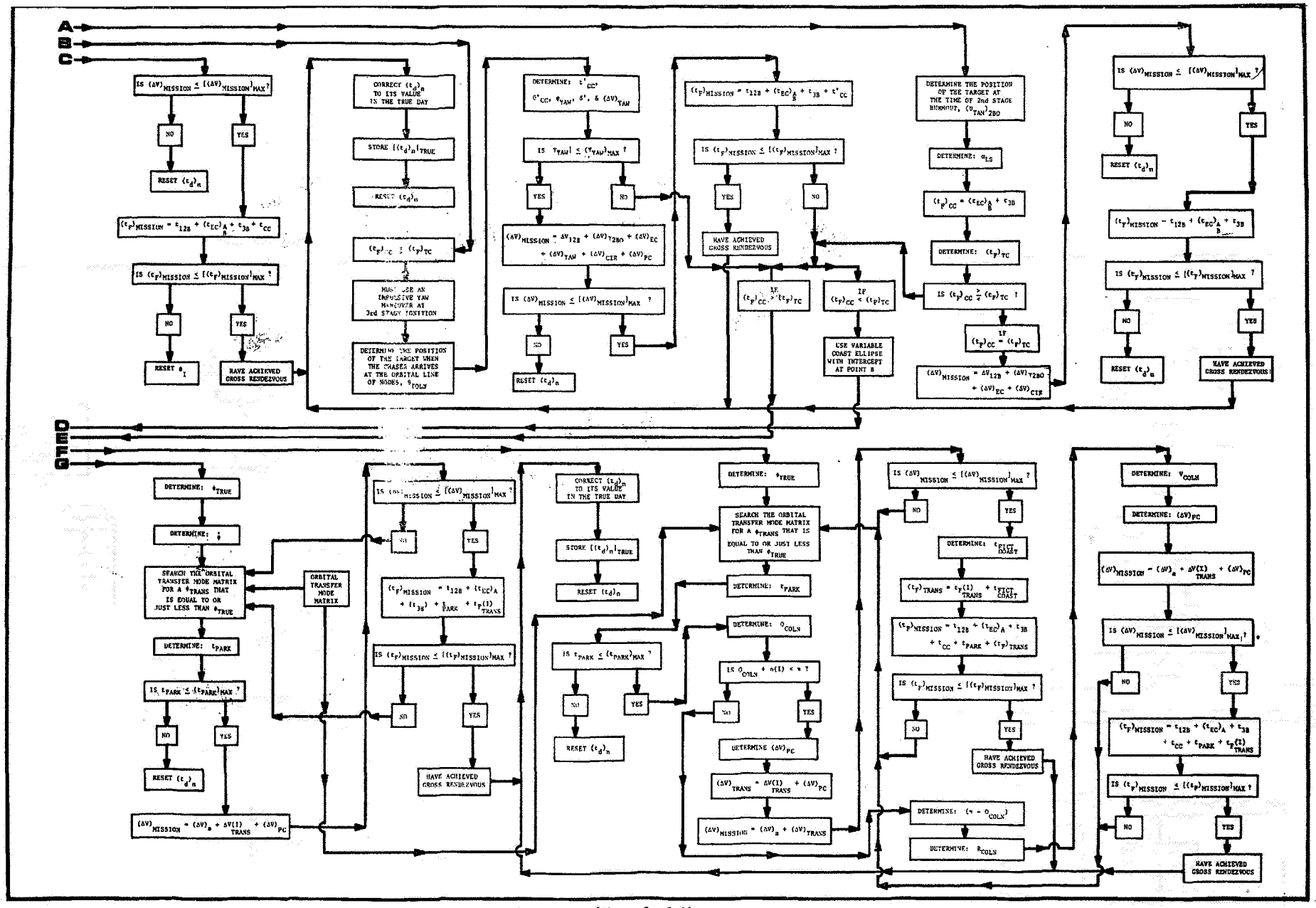

Figure 39. LOGIC FLOW CHART FOR THE SUBROUTINE (Sheet 2 of 2)

4.2 Recommendations

It has been assumed that the maximum allowable parking orbit time is relatively small, roughly on the order of one parking orbit revolution. Thus, in a first approximation, it is assumed that the differential nodal regression of the target and parking orbits is negligible. However, for longer parking times, equation(s) must be added to the subroutine to account for this unequal nodal regression.

It is recommended that the subroutine be programmed and checked out in the following steps:

1) Programming and checkout of various separate phases or parts of the subroutine. This will ensure the speed and accuracy of each independent phase.

2) Error analysis and improvement of each phase.

3) Programming and checkout of the entire subroutine to check the compatibility of all separate phases.

SECTION 5

REFERENCES

1. Berman, Arthur I., The Physical Principles of Astronautics, John Wiley & Sons, Inc., 1963.

2. Bird, John D., and Thomas, Jr., David F., "A Two-Impulse Plan for Performing Rendezvous on a Once-a-Day Basis," NASA TN-D-437, Langley Research Center, November 1960.

3. Blitzer, Leon, "On the Motion of a Satellite in the Gravitational Field of the Oblate Earth," GM-TM-0165-00279, Space Technology Laboratories, September 1958.

4. Brunk, William E., and Flaherty, Richard J., "Methods and Velocity Requirements for the Rendezvous of Satellites in Circumplanetary Orbits," NASA-TN-D-81, Lewis Research Center, October 1959.

5. Coates, G. L., "Optimization of Two-Burn Direct Ascent Trajectories for Rendezvous," TDR-269 (4550-20)-5, Aerospace Corp., February 1965.

6. Davis, H. A., and Chambers, L. H., Brief Course in Plane and Spherical Trigonometry, American Book Co., 1933.

7. Dowlen, E. M., and Seddon, J., "Orbital Rendezvous Techniques", Journal of the British Interplanetary Society, Vol. 19, 1963-64.

8. Ellison, Bobby, "A Parameter Study of Launch Windows for Orbit to Orbit Transfers About a Planet Keeping Required Energy Change Near a Minimum", Aeroballistics Internal Note No. 30-63, George C. Marshall Space Flight Center, Huntsville, Alabama, 1963.

9. Ehricke, Krafft A., Space Flight, Vol II Dynamics, D. Van Norstrand Co., Inc., 1962.

10. Kenehan, Martin F., "Analytic Determination of Launch Windows for Orbital Rendezvous," AIAA Paper No. 64-399, Paper Presented at 1st AIAA Annual Meeting, Washington, D.C., June 29 - July 2, 1964.

11. Koelle, Heinz H., ed., Handbook of Astronautical Engineering, McGraw-Hill Book Co., 1961.

12. Metzger, R. R., Kopp, R. J., and Rhodes, P., "Fortran IV Computer Program for the Determination of the Applicability of IGM to Coplanar Earth Orbital Rendezvous," Northrop Space Laboratories, Huntsville, Alabama, (to be published).

13. Nelson, Walter C., and Loft, Ernest E., Space Mechanics, Prentice-Hall, Inc., 1962.

14. Neilsen, Kaj J., and Vanlonkhuyzen, John H., Plane and Spherical Trigonometry, Barnes & Noble, 1964.

15. _____, Orbital Flight Handbook, Martin-Marietta, Space Systems Division.

16. Petersen, Norman V., and Swanson, Robert S., "Rendezvous Compatible Orbits, Astronautical Sciences Review, Oct. - Dec. 1959.

17. _____, Space Navigation Handbook, Navpers 92988.

18. Swanson, Robert S., and Petersen, Norman J., "Summary Report of Rendezvous Compatible Orbits," NSL 62-117, Northrop Space Laboratories, Hawthorne, California, July 1962.

APPENDIX A

DEFINITIONS

The reader is referred to Figures A-1 and A-2 with reference to the following definitions:

Celestial sphere - The celestial sphere is an imaginary sphere of infinite radius, with the Earth located at its center. All celestial bodies, including the First Point of Aries, are considered to lie on the surface of the celestial sphere. The Earth's equatorial plane is coplanar with the celestial sphere's equatorial plane and the Earth and celestial polar axes coincide. The celestial sphere remains fixed in inertial space while the Earth rotates about its axis.

Hour circle - The hour circle is the great circle that passes through the celestial poles and a point on the celestial sphere.

Vernal equinox - The vernal equinox is the intersection (ascending node) of the Earth's equatorial plane. This line points to the assumed space-fixed First Point of Aries, designated by the symbol γ.

Sidereal hour angle (SHA) - The sidereal hour angle is the central angle, measured in the equatorial plane, between the hour circle of a point on the celestial sphere and the hour circle of Aries. This angle is measured westward from Aries through 360°.

Local hour angle of Aries (LHAγ) - The local hour angle of Aries is the central angle between the hour circle of the launch site and the hour circle of Aries. This angle is measured westward from the launch site hour circle through 360°.

Greenwich hour angle of Aries (GHAγ) - The Greenwich hour angle of Aries is the central angle between the hour circle of the Earth's prime meridian and the hour of circle of Aries. This angle is measured westward from the Greenwich hour circle through 360°.

Local hour angle (LHA) - The local hour angle is the central angle between the hour circle of the launch site and the hour circle of the target orbit ascending node. This angle is measured westward from the launch site hour angle.

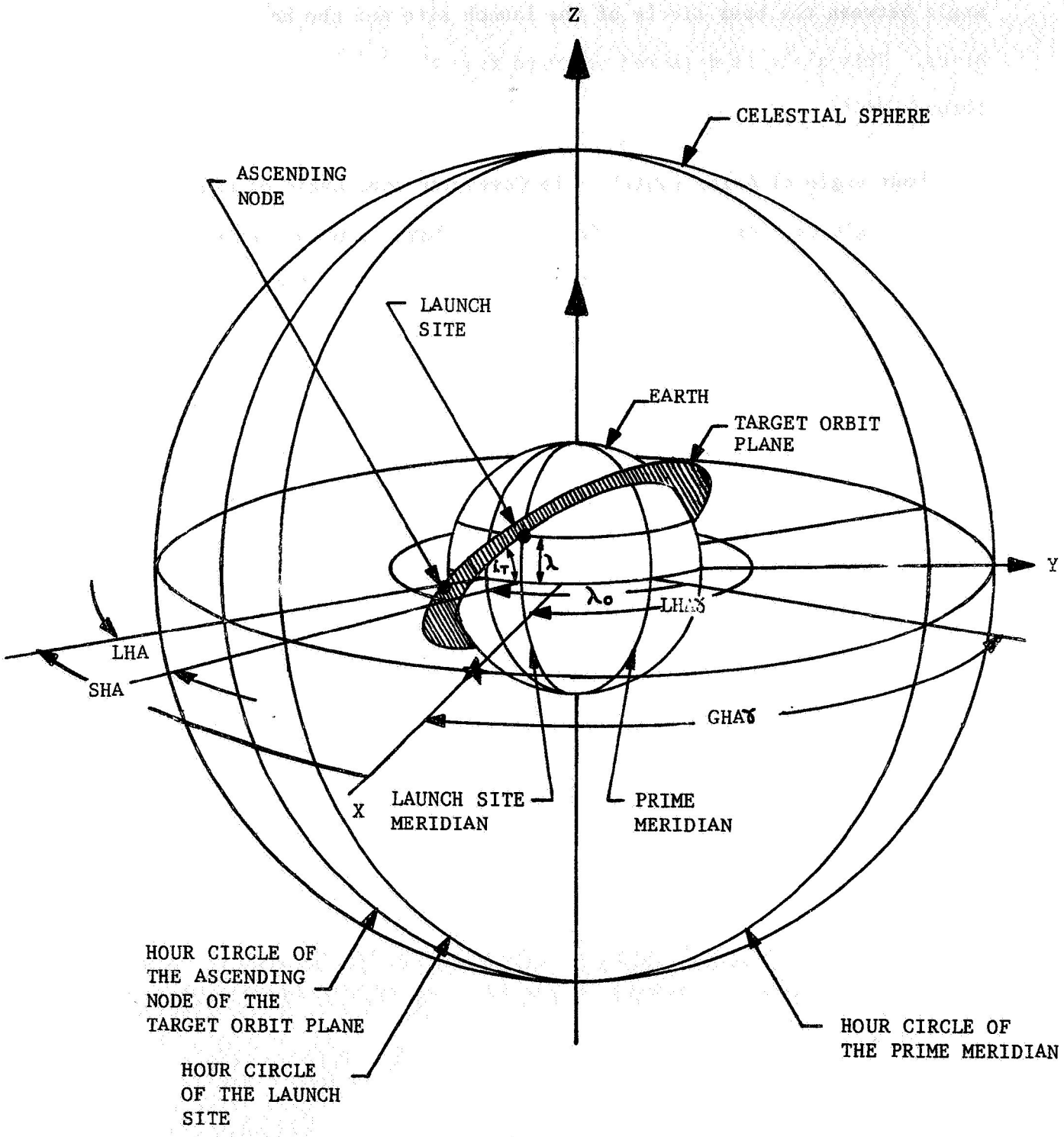

Figure A-1. CELESTIAL SPHERE AND THE EARTH

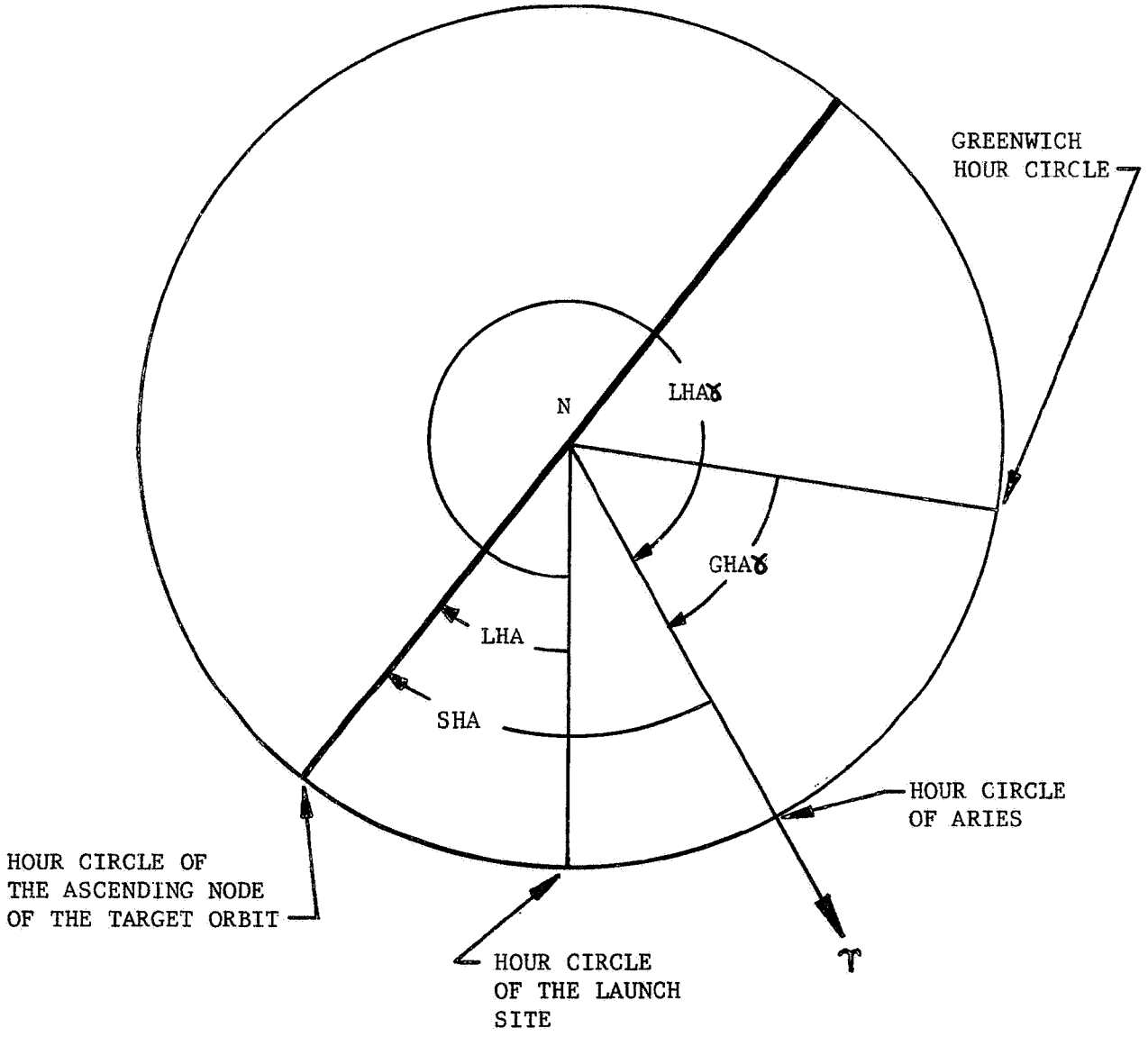

Figure A-2. CELESTIAL SPHERE AS VIEWED FROM THE NORTH POLE

APPENDIX B

TRIGONOMETRIC EQUATIONS FOR THE ASCENT TRAJECTORY MODES

This appendix presents the geometrical relationships for each ascent trajectory mode and the associated equations. These equations were developed assuming that the total intercept range angle θ_I was a variable, (for $\theta_I = 90$ degrees, minimum plane-change angle occurs). Furthermore, each ascent trajectory mode is restricted by range safety constraints placed on the launch azimuth, A_Z, and by the launch vehicle's capabilities to perform plane-change maneuvers. Thus, depending on these restrictions, the launch times for a given mission can be determined by examining all acceptable values of θ_I for the various ascent geometry cases, at each time point, $(t_d)_n$, after $(t_d)_n = 0$, for a given period of time.

With reference to Figure B-1, the following equations are required for determining the launch azimuth for the Coplanar Ascent Trajectory Mode:

$$A_Z = \sin^{-1}\left[\frac{\cos i_T}{\cos \lambda}\right] \tag{B-1}$$

or

$$A_Z = \pi - \sin^{-1}\left[\frac{\cos i_T}{\cos \lambda}\right] \tag{B-2}$$

With reference to Figure B-2, the equations applicable to Ascent Trajectory Mode 1 are as follows:

The central angle measured along the equator from the ascending node of the target orbit to the launch site meridian can be written as:

$$LHA = \sin^{-1}\left[\frac{\tan \lambda}{\tan i_T}\right] \tag{2-7}$$

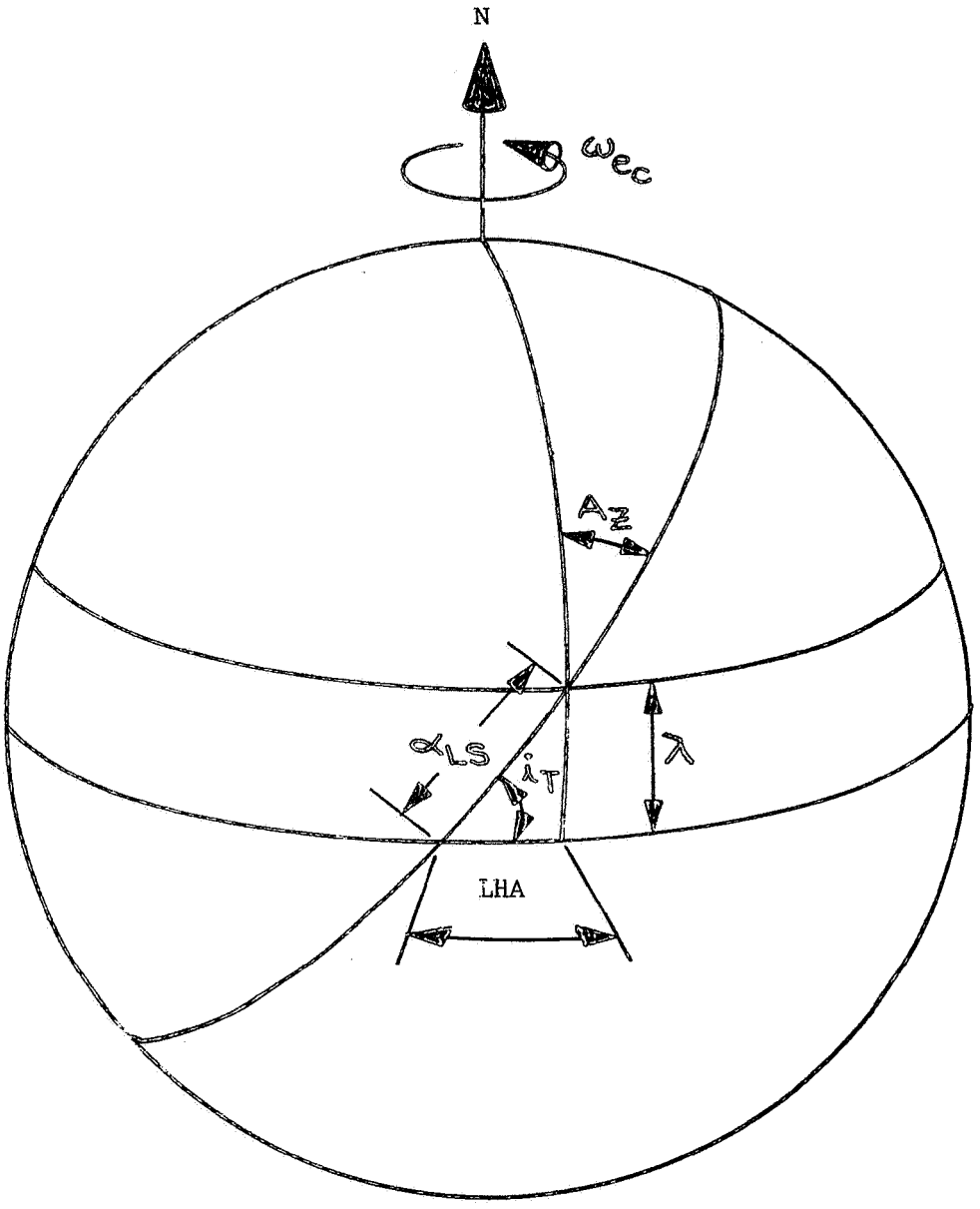

Figure B-1. COPLANAR ASCENT TRAJECTORY MODE GEOMETRY

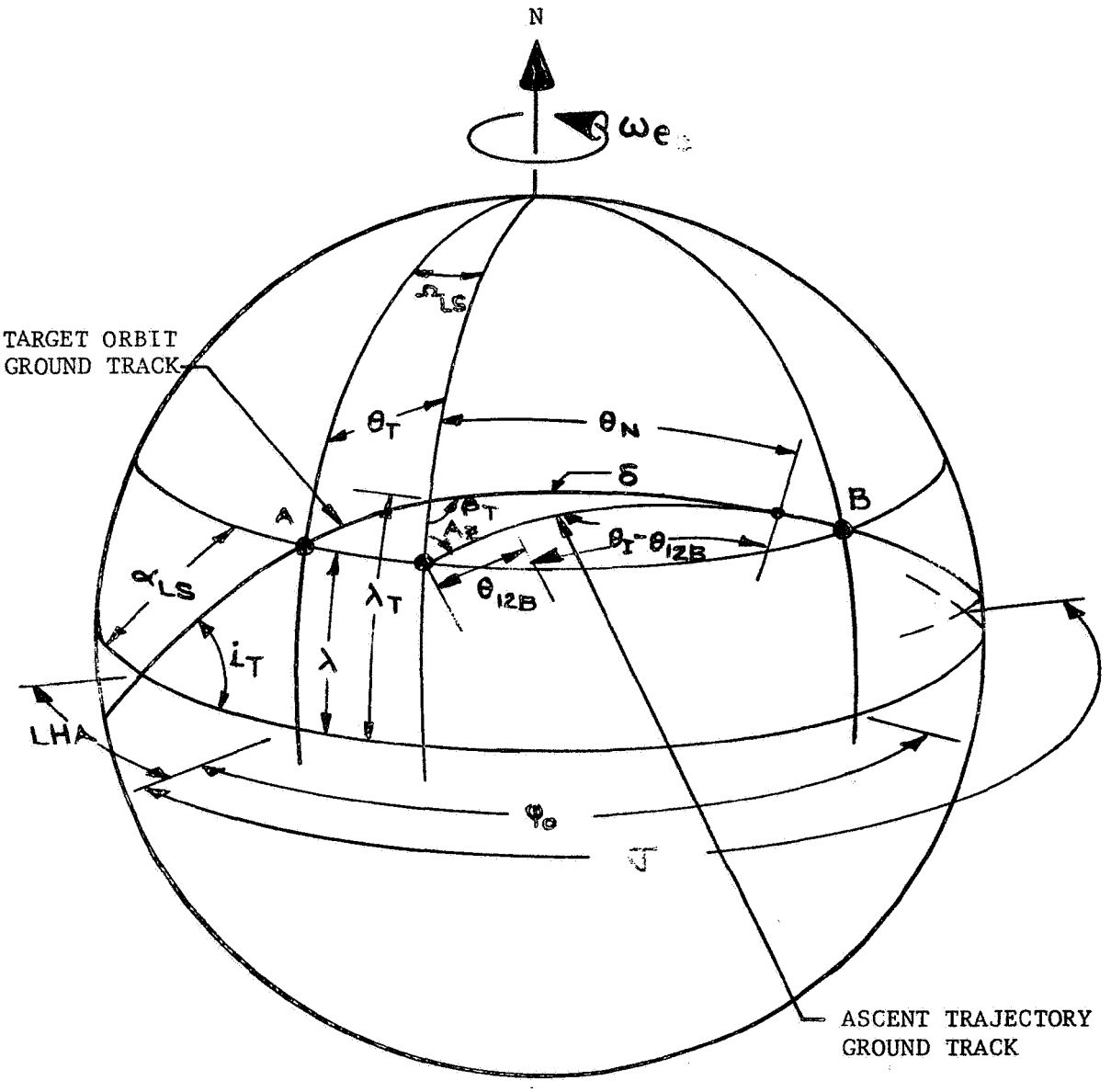

Figure B-2. ASCENT TRAJECTORY MODE 1 GEOMETRY

During a launch delay time of $(t_d)_n$, the Earth rotates through the angle Ω_{LS}, where

$$\Omega_{LS} = \omega_{e_c} (t_d)_n \tag{2-10}$$

The angle Ω_{LS} is the central angle measured from the launch site meridian at $(t_d)_n = 0$ to the launch site meridian at time $(t_d)_n$.

The latitude of the target orbit ground track when it intersects the launch site meridian at time $(t_d)_n$ is

$$\tan \lambda_T = \sin (\sigma - \Omega_{LS}) \tan i_T \tag{B-3}$$

where

$$\sigma = \psi_o + \text{LHA} \tag{B-4}$$

$$\psi_o = \pi - 2(\text{LHA}) \tag{3-1}$$

The angle ψ_o is the central angle measured from the launch site meridian at time $(t_d)_n = 0$ to the meridian passing through point B. Point B represents the point at which the target orbit ground track passes through the launch-site in a southerly direction. For Ascent Trajectory Mode 1, $\lambda_T > 0$.

The angle β_T is determined by the equation

$$\cos \beta_T = \cos(\sigma - \Omega_{LS}) \sin i_T \tag{B-5}$$

$$0 \leq \beta_T \leq \pi.$$

The plane-change angle, δ, can be computed from

$$\sin \delta = \frac{\sin(\lambda_T - \lambda) \sin \beta_T}{\sin \theta_I} \tag{B-6}$$

The central angle, measured in the target orbit plane, from the launch site meridian at $(t_d)_n = 0$ to the launch site meridian at $(t_d)_n$ is θ_T, and is determined by the equation

$$\cos \theta_T = \sin \lambda_T \sin\lambda + \cos \lambda_T \cos \lambda \cos \Omega_{LS} \qquad \text{(B-7)}$$

$$0 < \theta_T < \pi/2.$$

The angle θ_N is the central angle measured in the target orbit plane from the intersection of the target orbit ground track and the launch site meridian at $(t_d)_n$ to the intersection of the ascent trajectory plane and the target orbit plane (orbital line of nodes). This angle can be found by the equation

$$\tan \tfrac{1}{2}_N = \tan \tfrac{1}{2} [\theta_I + (\lambda_T - \lambda)] \left[\frac{\cos \tfrac{1}{2}(\beta_T + \delta)}{\cos \tfrac{1}{2}(\beta_T - \delta)}\right] \qquad \text{(B-8)}$$

The launch azimuth, A_Z, is determined by:

$$\cot \tfrac{1}{2}A_Z = \tan \tfrac{1}{2}(\beta_T + \delta) \left\{\frac{\cos \tfrac{1}{2} [\theta_I + (\lambda_T - \lambda)]}{\cos \tfrac{1}{2} [\theta_I - (\lambda_T - \lambda)]}\right\} \qquad \text{(B-9)}$$

With reference to Figure B-3, the equations applicable to Ascent Trajectory Mode 2 are:

$$\text{LHA} = \sin^{-1}\left[\frac{\tan \lambda}{\tan i_T}\right] \qquad \text{(2-7)}$$

$$\Omega_{LS} = \omega_e (t_d)_n \qquad \text{(2-10)}$$

$$\psi_o = \pi - 2(\text{LHA}) \qquad \text{(3-1)}$$

$$\sigma = \psi_o + \text{LHA} \qquad \text{(B-4)}$$

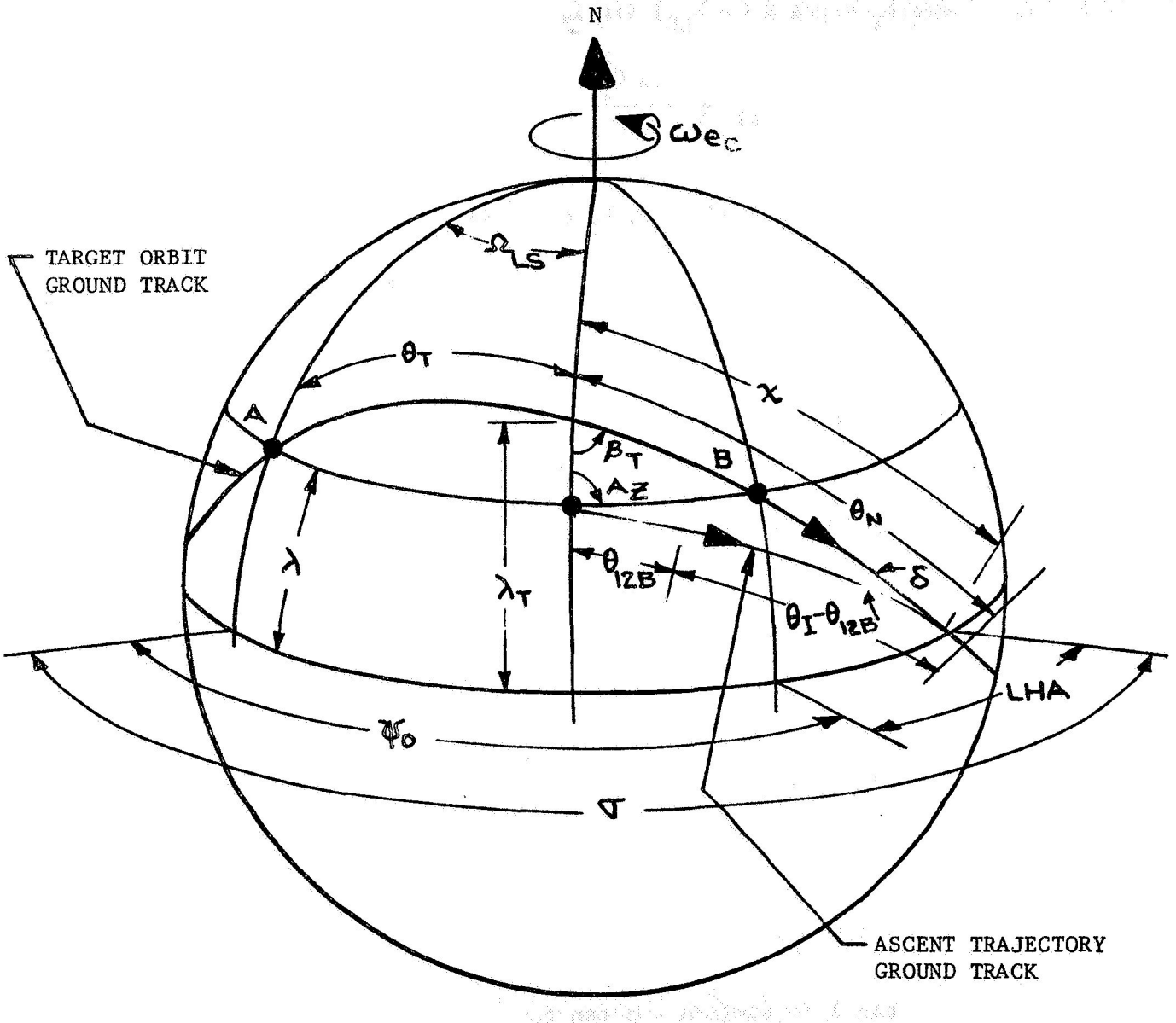

Figure B-3. ASCENT TRAJECTORY MODE 2 GEOMETRY

$$\tan \lambda_T = \sin (\sigma - \Omega_{LS}) \tan i_T \qquad \text{(B-3)}$$

$$\cos \beta_T = \cos (\sigma - \Omega_{LS}) \sin i_T \qquad \text{(B-5)}$$

$$\sin \delta = \frac{\sin(\lambda_T - \lambda)\sin \beta_T}{\sin \theta_I} \qquad \text{(B-6)}$$

$$\cos \theta_T = \sin \lambda_T \sin\lambda + \cos \lambda_T \cos \lambda \cos \Omega_{LS} \qquad \text{(B-7)}$$

$$\tan\tfrac{1}{2} \theta_N = \tan\tfrac{1}{2} [\theta_I + (\lambda_T - \lambda)] \left[\frac{\cos\tfrac{1}{2}(\beta_T + \delta)}{\cos\tfrac{1}{2}(\beta_T - \delta)}\right] \qquad \text{(B-8)}$$

$$\cot\tfrac{1}{2}A_Z = \tan\tfrac{1}{2}(\beta_T + \delta) \left\{\frac{\cos\tfrac{1}{2} [\theta_I + (\lambda_T - \lambda)]}{\cos\tfrac{1}{2} [\theta_I - (\lambda_T - \lambda)]}\right\} \qquad \text{(B-9)}$$

With reference to Figure B-4, the equations applicable to Ascent Trajectory Mode 3 are:

$$LHA = \sin^{-1} \left[\frac{\tan \lambda}{\tan i_T}\right] \qquad \text{(2-7)}$$

$$\Omega_{LS} = \omega_e (t_d)_n \qquad \text{(2-10)}$$

$$\psi_o = \pi - 2(LHA) \qquad \text{(3-1)}$$

$$\sigma = \Omega_{LS} - \psi_o \qquad \text{(B-10)}$$

$$\tan \lambda_T = \sin(LHA - \rho)\tan i_T \qquad \text{(B-11)}$$

$$\cos \beta_T = \cos(LHA - \rho)\sin i_T \qquad \text{(B-12)}$$

$$\sin\delta = \frac{\sin(\lambda_T - \lambda) \sin\beta_T}{\sin\theta_I} \qquad \text{(B-6)}$$

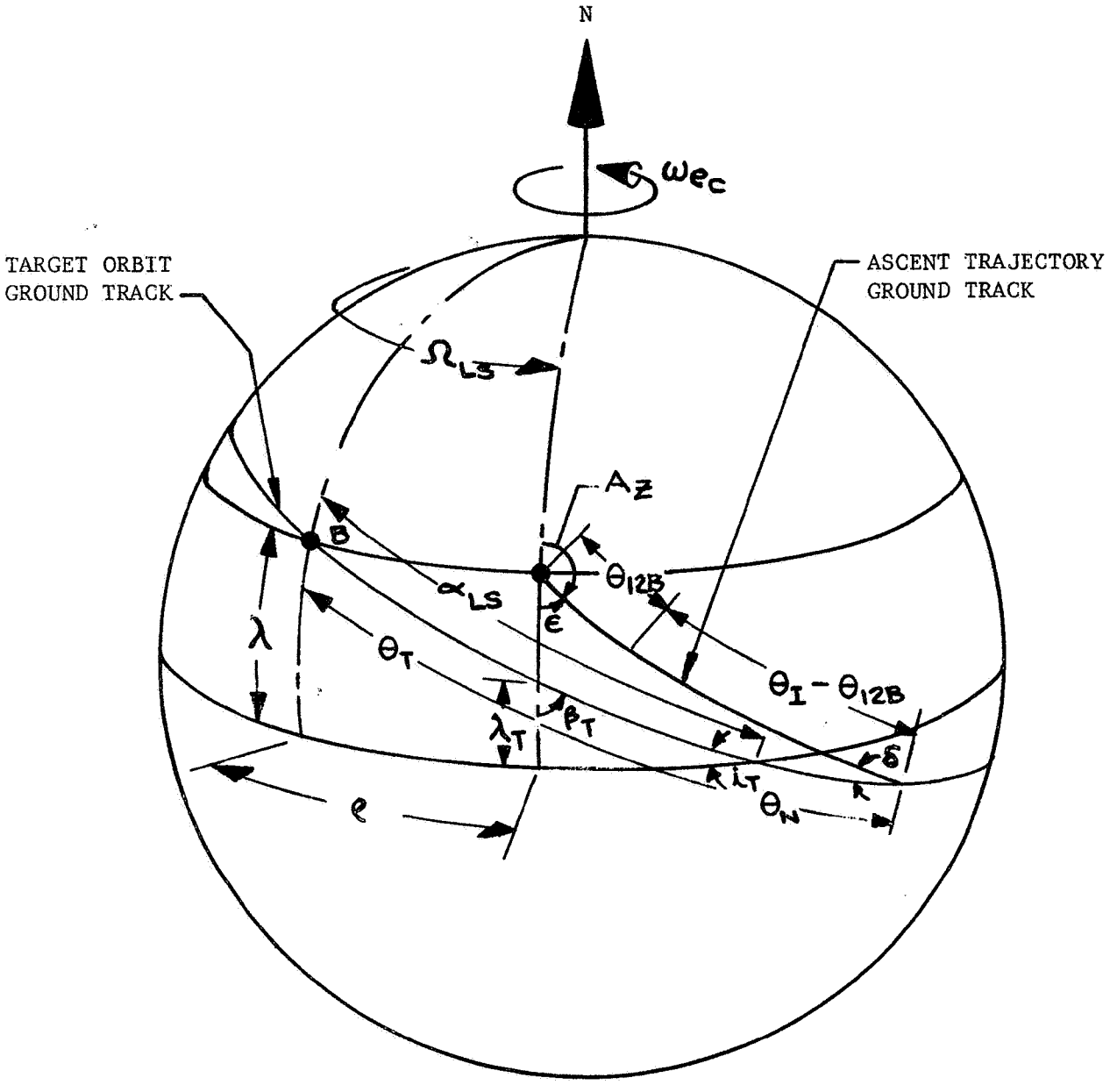

Figure B-4. ASCENT TRAJECTORY MODE 3 GEOMETRY

$$\cos\ \theta_T = \sin\ \lambda_T\ \sin\lambda + \cos\ \lambda_T\ \cos\lambda\ \cos\rho \tag{B-13}$$

$$\tan\tfrac{1}{2}\ \theta_N = \tan\tfrac{1}{2}[\theta_I + (\lambda_T - \lambda)]\left\{\frac{\cos\ \frac{1}{2}\ [(\pi - \beta_T) + \delta]}{\cos\ \frac{1}{2}\ [(\pi - \beta_T) - \delta]}\right\} \tag{B-14}$$

$$\cot\tfrac{1}{2}\ = \tan\tfrac{1}{2}\ [(\pi - \beta_T) + \delta\ ]\ \left\{\frac{\cos\tfrac{1}{2}[\theta_I + (\lambda_T - \lambda)]}{\cos\tfrac{1}{2}[\theta_I - (\lambda_T - \lambda)]}\right\} \tag{B-15}$$

$$A_Z = \pi - \varepsilon \tag{B-16}$$

With reference to Figure B-5, the equations applicable to Ascent Trajectory Mode 4 are:

$$\mathrm{LHA} = \sin^{-1}\left[\frac{\tan\ \lambda}{\tan\ i_T}\right] \tag{2-7}$$

$$\Omega_{LS} = \omega_e(t_d)_n \tag{2-10}$$

$$\rho\ = 2\pi - \Omega_{LS} \tag{B-17}$$

$$\psi_o = \pi - 2(\mathrm{LHA}) \tag{3-1}$$

$$\tan\ \lambda_T = \sin(\mathrm{LHA} - \rho\ )\tan\ i_T \tag{B-11}$$

$$\cos\ \beta_T = \cos(\mathrm{LHA} - \rho\ )\sin\ i_T \tag{B-12}$$

$$\sin\ \delta = \frac{\sin(\lambda_T - \lambda)\ \sin\ \beta_T}{\sin\ \theta_I} \tag{B-6}$$

$$\cos\theta_T = \sin\lambda_T\ \sin\lambda + \cos\lambda_T\ \cos\lambda\ \cos\rho \tag{B-13}$$

$$\tan\tfrac{1}{2}\ \theta_{NT} = \tan\tfrac{1}{2}[\theta_I + (\lambda_T - \lambda)]\left\{\frac{\cos\tfrac{1}{2}[(\pi - \beta_T) + \delta]}{\cos\tfrac{1}{2}[(\pi - \beta_T) - \delta]}\right\} \tag{B-18}$$

$$\cot\tfrac{1}{2}\varepsilon = \tan\tfrac{1}{2}\ [(\pi - \beta_T) + \delta]\left\{\frac{\cos\tfrac{1}{2}\ [\theta_I + (\lambda_T - \lambda)]}{\cos\tfrac{1}{2}\ [\theta_I - (\lambda_T - \lambda)]}\right\} \tag{B-15}$$

$$A_Z = \pi - \varepsilon \tag{B-16}$$

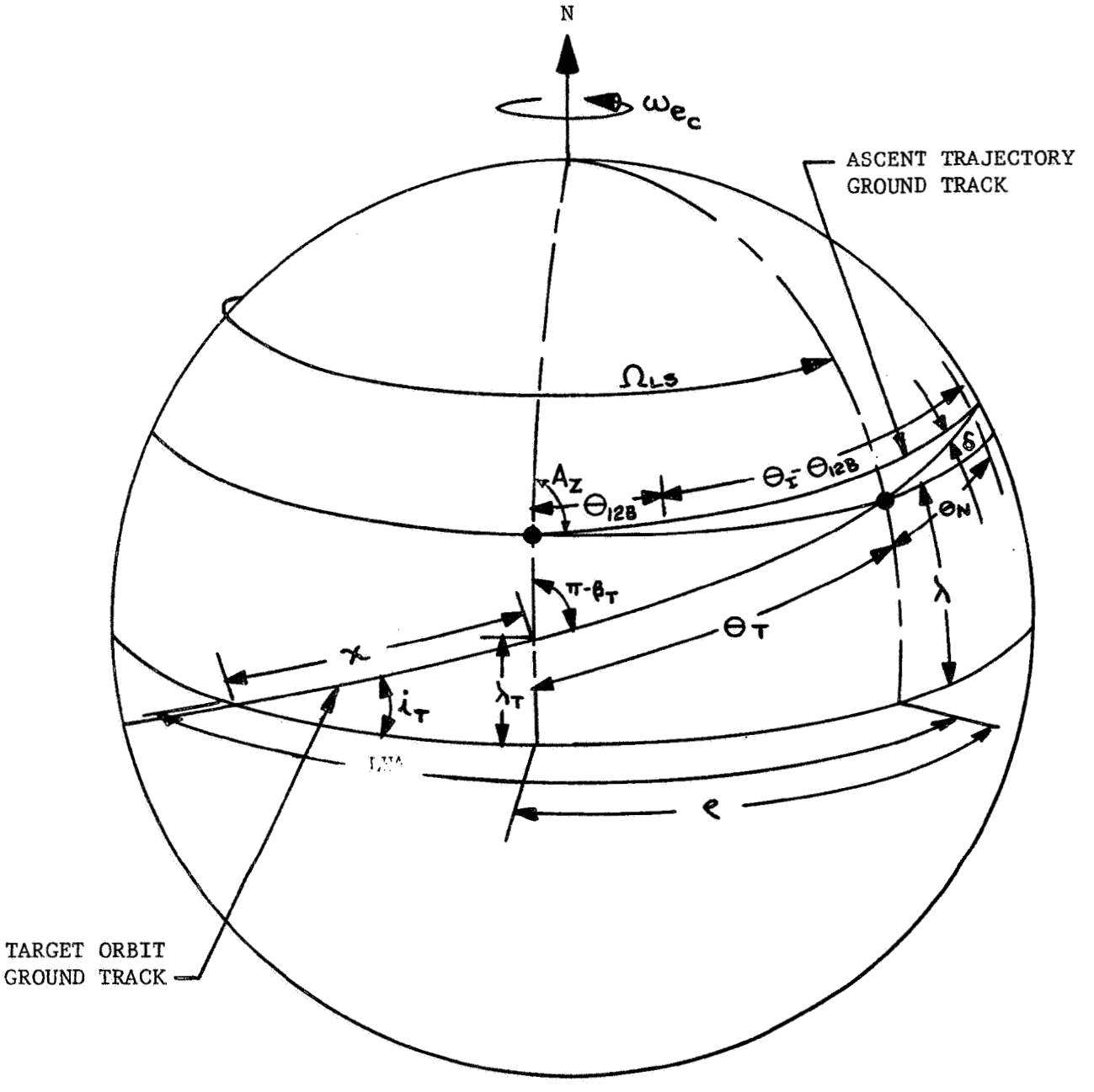

Figure B-5. ASCENT TRAJECTORY MODE 4 GEOMETRY

With reference to Figure B-6, the equations applicable to Ascent Trajectory Mode 5 are:

$$\sigma = \pi/2 \tag{B-19}$$

$$\Omega_{LS} = \omega_e(t_d)_n \tag{2-10}$$

$$\tan\lambda_T = \sin(\sigma - \Omega_{LS})\tan i_T \tag{B-3}$$

$$\cos\beta_T = \cos(\sigma - \Omega_{LS})\ \sin i_T \tag{B-5}$$

$$\sin\delta = \frac{\sin(\lambda_T - \lambda)\sin\beta_T}{\sin\theta_I} \tag{B-6}$$

$$\cos\theta_T = \sin\lambda_T\ \sin\lambda + \cos\lambda_T\ \cos\lambda\ \cos\Omega_{LS} \tag{B-7}$$

$$\tan\tfrac{1}{2}\theta_N = \tan\tfrac{1}{2}\ [\theta_I + (\lambda_T - \lambda)]\left\{\frac{\cos\tfrac{1}{2}[(\pi - \beta_T) + \delta]}{\cos\tfrac{1}{2}[(\pi - \beta_T) - \delta]}\right\} \tag{B-14}$$

$$\cot\tfrac{1}{2}\varepsilon = \tan\tfrac{1}{2}[(\pi - \beta_T) + \delta]\left\{\frac{\cos\tfrac{1}{2}[\theta_I + (\lambda_T - \lambda)]}{\cos\tfrac{1}{2}[\theta_I - (\lambda_T - \lambda)]}\right\} \tag{B-15}$$

$$A_Z = \pi - \varepsilon \tag{B-16}$$

With reference to Figure B-7, the equations applicable to Ascent Trajectory Mode 6 are:

$$\sigma = \pi/2 \tag{B-19}$$

$$\Omega_{LS} = \omega_e(t_d)_n \tag{2-10}$$

$$\rho = 2\pi - \Omega_{LS} \tag{B-17}$$

$$\tan\lambda_T = \sin(\sigma - \rho)\sin i_T \tag{B-20}$$

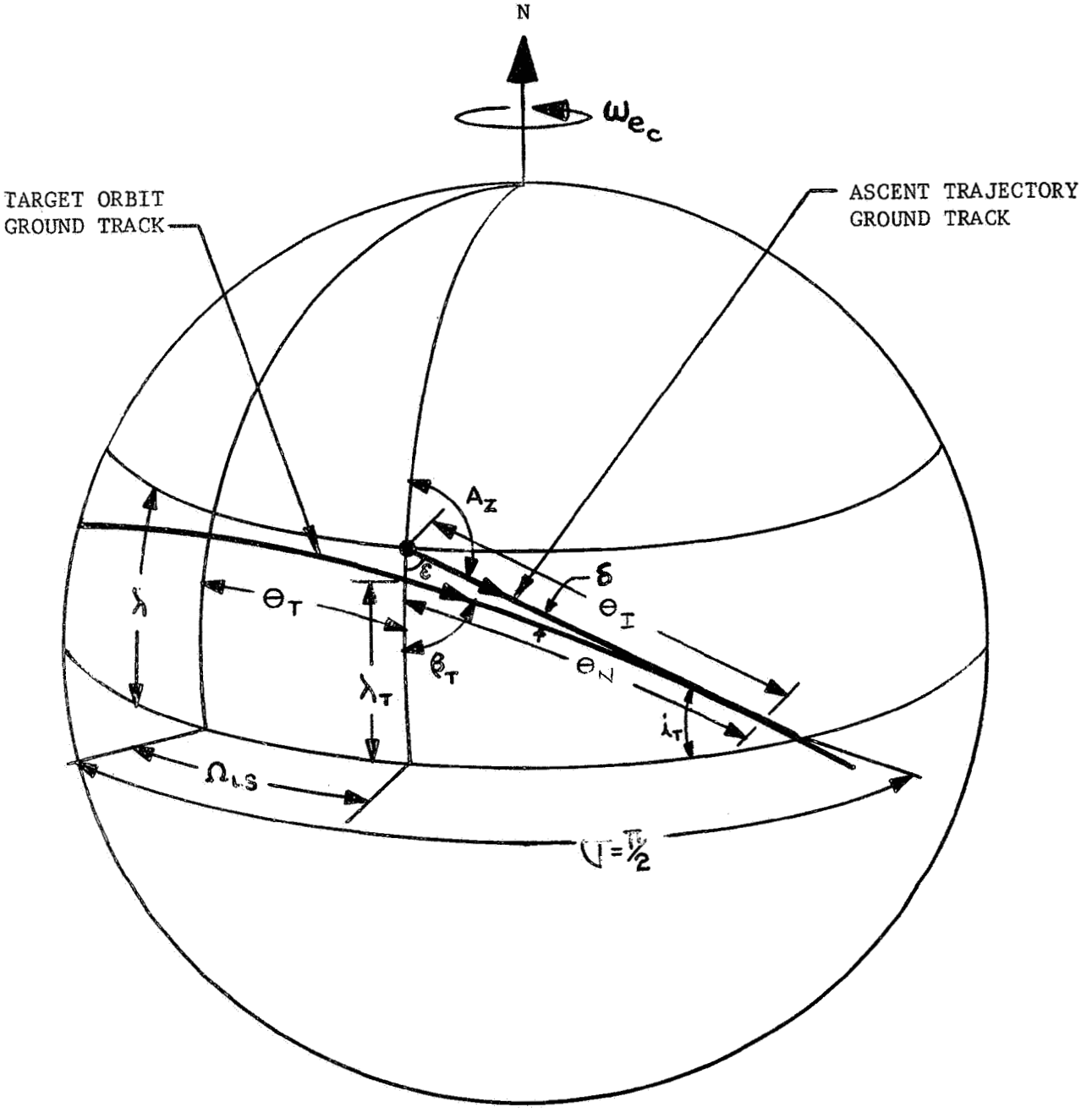

Figure B-6. ASCENT TRAJECTORY MODE 5 GEOMETRY

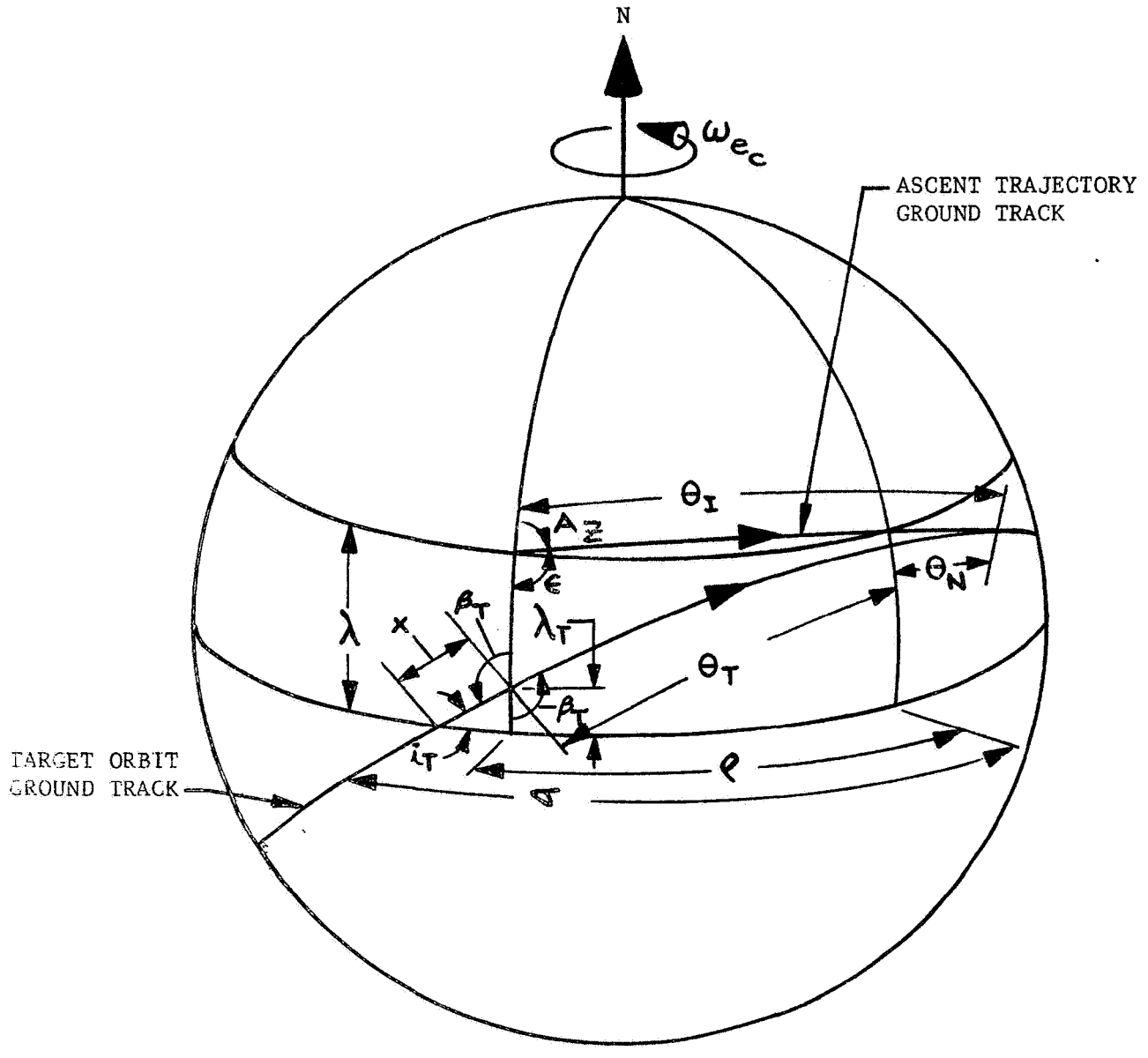

Figure B-7. ASCENT TRAJECTORY MODE 6 GEOMETRY

$$\cos\beta_T = \cos(\sigma - \rho)\sin i_T \tag{B-21}$$

$$\sin\delta = \frac{\sin(\lambda_T - \lambda)\sin\beta_T}{\sin\theta_I} \tag{B-6}$$

$$\cos\theta_T = \sin\lambda_T \sin\lambda + \cos\lambda_T \cos\lambda \cos\rho \tag{B-13}$$

$$\tan\tfrac{1}{2}\theta_{NI} = \tan\tfrac{1}{2}[\theta_I + (\lambda_T - \lambda)]\left\{\frac{\cos\tfrac{1}{2}[(\pi - \beta_T) + \delta]}{\cos\tfrac{1}{2}[(\pi - \beta_T) - \delta]}\right\} \tag{B-18}$$

$$\cot\tfrac{1}{2}\varepsilon = \tan\tfrac{1}{2}[(\pi - \beta_T) + \delta]\left\{\frac{\cos\tfrac{1}{2}[\theta_I + (\lambda_T - \lambda)]}{\cos\tfrac{1}{2}[\theta_I - (\lambda_T - \lambda)]}\right\} \tag{B-15}$$

$$A_Z = \pi - \varepsilon \tag{B-16}$$

APPENDIX C

ADDITIONAL EQUATIONS FOR COPLANAR ORBITAL TRANSFER MODES

This appendix presents a brief listing of the coplanar orbital transfer modes generated by the Orbital Transfer Mode Matrix and any additional equations that may be needed for their complete solution.

REFERENCE AXIS AND MAJOR AXIS
OF THE TRANSFER ELLIPSE

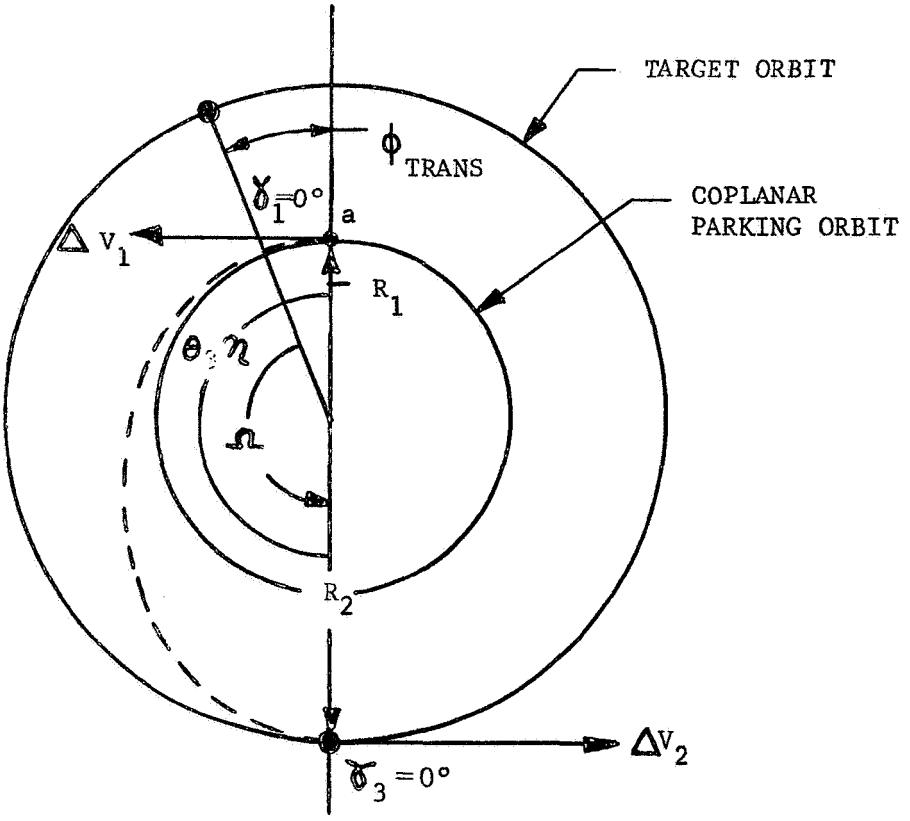

$$\theta_1 = 0°$$

$$\eta = \pi$$

Figure C-1. HOHMANN TRANSFER MODE

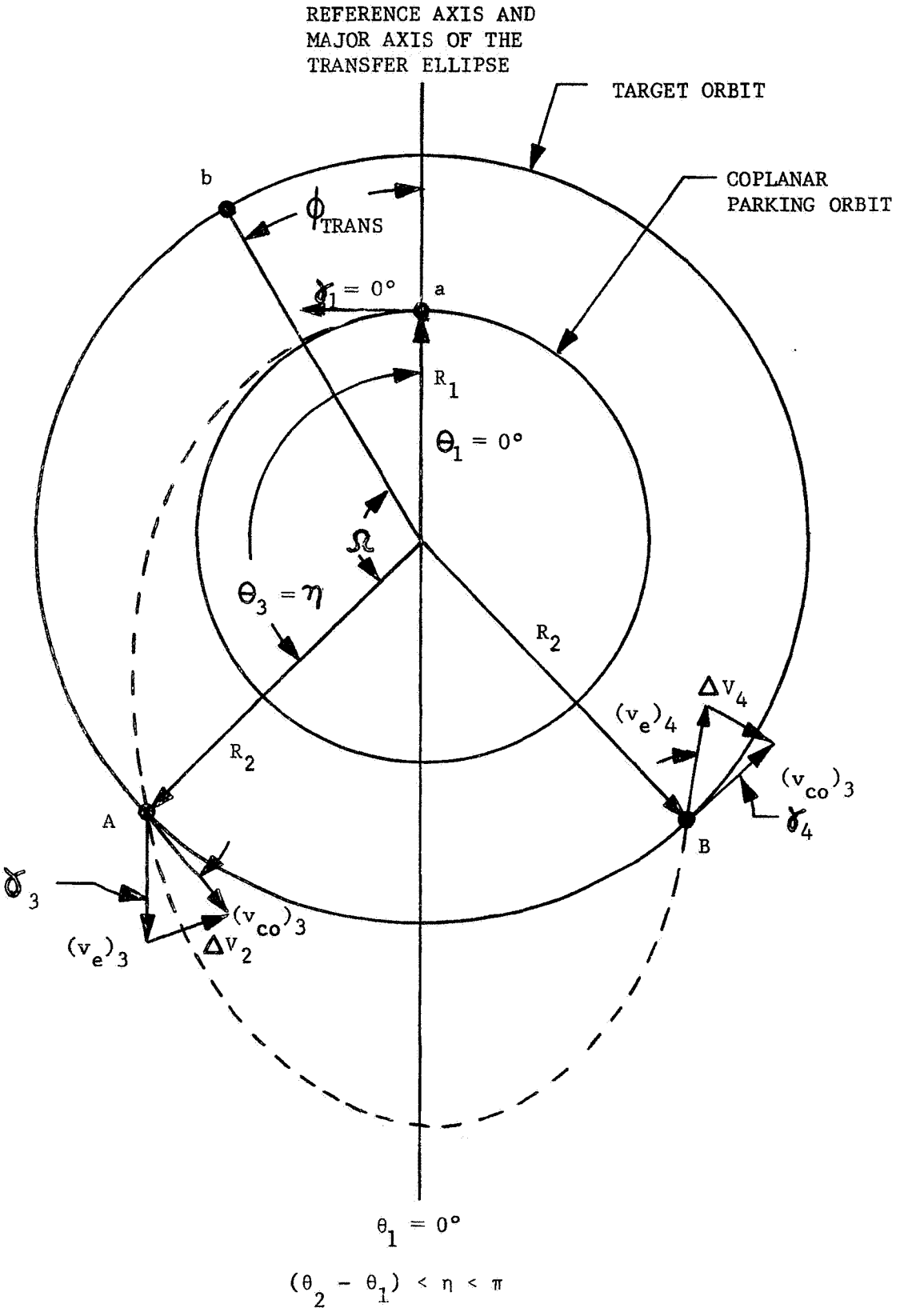

Figure C-2. MODIFIED HOHMANN TRANSFER MODE

NOTE: See Coplanar Gamma-Change Transfer Mode for the equations for "Rendezvous at B".

With reference to Figure C-3, the following equations are required for "Rendezvous at B."

$$\theta_3 = \theta_1 + \eta \tag{3-55}$$

$$\theta_4 = 2\pi - \theta_3 \tag{C-1}$$

$$e = \frac{R_2 - R_1}{R_1 \cos\theta_1 - R_2 \cos\theta_4} \tag{3-57}$$

$$\sin E_1 = \sin^{-1} \frac{(1 - e^2)^{\frac{1}{2}} \sin\theta_1}{1 + e\cos\theta_1} \tag{3-60a}$$

$$E_1 = \sin^{-1} \frac{(1 - e^2)^{\frac{1}{2}} \sin\theta_1}{1 + e\cos\theta_4} \tag{3-60b}$$

$$\sin E_4 = \frac{(1 - e^2)^{\frac{1}{2}} \sin\theta_4}{1 + e\cos\theta_4} \tag{C-2a}$$

$$E_4 = \sin^{-1} \frac{(1 - e^2)^{\frac{1}{2}} \sin\theta_4}{1 + e\cos\theta_4} \tag{C-2b}$$

$$M_1 = E_1 - e \sin E_1 \tag{3-62}$$

$$M_4 = E_4 - e \sin E_4 \tag{C-4}$$

$$(t_F)_{TRANS} = (M_4 - M_1)\sqrt{\frac{a^3}{\mu}} \tag{C-5}$$

$$\omega_2 = \sqrt{\frac{\mu}{R_2^3}} \tag{3-67}$$

$$\phi_{TRANS} = \eta - \omega_2 (t_F)_{TRANS} \tag{3-68}$$

$$\gamma_1 = \left| \tan^{-1} \left[\frac{e \sin\theta_1}{1 + e \cos\theta_1} \right] \right| \tag{3-69b}$$

$$(v_{co})_1 = \sqrt{\frac{\mu}{R_1}} \tag{3-70}$$

$$(v_e)_1 = \sqrt{\frac{2\mu}{R_1} - \frac{\mu}{a}} \tag{3-71}$$

$$\Delta V_1 = \left| \left[(v_e)_1^2 + (v_{co})_1^2 - 2(v_e)_1 (v_{co})_1 \cos\gamma_1 \right]^{\frac{1}{2}} \right| \tag{3-72}$$

$$\gamma_4 = \left| \tan^{-1} \left[\frac{e \sin\theta_4}{1 + e \cos\theta_4} \right] \right| \tag{C-6}$$

$$(v_{co})_3 = \sqrt{\frac{\mu}{R_2}} \tag{3-74}$$

$$(v_e)_4 = \sqrt{\frac{2}{R_2} - \frac{\mu}{a}} \tag{C-7}$$

$$\Delta V_4 = \left| \left[(v_e)_4^2 + (v_{co})_3^2 - 2(v_e)_4 (v_{co})_3 \cos\gamma_4 \right]^{\frac{1}{2}} \right| \tag{C-8}$$

$$(\Delta V)_{TRANS} = \Delta V_1 + \Delta V_4 \tag{C-9}$$

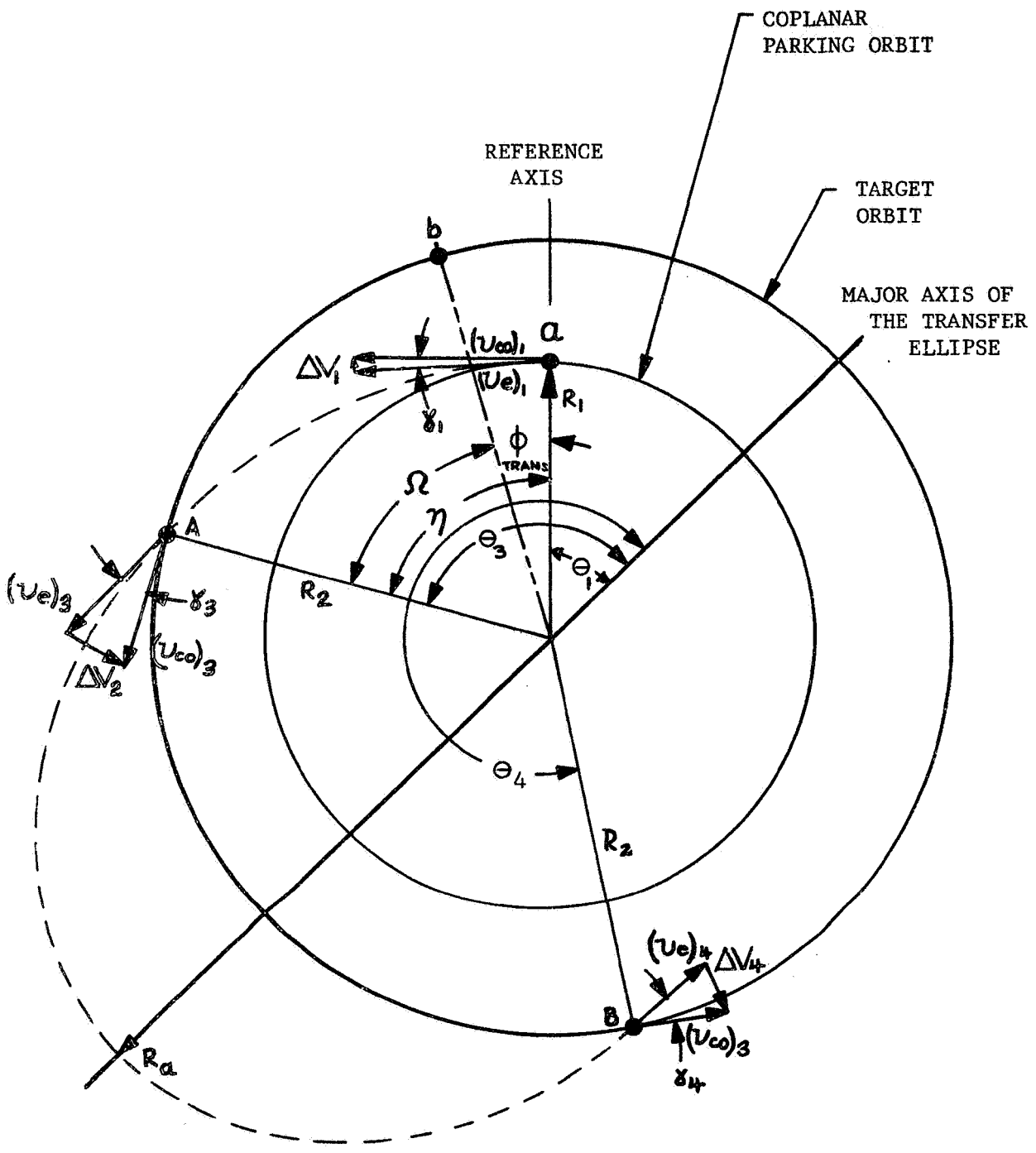

$$0 \leq \theta_1 < 2\pi$$

$$(\theta_2 - \theta_1) < \eta < (\pi - \theta_1)$$

Figure C-3. GAMMA-CHANGE TRANSFER MODE

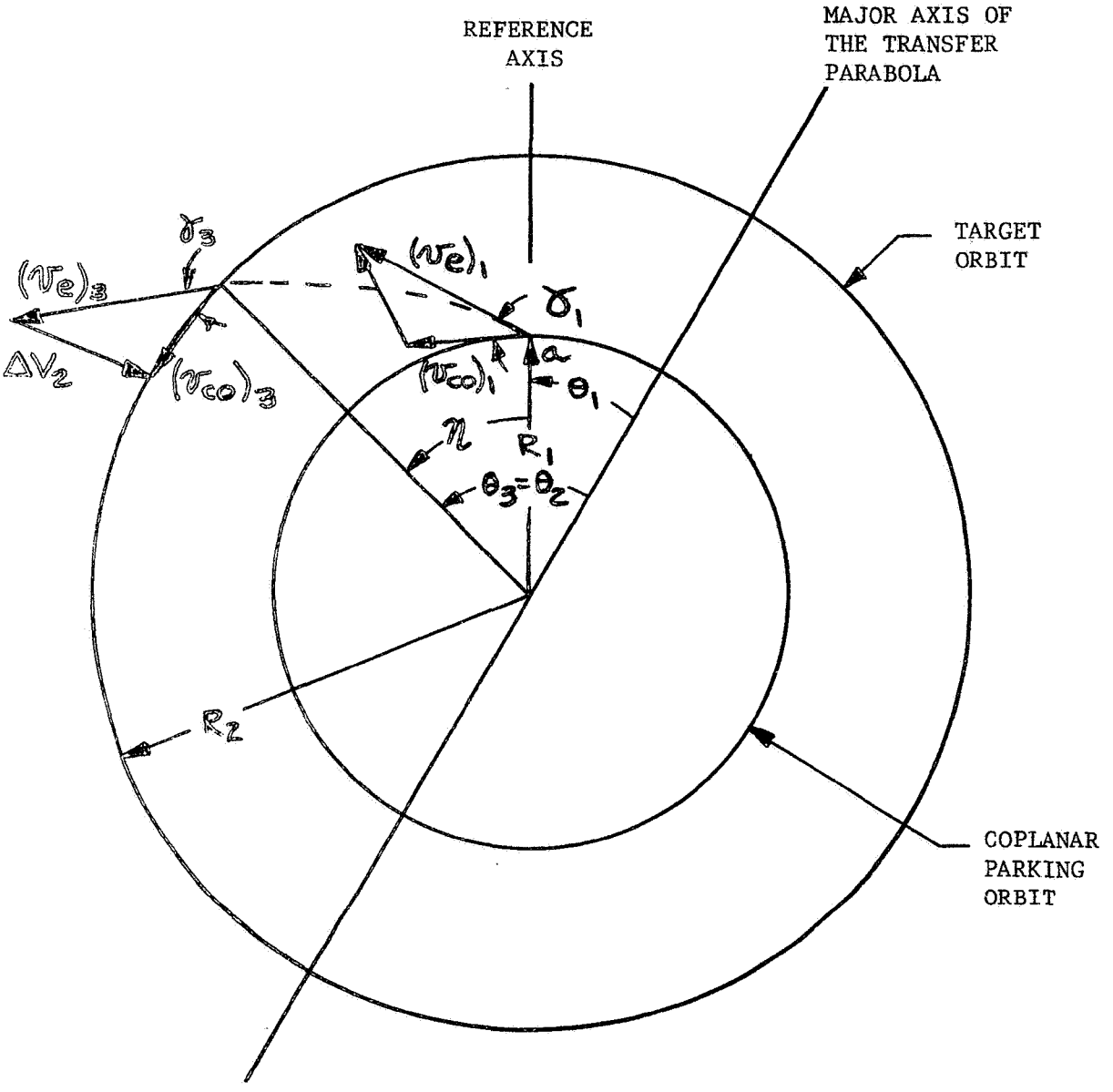

$$0 \leq \theta_1 < 2\pi$$

$$\eta = \theta_2 - \theta_1$$

Figure C-4. PARABOLIC TRANSFER MODE

With reference to Figure C-5, the following equations are needed for the Concentric Three-Impulse Elliptic Transfer Mode.

$$e = \frac{R_2 - R_1}{R_1\cos\theta_1 - R_2\cos\theta_3} \tag{3-57}$$

$$P = R_1(1 + e\cos\theta_1) \tag{3-58}$$

$$a = \frac{P}{1 - e^2} \tag{3-59}$$

$$\sin E_1 = \frac{(1 - e^2)^{\frac{1}{2}}\sin\theta_1}{1 + e\cos\theta_1} \tag{3-60a}$$

$$E_1 = \sin^{-1}\left[\frac{(1 - e^2)^{\frac{1}{2}}\sin\theta_1}{1 + e\cos\theta_1}\right] \tag{3-60b}$$

$$\sin E_3 = \frac{(1 - e^2)^{\frac{1}{2}}\sin\theta_3}{1 + e\cos\theta_3} \tag{3-61a}$$

$$E_3 = \sin^{-1}\left[\frac{(1 - e^2)^{\frac{1}{2}}\sin\theta_3}{1 + e\cos\theta_3}\right] \tag{3-61b}$$

$$M_1 = E_1 - e\sin E_1 \tag{3-62}$$

$$M_3 = E_3 - e\sin E_3 \tag{3-63}$$

$$(t_F)_{E_1} = (M_3 - M_1)\sqrt{\frac{a^3}{\mu}} \tag{C-10}$$

R_{P_2} = chosen perigee radius of transfer ellipse 2

$$e_2 = \frac{R_2 - R_{P_2}}{R_2 + R_{P_2}} \tag{C-11}$$

$$a_2 = \frac{R_{P_2} + R_2}{2} \tag{C-12}$$

$$(t_F)_{E_2} = 2\pi\sqrt{\frac{a_2^3}{\mu}} \tag{C-13}$$

$$(t_F)_{TRANS} = (t_F)_{E_1} + (t_F)_{E_2} \tag{C-14}$$

$$\omega_2 = \sqrt{\frac{\mu}{R_2^3}} \tag{3-67}$$

$$\phi_{TRANS} = \eta + 2\pi - \omega_2(t_F)_{TRANS} \tag{C-15}$$

$$(v_{co})_1 = \sqrt{\frac{\mu}{R_1}} \tag{3-70}$$

$$(v_e)_1 = \sqrt{\frac{2\mu}{R_1} - \frac{\mu}{a}} \tag{3-71}$$

$$\gamma_1 = \left|\tan^{-1}\left[\frac{e\sin\theta_1}{1 + e\cos\theta_1}\right]\right| \tag{3-69b}$$

$$\Delta V_1 = \left|\left[(v_e)_1^2 + (v_{co})_1^2 - 2(v_e)_1(v_{co})_1\cos\gamma_1\right]^{\frac{1}{2}}\right| \tag{3-72}$$

$$(v_a)_1 = \sqrt{\frac{2\mu}{R_2} - \frac{\mu}{a}} \tag{C-16}$$

$$(v_a)_2 = \sqrt{\frac{2\mu}{R_2} - \frac{\mu}{a_2}} \tag{C-17}$$

$$\Delta V_2 = (v_a)_2 - (v_a)_1 \tag{C-18}$$

$$(v_{co})_3 = \sqrt{\frac{\mu}{R_2}} \tag{3-75}$$

$$\Delta V_3 = (v_{co})_3 - (v_a)_2 \tag{C-19}$$

$$(\Delta V)_{TRANS} = \Delta V_1 + \Delta V_2 + \Delta V_3 \tag{C-20}$$

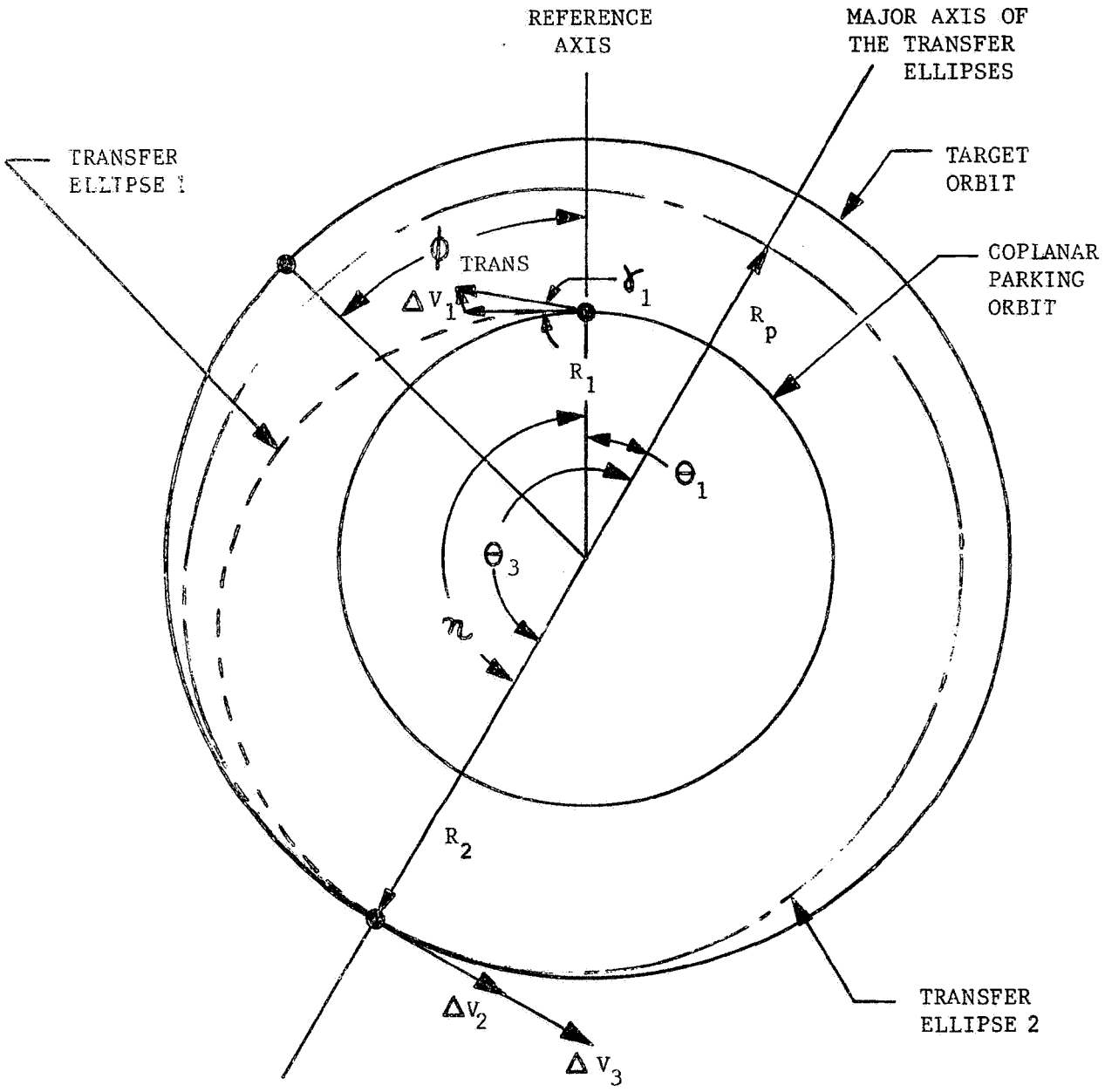

$$0 \leq \theta_1 < 2\pi$$

$$n = (\pi - \theta_1)$$

Figure C-5. CONCENTRIC THREE-IMPULSE ELLIPTIC TRANSFER MODE

With reference to Figure C-6, the following equations are needed for the Bi-Elliptic Three-Impulse Transfer Mode.

$$e = \frac{R_2 - R_1}{R_1\cos\theta_1 - R_2\cos\theta_3} \tag{3-57}$$

$$P = R_1(1 + e\cos\theta_1) \tag{3-58}$$

$$a = \frac{P}{1 - e^2} \tag{3-59}$$

$$\sin E_1 = \frac{(1 - e^2)^{\frac{1}{2}}\sin\theta_1}{1 + e\cos\theta_1} \tag{3-60a}$$

$$E_1 = \sin^{-1}\left[\frac{(1 - e^2)^{\frac{1}{2}}\sin\theta_1}{1 + e\cos\theta_1}\right] \tag{3-60b}$$

$$M_1 = E_1 - e\sin E_1 \tag{3-62}$$

$$M_a = \pi \tag{C-21}$$

$$(t_F)_{E_1} = (M_a - M_1)\sqrt{\frac{a^3}{\mu}} \tag{C-22}$$

$$R_a = a(1 + e) \tag{C-23}$$

$$e_2 = \frac{R_a - R_2}{R_a + R_2} \tag{C-24}$$

$$a_2 = \frac{R_a + R_2}{2} \tag{C-25}$$

$$(t_F)_{E_2} = \pi\sqrt{\frac{a_2^3}{\mu}} \tag{C-26}$$

$$(t_F)_{TRANS} = (t_f)_{E_1} + (t_f)_{E_2} \qquad (C\text{-}15)$$

$$\omega_2 = \sqrt{\frac{\mu}{R_2^3}} \qquad (3\text{-}67)$$

$$\phi_{TRANS} = (2\pi - \theta_1) - \omega_2 (t_F)_{TRANS} \qquad (C\text{-}27)$$

$$(v_{co})_1 = \sqrt{\frac{\mu}{R_1}} \qquad (3\text{-}70)$$

$$(v_e)_1 = \sqrt{\frac{2\mu}{R_1} - \frac{\mu}{a}} \qquad (3\text{-}71)$$

$$\gamma_1 = \left| \tan^{-1} \left[\frac{e \sin\theta_1}{1 + e \cos\theta_1} \right] \right| \qquad (3\text{-}69b)$$

$$\Delta V_1 = \left| \left[(v_e)_1^2 + (v_{co})_1^2 - 2(v_e)_1 (v_{co})_1 \cos\gamma_1 \right]^{\frac{1}{2}} \right| \qquad (3\text{-}72)$$

$$(v_a)_1 = \sqrt{\frac{2\mu}{R_a} - \frac{\mu}{a}} \qquad (C\text{-}28)$$

$$(v_a)_2 = \sqrt{\frac{2\mu}{R_a} - \frac{\mu}{a_2}} \qquad (C\text{-}29)$$

$$\Delta V_2 = (v_a)_2 - (v_a)_1 \qquad (C\text{-}18)$$

$$(v_{co})_3 = \sqrt{\frac{\mu}{R_2}} \qquad (3\text{-}75)$$

$$(v_p)_2 = \sqrt{\frac{2\mu}{R_2} - \frac{\mu}{a_2}} \qquad (C\text{-}30)$$

$$\Delta V_3 = (v_{co})_3 - (v_p)_2 \qquad (C\text{-}31)$$

$$(\Delta V)_{TRANS} = \Delta V_1 + \Delta V_2 + \Delta V_3 \qquad (C\text{-}20)$$

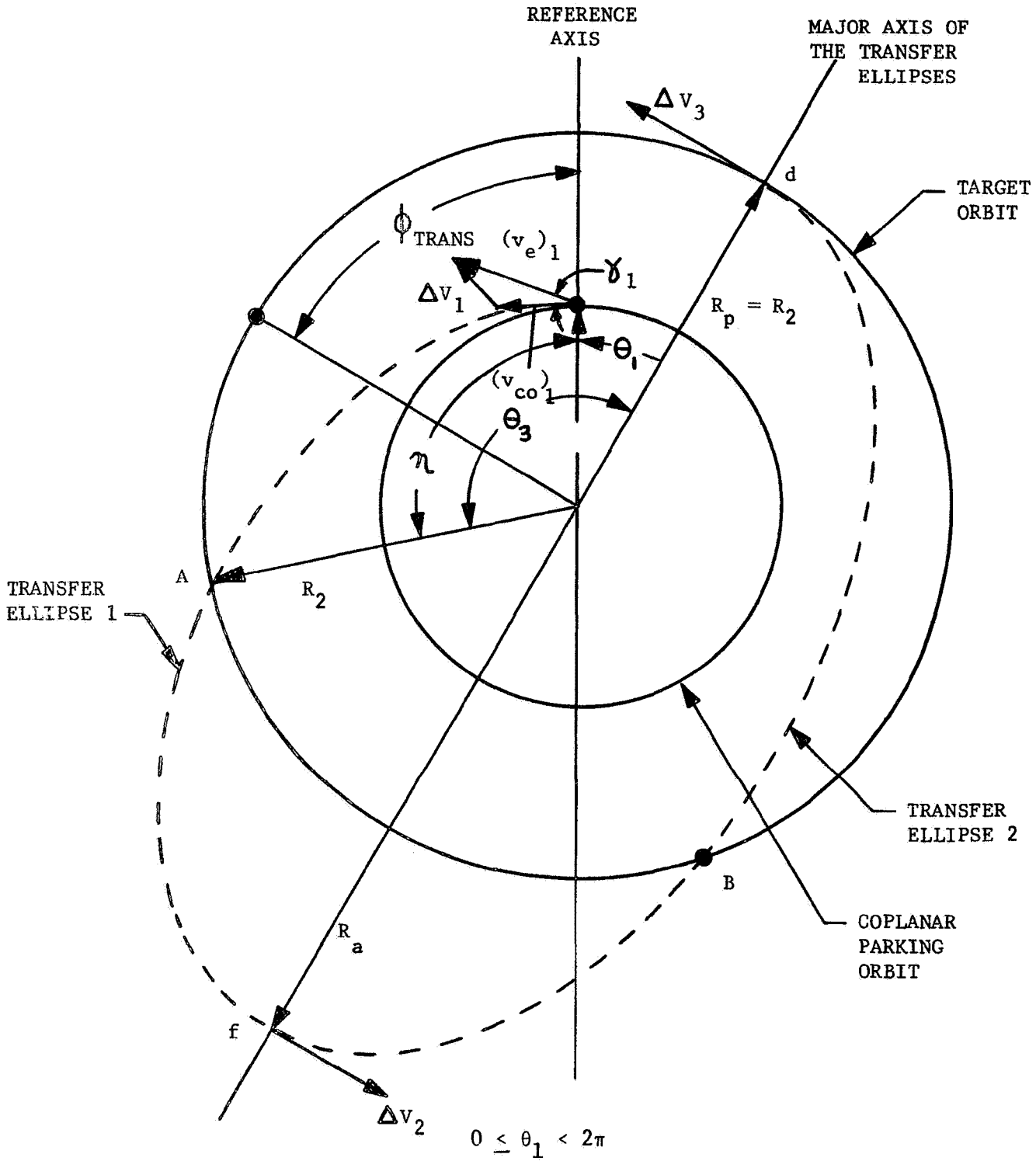

Figure C-6. BI-ELLIPTIC THREE-IMPULSE TRANSFER MODE

APPENDIX D

ADDITIONAL EQUATIONS REQUIRED FOR NON-COPLANAR ORBITAL TRANSFER MODES

This appendix presents the additional equations required to determine the orbital transfer parameters if the point of departure and the point of arrival on the fictitious target orbit (points a and A, respectively, in Figure D-1) lie on the same side of the orbital line of nodes.

The position of the chaser at the end of required parking time, relative to the orbital line of nodes, is

$$\theta_{COLN} = \omega_1(t_{PARK}) \tag{3-85}$$

The point of orbital transfer departure (a) and the point of arrival on the fictitious target orbit (A), lie on the same side of the orbital line of nodes when

$$[\theta_{COLN} + \eta] < \pi \tag{D-1}$$

Therefore, this method of accomplishing non-coplanar gross rendezvous, by a given transfer mode, is permissible only when equation (D-1) is satisfied.

The time spent by the chaser in coasting from point A to point e along the fictitious target orbit is

$$t_{\substack{FICT \\ COAST}} = \frac{\pi - [\theta_{COLN} + \eta]}{\omega_2} \tag{D-2}$$

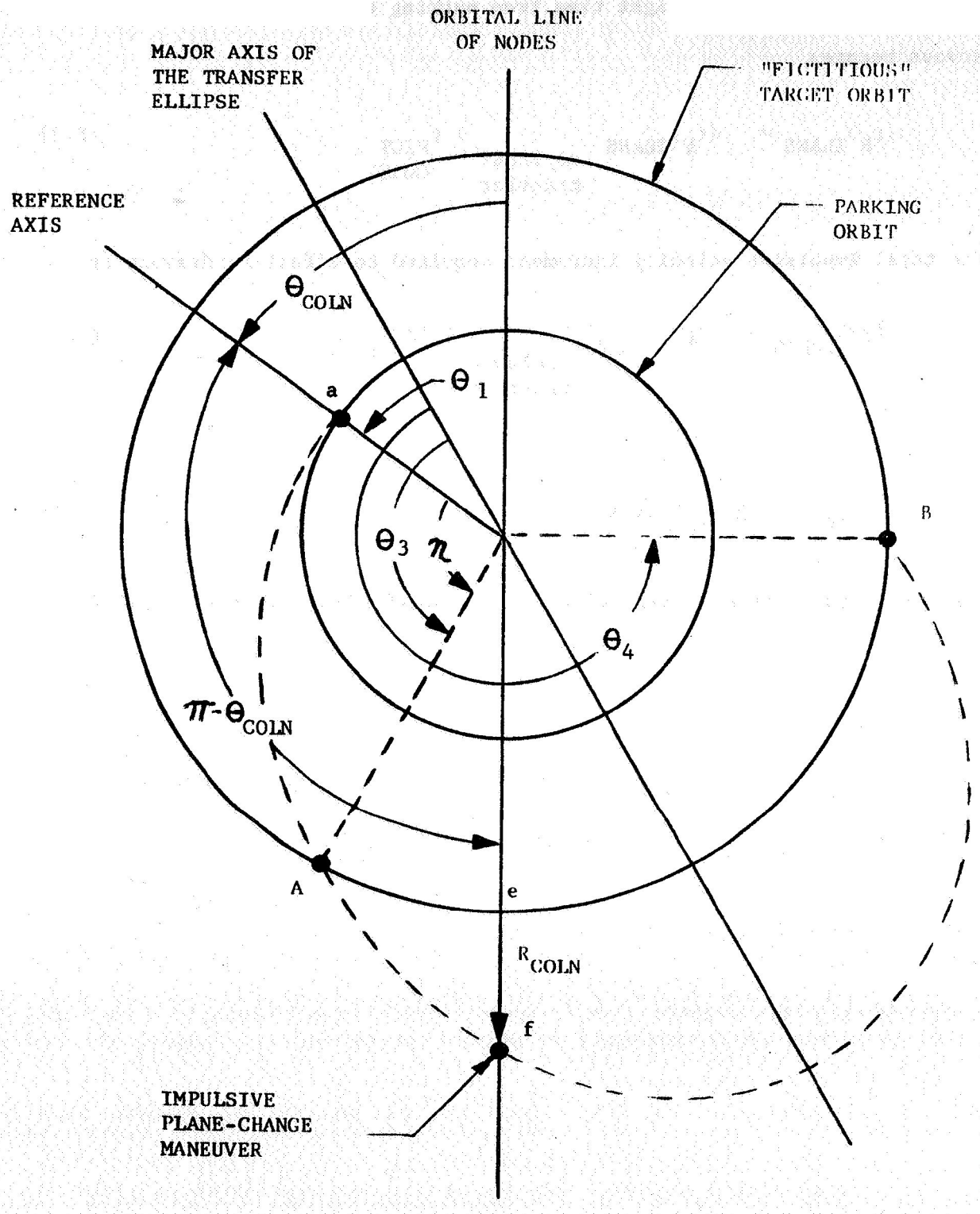

Figure D-1. NON-COPLANAR GAMMA-CHANGE TRANSFER MODE

Thus, the total chaser flight time from parking orbit departure to gross rendezvous becomes

$$(t_F)_{TRANS} = (t_F)_{\substack{TRANS \\ coplanar \\ transfer}} + t_{\substack{FICT \\ COAST}} \tag{D-3}$$

The total impulsive velocity increment required to effect rendezvous is

$$(\Delta V)_{TRANS} = (\Delta V)_{\substack{TRANS \\ coplanar \\ transfer}} + (\Delta V)_{PC} \tag{D-4}$$

where

$$(\Delta V)_{PC} = 2(v_{co})_3 \sin\tfrac{1}{2}\delta \tag{D-5}$$

The above equations are also valid for the Non-Coplanar Three-Impulse Transfer Modes.